Mathematical modelling of predator-prey dynamics in complex environments

Thesis submitted for the degree of

Doctor of Philosophy at the

by

Halil Ibrahim Egilmez

Department of Mathematics
University of Leicester
UK

September 2017

Abstract

The main aim of mathematical ecology is to explore interactions among organisms and the environment where they live, and predator-prey interaction is one of the major type of interactions observed in nature. Models of predator-prey systems - mathematically described by ODEs, PDEs or integro-differential equations - have a long and illustrious history starting from the seminal works by Lotka and Volterra. However, despite a large number of existing publications in the literature, some fundamental questions related to this type of systems still remain open. For example, the spatial heterogeneity of the environment and its role in stabilisation of predator-prey dynamics and persistence of species is still not well understood. Another major challenge is the effect of external forcing (e.g. daily, seasonal, or other variation of model parameters) on long-term dynamics of the predator-prey or host parasite models. Finally, the parameterisation of model functions describing species interactions, for instance, formulation of the functional response of predator, can play a crucial role in the model outcomes.

In the present dissertation, we explore the three above challenging issues (i.e. space heterogeneity, external forcing and model parametrisation) on the patterns of spatio-temporal dynamics of predator-prey or/and host-parasite systems and their stability. In particular, we revisit the famous paradox of enrichment which is classical in mathematical biology and explain how the spatial heterogeneity and animal movement on various time scales can stabilise the system characterised by an infinitely large carrying capacity (Chapter 2). Mathematically, we use a

system of integro-differential equations and consider a tri-trophic planktonic system as a case study. In the two next chapters, we consider the role of daily and seasonal variation of temperature on the control of pathogenic bacteria by their predators: bacteriophages (i.e. bacterial viruses). As an important ecological case study, we explore seasonable dynamics of the infectious bacteria causing the lethal disease Melioidosis in Thailand. In the beginning we model interaction in the top water of a rice field (Chapter 3). Here we build two different models of host-parasite interactions based on ODEs and DDEs (delay differential equations). In Chapter 4, by using reaction-diffusion framework, we extend the previous model of bacteria-phage interactions to consider bacteria-phage dynamics in soil. Using our modelling approach we can make predictions about disease management of Melioidosis in tropic environments.

Dedication

To my wife and son

Acknowledgements

Firstly, I would like to express my sincere gratitude to my advisor Dr Andrew Morozov for the continuous support of my PhD study and related research, for his patience, motivation, and immense knowledge. His guidance helped me in all the time of research and writing of this thesis. I could not have imagined having a better advisor and mentor for my PhD study.

Besides my advisor, I would like to thank Prof Sergei Petrovskii, Prof Ruslan Davidchack and all the honourable staff members of the mathematics department for their insightful comments and encouragement. My thanks also goes to Dr Edouard Galyov and Prof Martha Clokie (Department of Infection, Immunity and Inflammation, University of Leicester), who support us for biological part of chapters 3-4 with their precious knowledge and some experiments.

My sincere thanks to my wife, Sinem, who always supports me with love and patience in tough time for me. Endless thanks also to my parents and parents-in-law for supporting me spiritually throughout writing this thesis and my life in general. I remember with respect my father who passed away in my writing process of the thesis. He is always in my thoughts and prayers.

Last but not the least, I would like to thank my sponsor, Turkish Ministry of National Education, for financial support to do my PhD. I cannot study for doctorate degree abroad without their support.

Contents

Chapter 1

Introduction

1.1 Single species population models

Mathematical modelling in ecology is a powerful and an efficient tool to explain the observed population dynamics and to predict future fate of ecosystems. Simple population models consider dynamics of a single species. For example, the simplest single population model (known as the Malthusian model) is given by the following equation

$$\frac{dP}{dt} = bP - dP = rP, \tag{1.1}$$

where b and d birth and death rate, respectively [71, 52]. Its solution is given by

$$P = P_0 e^{rt}, \tag{1.2}$$

where P_0 is initial value and t is time. If the parameter $r = b - d$ is negative, then the population dies out; If it is positive, then the population grows exponentially with no upper limit which means infinite resources and ecosystem (see Fig 1.1(a)). In reality, however, populations of all species are limited by available resources which results in a decrease of their growth ability at high species densities. The

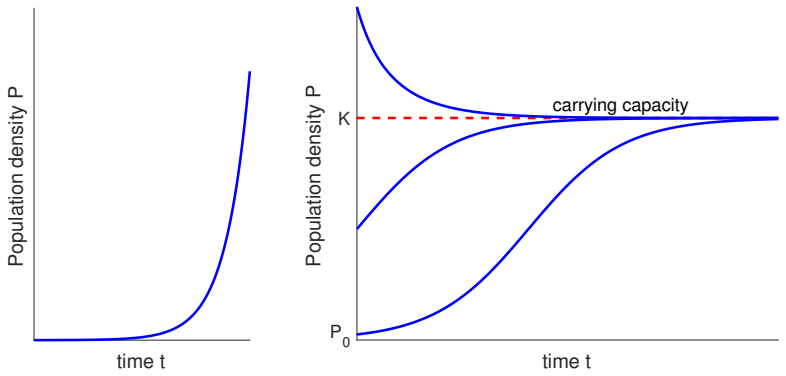

(a) **(b)**

Figure 1.1: Generic behaviour of simple population dynamics given by (1.1) and (1.3). (a) Populations grow exponentially for unlimited resources and display a J-shaped curve while (b) populations had limited resources exhibit logistic growth and the density of population approaches to carrying capacity as S-shaped curve.

logistic equation

$$\frac{dP(t)}{dt} = r\Big(1 - \frac{P(t)}{K}\Big)P(t), \tag{1.3}$$

provides a more realistic description of the population growth for large population sizes which takes into account intraspecific competition (e.g. for space or resources).

The maximal population size which the environment can sustain is called the carrying capacity and is denoted by K. Fig 1.1(b) shows that after long time the population equilibrium is given by the carrying capacity [117, 92].

More complicated single species models include time delays to take into consideration population structuring and describe incubation/maturation time to account for competition between adults and juveniles [13]. The resultant equation becomes a delay differential equation (DDE), where the derivative at the current time is given in terms of the solution of function at the previous times, i.e. the population history. DDEs under different model settings have been studied for a long time to describe single species dynamics [123, 48] including integro-differential modelling frameworks [69]. For simple example, in the classical logistic equation

the effect of maturation delay can be described as

$$\frac{dP}{dt} = rP(t)\Big[1 - \frac{P(t-T)}{K}\Big], \tag{1.4}$$

where T is maturation time; $P(t-T)$ is population density at time $t-T$, and it is mostly referred *Hutchinson-Wright equation* [48, 122]. In the ordinary logistic equation (1.3), it is assumed that the population size at time t instantly changes the growth rate of population size at that moment, whereas in Eq (1.4) changing in population density influences the growth rate of the species after maturation. Adding delay into equation can change the stability of the system equilibria and it can result in not only periodical oscillations but also in chaotic dynamics [29]. Interestingly, in delay model long term transients dynamics can arise where the population size can go to equilibrium or extinct after it oscillates for hundreds of generations [87].

Earlier ecological models have generally assumed that the densities of species are spatially homogeneous or the environment is well mixed (for example, considering that the species mobility is high enough). In this case, system of ODEs or DDEs would be an adequate modelling tool. However, such a simplistic assumption is generally wrong and the species distributions in spaces are highly heterogeneous. To cope with spatial heterogeneity one can use the reaction-diffusion modelling framework, where diffusion terms are added to local population dynamics (described by the reaction terms). In the simplest case of a single species and a constant spatial diffusion, the model equation is given by

$$\frac{\partial P(t,x)}{\partial t} = D\frac{\partial^2 P(t,x)}{\partial x^2} + F(P), \tag{1.5}$$

where $D\frac{\partial^2 P(t,x)}{\partial x^2}$ is diffusion term with constant diffusion coefficient D and $F(P)$ is the local population growth rate (which might be, for simplicity, logistic). $P(t,x)$ is the population density at time t and position x. The above equation was firstly studied by Fisher and Kolmogorov et al in 1930s [31, 51]. On the other hand,

spatially extended models are much harder to investigate analytically (as compared to non-spatial models), especially in the case where model coefficients are space dependent: very often only numerical methods are the only possible investigation tool.

1.2 Predator-prey modelling framework

Any species lives in a community and interacts with some other species along with the environment. Thus for better predictions it is important to include other species in the model as dynamic variables. For this reason, researchers have been greatly interested in the population dynamics of interacting species in recent years. Overall, there are three main types of pairwise interaction between species: (i) competition (where the population growth rate of interacting species mutually decrease in the presence of each other); (ii) symbiosis (where two species stimulate the population growth of each other); and (iii) predator-prey and host-parasite interaction (where an decrease in the growth rate of the pre/host is due to its consumption/use by the predator/parasite species which actually increases its own density) [92, chapter 3]. In this thesis, we will focus on predator-prey and/or host-parasite interactions.

Predator prey models were firstly introduced by Lotka in 1925 and Volterra in 1926 in their seminal works [65, 66, 68, 118]. In the classical Lotka-Volterra model the consumption of prey follows the mass action law, i.e. it is proportional to the product of the population density of prey and predator [67]. The model equations are given by

$$\frac{dP}{dt} = rP - gPM, \tag{1.6}$$

$$\frac{dM}{dt} = \gamma gPM - \mu M \tag{1.7}$$

where $P(t)$ is prey and $M(t)$ is predator densities at time t. The parameters r (proportional increase of the population P), γ (conversion efficiency), μ (mortality

rate of predator) and searching efficiency/attack rate g are positive. The model has two equilibrium states; the trivial equilibrium (0,0) is a saddle and the non-trivial equilibrium $(P^*, M^*) = (\mu/\gamma g,\ r/g)$ is neutrally stable because of purely imaginary eigenvalues [2]. Thus the model is structurally unstable: its slight modification would result in alteration of the dynamics. This makes the application of the initial Lotka-Volterra model to describe realistic ecological systems rather questionable.

To make model (1.6)-(1.7) more realistic, it has been improved by many authors, for instance by introducing the logistic growth and a non-linear functional response of predator. This results in the following modification

$$\frac{dP}{dt} = rP(1 - \frac{P}{K}) - f_P M, \tag{1.8}$$

$$\frac{dM}{dt} = \gamma f_P M - \mu M, \tag{1.9}$$

where K is carrying capacity and f_P is functional response of the predator.

In the initial Lotka-Volterra model the functional response f_P was linear which is the simplest parameterisation based on the mass-action assumption (The rate of food consumption is proportional to the product of the concentrations of the prey and the predator and this is similar to chemical reactions [119]). It is referred to as Holling type I. In 1959, C.S. Holling amended this expression by suggesting two new types of a single resource functional response [44, 42] with further explaining mechanisms of emerging of such responses (see [43] and 1965 [45]).

- $f_P = \frac{gP}{k+P}$ (Holling Type II) [44, 79]
- $f_P = \frac{gP^2}{k^2+P^2}$ (Holling Type III)[42]

where k is half saturation rate. The above functional responses are known as Holling Type II (concave upward) and Holling Type III (sigmoid) and have been used by many researches under original or slightly modified forms such as [107] for

Holling Type II and [47, 85] for type III. Examples of functional responses of types I-III are shown in Fig 1.2: Early predator-prey models such as (1.8)-(1.9) with the functional response of Holling type II predicted the occurrence of large amplitude population cycles in nutrient rich environment (large carrying capacity K of the prey) resulting in a further extinction of species [100]. On the other hand, empirical literature indicates the predators can keep prey density constant at low level even in highly eutrophic environment [17, 9]. This apparent mismatch between the theoretical predictions and empirical observations is known as the "paradox of enrichment" and it remains one of important open questions of mathematical biology. There have been proposed a number of solutions to resolve the paradox of enrichment [3, 35]. For example, this can be done by including evolution of traits of prey and predator [88]. A possible solution can be the existence of more vulnerable and less vulnerable prey subpopulations [101]. Spatial heterogeneity of predator-prey interactions can be a possible solution of the paradox since the initial models considered well-mixed systems [26, 96, 85]. However, the question of finding appropriate solutions the paradox of enrichment is still an open problem.

An appropriate choice of the functional response of predator may explain an efficient top-down control and resolve the paradox of enrichment in plankton ecosystems [85]. The use of sigmoid functional response provides a possible solution

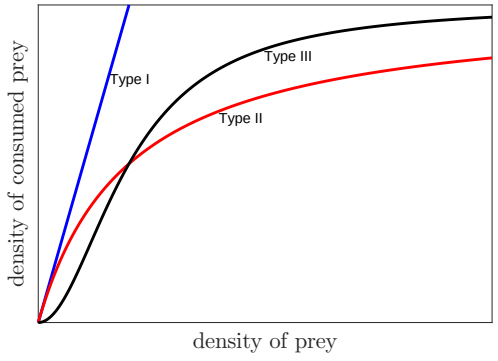

Figure 1.2: Functional responses of predators are generally classified into three types known as Holling type I, II, and III. For details see the text.

such that it enhances the stability of predator-prey model in the case where clearance rate is an increasing function of the food density for grazing zooplankton [94]. In the current thesis we shall also address the question of the influence of the shape and the type of the functional response on the stability of predator-prey systems.

We should say that in a two-species predator-prey model is often a simplification of reality and species are embedded into a food chain or a food web which includes interactions between different trophic levels as well as interaction within the same trophic level (for instance, two predators can compete for the same prey). Thus, some models may involve both competition and predation simultaneously. A predator can consume different resources from the same or several trophic levels: in this case the functional response will be a multi-prey functional response. Unlike a single prey functional response, the multi-prey functional response is not well studied in the literature and choosing a suitable parameterisation for such a response (especially, the one including switching) is an open problem in mathematical biology [83, 102].

Host-parasite interactions are usually similar to predator-prey interactions, however, their modelling may present some particularities, especially this concerns modelling interaction between bacteriophage (viruses of bacteria) and bacteria. In particular, phages can live inside bacteria for long time and result in burst only under some environmental conditions as temperature or pH [104]. Also, phages do not immediately kill their bacterial hosts but do it after some latency time.

Finally, there is a growing understanding that predator-prey and host-parasite interactions can be strongly affected by seasonality: in earlier predator-prey models seasonality was generally neglected. Including seasonality can entirely change model dynamics [103]. Among important seasonal factors which affect the population dynamics are temperature, sunlight level, wind, precipitation, etc. [89]. Considering periodically varying some parameters in interacting population models could make our predictions more realistic even though they would often make

the model more complicated.

In this thesis, we examine some key features affecting predator-prey interactions. These include the role of spatial heterogeneity (particularly shown in chapter 2), the importance of time and space scales, daily and seasonal variations (Chapter 3) and the overall system complexity (Chapter 4). As the relevant ecological case studies, we considered a eutrophic plankton ecosystems, (Chapter 2), bacteria-phage interactions in surface water of a field (Chapter 3) and in the top soil (Chapter 4). In the next two sections of this chapter, to better understand our modelling results, we provide a short introduction into plankton modelling and bacteria-phage interactions.

1.3 Modelling plankton dynamics

1.3.1 Biological background

Plankton means drifting in Greek since planktonic organisms typically flow with surrounding currents and turbulence. They are generally microscopic organisms, but also they cover a wide range of sizes and live in oceans or other bodies of water [60, Chapter 7]. Some of plankton species are capable of actively moving in the vertical direction, but generally they are unable to actively swim in horizontal directions to resist currents and the turbulent diffusion. Plankton can be classified by their size or development stage. In addition, they are divided into trophic levels: two of them are phytoplankton (plants) and zooplankton (animals).

Phytoplankton are the large majority of the plants in the aquatic environment. There are some macroscopic phytoplankton although they are generally microscopic plants. Their sizes are generally between 63 μm and 153 μm. Phytoplankton have chlorophyll to capture sunlight and they photosynthesise like land plants, therefore they need sunlight, nutrients and carbon dioxide (CO_2) to reproduce. Phytoplankton consume carbon dioxide and release oxygen on a scale equivalent to all land plants and this makes them and their life critically import-

ant. On the other hand they also depend on minerals. In this way they populate well-lit surface layer of water and they go down to nutrient-rich water via biological pump and up-welling [75]. They are called the primary producers in aquatic food web since many zooplankton and some animals graze on them and thus the form the basis of the food chain in the ocean and lakes. They also play key role in estimating the potential consequences of global warming according to their range of the sea surface [56, Chapter 3] [21].

Zooplankton are typically tiny animals in the water and they are generally found near the surface since their resource (phytoplankton) dwell there. They are usually microscopic, but some of them are larger and are capable of active swimming in the vertical direction [56, Chapter 4]. Microzooplankton are organisms with the body size between 20 and 200 μm. Mesozooplankton are larger zooplankton with the size between 0.2 and 20 mm among which copepods are one of the most abundant group which serves an important source of food for upper trophic levels including fish and whales. Copepods are classified by the development stage which name comes from greek as cope (kope) means in Greek for "oar" and "podes" (podos) in Greek for "foot" so Copepod = oar-footed. Fig 1.3 gives an illustration of phytoplankton, microzooplankton and mesozooplankton.

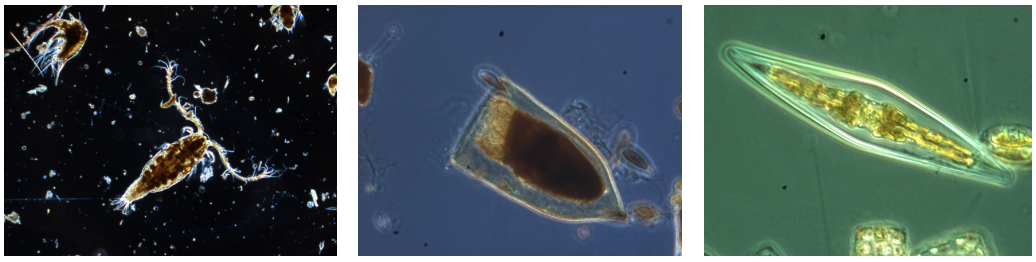

(a) **(b)** **(c)**

Figure 1.3: Sample figures of copepods in (a); microzooplankton in (b) and phytoplankton in (c) (source from microthalassia.ca).

1.3.2 Modelling plankton interaction

Mathematical modelling of plankton dynamics is critical for understanding of the structure of aquatic food chains, growth of plankton and long term predictions. This research area has quickly developed due to a recent development of computer power allowing for efficient numerical simulations [77].

Among other interestingly open problems, the question of the possibility of top-down control of phytoplankton by their gazers remains among the most important ones: in other words the main question is whether or not zooplankton grazers can keep phytoplankton density low in the case of high nutrient concentration in the water. This question is obviously related to the previously mentioned paradox of enrichment. Note that understanding the mechanisms of stabilisation in the nutrient-rich waters can be important for modelling some other ecosystems with eutrophication as, for instance, some terrestrial ecosystems. Lewis et al. (2012) [62] examined a model between three trophic levels which are phytoplankton, microzooplankton and mesozooplankton. They showed that some chemicals released owing to microzooplankton grazing on phytoplankton and those chemicals influenced the system stabilities and copepods predation rate. The article assumed the plankton food web in well-mixed space and ignore spatial distribution.

Previously, it was found that spatial heterogeneity of plankton distribution is one of the most important promoters of top-down control in eutrophic ecosystems and can potentially resolve the paradox of enrichment [96, 81, 84]. Vertical heterogeneity of plankton distribution is mainly caused by pronounced gradients of distributions of environmental factors such as sunlight and nutrients (see Fig 1.4), which strongly affect the growth of phytoplankton. Surprisingly, such heterogeneity has rarely been taken into account when exploring top-down control in nutrient-rich waters. On the other hand, zooplankton grazers (e.g. microzooplankton) can be classified according to their dispersal ability. In the case where they move very slow and feed at the depth where they were born, we refer to this type

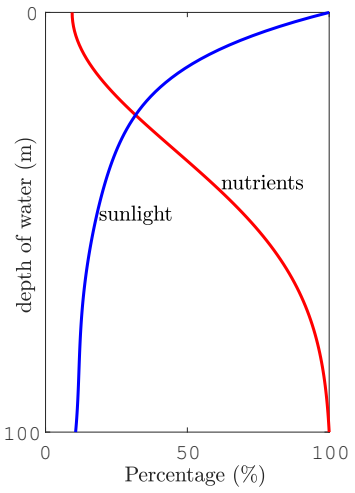

Figure 1.4: Typical vertical distribution of light (blue) and nutrients (red) across the vertical water column: the curves are expressed, respectively, in terms of the percentage of the maximal light intensity at the surface and the maximal nutrient concentration at deep waters.

of predator as a **local** predator. Modelling results show that local predators may be efficient for system stabilization in the case of slow vertical mixing. Omnivrous zooplankton such as copepods, in contrast, are able to quickly move across the entire euphotic zone of the water column within few hours; the dispersal time is small as compared to their own generation time (several months). We refer to this type of zooplankton as a **global** predator; the important particularity of this type is that grazers cannot be assigned to a particular location for long period of time. Therefore, the global predator can be described in models using a global variable [81, 84, 27]: the population size of the global predator should be described by an integral quantity (e.g. spatially averaged value). As a result we have a hierarchy of time and space scales to describe slow moving but fast growing microzooplankton and fast moving but slow growing mesozooplankton [86].

In a realistic plankton food web model we need to include both global predators and local grazers simultaneously [98]. The food web model consisting of traditionally two predators (local such as microzooplankton and global as copepods)

and the primary producer phytoplankton) is called tri-trophic [38, 37]. The key issue which is unknown so far is the potential effect of the combined predators in the stabilization and persistence of planktonic ecosystem. Mathematically some models consider a continuous vertical distribution of species across the column [61, 74] whereas some others split the whole euphotic zone into discrete layers [80].

Integro-differential equations are differential equations involving integrals of unknown functions. An example of a first order linear integro-differential equation is provided below:

$$\frac{dP(h,t)}{dt} = \int_a^h F(h,t,P(h,t))dt + G(h,t,P(h,t)).$$

Using a spatially-continuous approach based on integro-differential equations Lewis et al. (2013) presented a spatial tri-trophic plankton model with local and global predators and analyse the stability [61]. Vertical distributions of phytoplankton, local grazer microzooplankton and grazing-induced production of chemicals were simulated by extending the article [62]. According to Lewis et al. (2013), primary producers can be controlled by grazers, although the phytoplankton density can 'bloom' and have their high values near the surface. However, some simplistic assumptions have been made suggesting a 'linear' food chain, where mesozooplankton could only consume microzooplankton and could not consume phytoplankton. This is often not true for ecosystems where phytoplankton constitute important food source for the copepods [8, 32, 40, 37, 82] even though they try to select nutritiously superior microzooplankton [41]. Therefore it would be more realistic to consider omnivorous copepods, even if their consumption of phytoplankton may be relatively small. In theoretical ecology such predation is known as 'intragild' predation, and it is a widespread phenomenon in food webs [97]. Another important assumption in [61] was that the spatial distribution of copepods followed info-chemicals released as a result of grazing of phytoplankton by microzooplankton, which may not always be correct [10].

In the dissertation (Chapter 2), we reconsider the results obtained by Lewis et al. (2013) [61] by introducing more realistic assumptions about omnivorous copepods. For this purpose we consider several multi-prey functional responses and also revisit the choice of a correct parameterisation of the multi-prey functional response with switching, which is currently a challenge in mathematical biology [36, 116, 115, 81, 61]. The obtained results here would contribute in resolving the paradox of enrichment.

1.4 Bacteria-phage interactions and applications to disease modelling

Another type of predator-prey interaction which we examine in the thesis is bacteria-phage interaction. Below we present a short introduction into the topic from the biological and modelling points of view.

1.4.1 Biological background

Living organisms are classified as either prokaryotes or eukaryotes according to the complexity of composed cells. Bacteria consists of a single cell. They are prokaryotes and they have simple internal structure. Eukaryotes have a nucleus while bacterial DNA floats free which is called nucleoid [6]. Other essential structural compartments are ribosomes, cell membrane, cell wall.

Bacteriophage is a virus which attacks and kills bacteria. The term bacteriophage comes from bacteria and Greek "phagein", which translates as 'to devour'. We will call bacteriophage as phage for short. Phage has a very simple structure that they are composed of a nucleic acid which is either DNA or RNA genome and synthesis of protein coat and tail [73] (Fig 1.5). They have no organelles to copy itself. They do not have ribosomes to produce protein and also they cannot generate or store energy as a form of adenosine triphosphate (ATP). Thus they cannot reproduce or carry out their life-sustaining functions without host cells

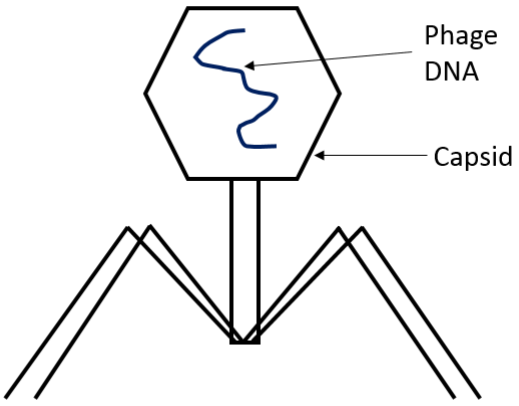

Figure 1.5: A typical *bacteriophage* is composed of a capsid which is protein shell and DNA. [73]

[73]. Therefore, they need host cells and attack them.

An important ecological study case considered in this thesis includes interactions between a highly pathogenic bacteria *Burkholderia pseudomallei* and its phage. Note that *B. pseudomallei* is highly abundant in north Australia and south east Asia (i.e. Thailand, Laos) causes an infectious disease *Melioidosis* which exist acute and chronic forms. *Melioidosis* is a serious environmental-acquired bacterial infection. It is hazardous for the people with chronic health problems, like diabetes, lung disease and heavy alcohol use. This disease leads to death of around 40% of the infected people. Especially, it affects low paid agricultural workers in South-east Asian countries [53]. The bacteria are native and live in water and soil. Those bacteria are highly versatile and they can manage to colonise areas easily. Phages can be a natural agent which would reduce bacterial numbers. Mathematical modelling of *B. pseudomallei*-phage interaction can improve our understanding of the most dangerous seasons and locations to be avoided by workers. Modelling can provide predictions about the probability of disease acquisition.

The interaction between bacteriophage and bacteria is strongly temperature dependent and it occurs either via lytic or lysogenetic infection cycles [104] (Fig 1.6). To reproduce, phages need to infect the host cell by firstly attaching the

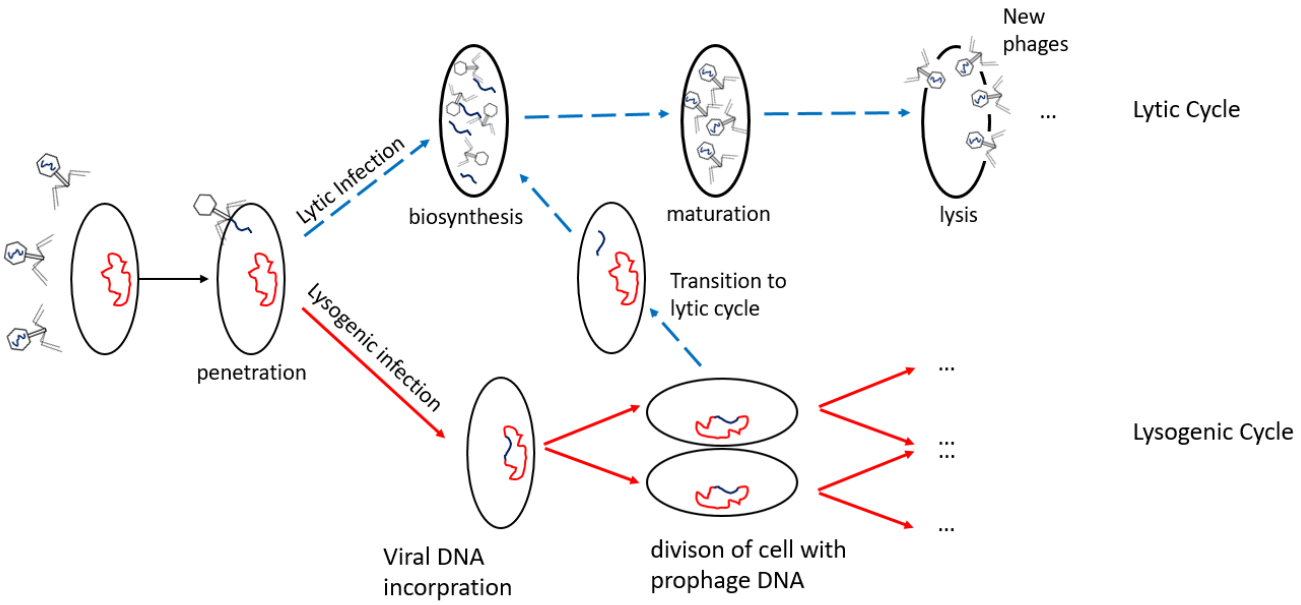

Figure 1.6: Lytic and lysogenic cycle: Phages kill the bacteria after infecting them in lytic cycle and release tens of new phages but in lysgogenic cycle the phages maintain their life inside the bacteria depending on some condition such as temperature, PH etc.

cell wall of bacteria by their tail (adsorption phase). In the next step, they inject their nucleic acid into the cell (penetration phase). After this step, bacteriophage may have one of two different ways which are lytic and lysogenic cycle depending on temperature and ultraviolet (UV) light.

Lytic cycle

At high temperatures (e.g. 37 °C, for details see chapter 3), the infection cycle is lytic. In this case, when DNA of bacteriophages inside the bacterial cell has taken control to synthesize the DNA and protein, they start to multiply in the cell (biosynthesis) and also destroy the host DNA. The next, viral DNA produces large amount of viral components by using metabolic machinery of host cell. The cell walls are broken and the bacteria are lysed when sufficient amount of bacteriophage is formed. Around 100 bacteriophage are released on lysis of bacteria. These free phage can find new host to destroy [34].

Lysogenic cycle

At low temperatures (e.g. at 25 °C), the infection cycle is lysogenic. In this case, the adsorbed phages do not immediately lyse the bacteria. Instead, DNA of bacteriophage replicates with the replication of the chromosome of bacterium by becoming incorporated into the bacterium chromosome. Host cells usually do not recognise this and replicate together for many cell generations. Thus viral DNA passes on to daughter cell of host. It is called lysogenic. Under some condition, the phage DNA leaves the host chromosomes and go into lytic cycle. Notice that some properties of bacteria in lysogenic cycle might change and lysogenized bacteria can resist to superinfection by the same or related phages [70].

In ecosystems such as agricultural fields in South-East Asia, variation of temperature on the daily and seasonal basis should result in a constant switch between the two types of infection.

1.4.2 Bacteria-phage models

Overall, currently there exist no bacteria-phage models with temperature-dependent lysogeny and one of the goal of the thesis was to build such a model. However, there exists a large number of previous publications on modelling bacteria-phage interaction at a constant temperature resulting in a lytic cycle infection [78, 54]. Historically, the first and the simplest computational modelling of bacteria-phage interaction dynamics was studied by Campbell in 1961 [15]. The system consists of one ordinary differential equation (ODE) and one delay differential equation (DDE) for constant latency period. The density of infected bacteria is not included as a dynamical variable. The model equations are given by

$$\frac{dS(t)}{dt} = \alpha S(t)\Big(1 - \frac{S(t)}{C}\Big) - \mu S(t) - KP(t)S(t), \tag{1.10}$$

$$\frac{dP(t)}{dt} = -KP(t)S(t) + KbS(t-\tau)P(t-\tau) - \mu P(t) - K_I P(t), \tag{1.11}$$

where $S(t)$ and $P(t)$ are densities of bacteria and phages at time t. τ shows constant delay time of infection, α is growth rate of bacteria, μ is the flow rate constant, K is adsorption rate, b is burst size, C is carrying capacity. We can easily see that the functional response is Holling type I as $f_S = KS$. Also, the burst size b can be understood as conversion efficiency of predation but unlike in predator-prey models this value is greater than one. On the other hand, predators (phages) die after predation (infection) to prey (bacteria) which is described by the term $-KPS$.

Campbell also examined host competing with two different species of bacteria. The Levin et al. [59] considered multiple resources and multiple species of bacteria and phages by extended the resource limited population model [110]. Therefore, phages compete between each other in addition to bacterial competition. Bremermann presented the model which was similar formulation with Campbell's [15] and Levin et al [59] but he considered the concentration of infected bacteria and didn't use DDE in order to discuss stability of equilibria [11]. The model equations become

$$\frac{dS(t)}{dt} = \alpha S(t)(1 - \frac{S(t)}{C}) - KS(t)P(t), \tag{1.12}$$

$$\frac{dI(t)}{dt} = KS(t)P(t) - \lambda I(t), \tag{1.13}$$

$$\frac{dP(t)}{dt} = \lambda_2 I(t) - \mu P(t), \tag{1.14}$$

where $I(t)$ is the density of infected bacteria, λ is death rate of infected bacteria, λ_2 is release rate of phages.

There have been several modifications of the above two models. For example, the model by Lenski and Levin is similar to the above previous delay models [58], however, the authors consider that infected bacteria do not consume resources and they are unable to grow. Beretta and Kuang made the previous models mode complicated [11] and describe dynamics marine bacteriophage infection by taking into account this decrease in the density of phages [4]. The authors modify

their previous model and included a constant latency period corresponding to the replication time of phage [5]. Gourley and Kuang studied the influence of phage mortality and space in the dynamics [39]. Payne and Jansen proposed the model with that both susceptible and infected bacteria grow exponentially (Malthusian) instead of logistic growth [95]. Multiple adsorption and multiple host binding sites has been studied in the recent published papers [108, 109]. In the article [121], host-phage model was considered only two equations (for susceptible (healthy bacteria and phages) controlled by adsorption and the carrying capacity. Cairn et al [14] focused on both infected and resistant bacteria in addition to susceptible bacteria and phages with delay equation for latency time. Krysiak-Batyn et al. reviewed and classified all existing articles of mathematical models of bacteriophage-host interactions [54].

However, we should emphasize again that none of the previous model was suitable to describe bacteria-paghe interactions with temperature-dependent lygogeny.

1.5 Major objectives of the thesis

In this thesis, we examine several key features affecting predator-prey dynamics in complex environment. Our original results are presented in three main chapters.

In Chapter 2, we analyse the role of heterogeneity in plankton model with vertical resolution. The predator prey model is constructed to describe a tri-trophic plankton population in eutrophic environment. We obtain this model by extending the vertically heterogeneous spatial model in [61] with omnivorous top predator and explore different parameterisations of the predator functional response. This chapter demonstrates the importance of spatial distributions, choosing of an appropriate functional response (with a correctly parametrized switching) and its parameterisation in the system stability.

In Chapter 3, we explored the role of daily and seasonal variation of the possibility of control of bacterial numbers by its phage. We considered interactions in a homogeneous environment mimicking surface water of a typical rice field. Technically, we build two mathematical models (using ordinary and delay differential models; we call them Model I and Model II, respectively). We assume that only the temperature, ultraviolet (UV) ray and sunrise/sunset time change with seasonal variations. Particularly, we examined the model in some Asian regions because of high risk *Melioidosis* (infectious disease) caused by *Burkholderia Pseudomallei*. This chapter shows the influences of the temperature and UV radiation with seasonal variation in the density of phage-free bacteria and the differences of the result between Model I and Model II. We used realistic model parameters obtained by our colleagues from the Department of the Immunity, Infection and Inflammation as well as from the literature.

In Chapter 4, we extended the same system as in Chapter 3 (*Burkholderia Pseudomallei*-phage interaction) to the case of spatially heterogeneous environment. We construct new vertically heterogeneous bacteria-phage model in upper layer of soil within 1 meter. Vertical distribution of temperature is modelled via diffusion equation. On the other hand, we consider that the carrying capacity C of the system decreases with depth according to the experimental data while UV cannot affect phages after around 5 cm in soil. Vertical displacement of bacteria and phages is described via reaction-diffusion model with diffusion coeeficients being very small. The chapter predicts the density of bacteria in the depth of soil in two main endemic provinces of Thailand. Our goal is to make predictions regarding possible disease acquisition across seasons under different level of eutrophication of the soil.

The final chapter (Chapter 5) provides conclusions and a general discussion of future perspectives of modelling predator-prey interactions in planktonic and bacteria-phage systems.

A version of Chapter 2 has been published in [26] and Chapter 3 has been

submitted in Journal "Scientific Report". We are now preparing chapter 4 as an article to submit.

Chapter 2

Spatio-temporal dynamics of tri-trophic plankton food chain with eutrophication

2.1 Introduction

Plankton communities are usually complex systems and their dynamics can be very rich which is reflected in our models. They have served as a paradigm in respect to modelling of complex ecosystems in ecology. An important open question in modelling of planktonic dynamics is to understand the possibility of efficient top-down control of the primary producer (phytoplankton) in nutrient rich water body (eutrophic) by their zooplankton grazers. It is known that phytoplankton densities may remain low despite high nutrient concertation in the water [9, 49] whereas theoretical models predict large-amplitude oscillations in such systems. As mentioned in Chapter 1, this mismatch is called the paradox of enrichment and it isn't limited to the plankton dynamics only [99, 76].

In this chapter, we reconsider the previous results on top-down control in tri-trophic eutrophic systems in heterogeneous environment under eutrophication

for the realistic situation, where a fast moving top predator is omnivorous and its spatial distribution follows the distribution of organisms of both lower trophic levels. We also explore the role of parametrization of the functional response of predators on the persistence and stability of the system. We demonstrate that the interplay between heterogeneity of environment and trophic interaction results in a strong top-down control which would be otherwise impossible in the same system without space. On the other hand, investigation of the model within the realistic parameter range shows that consumption of phytoplankton by copepods generally results in a collapse of the ecosystem: microzooplankton and copepods (mesozooplankton) cannot coexist together. The coexistence of the three trophic levels becomes possible only after introducing a particular assumption regarding the shape the functional response of copepods (the functional response should exhibit an active switching). We also find a bistability of the system with omnivorous copepods: successful establishment of copepods in the system requires a supercritical initial number of copepods.

The material of this chapter has been published in "Mathematical Modelling of Natural Phenomena" (see [26]).

Notations related to chapter 3

t	Time
h	Length (m)
$P(h,t)$	Phytoplankton density at depth h and at time t
$M(h,t)$	Microzooplankton density at depth h and at time t
$\overline{Z}(t)$	Copepods density at time t
K	Phytoplankton carrying capacity
r	Maximum growth rate of phytoplankton
ϕ	Light attenuation coefficient
ω	The self-shading coefficient
m	Mortality rate of phytoplankton
μ	Mortality rate of microzooplankton
δ	Mortality rate of copepods
f_{P_1}	Functional response of microzooplankton
f_{P_2}	copepods grazing on phytoplankton
f_M	feeding on microzooplankton
g	Microzooplankton grazing rate
β_1	Copepods grazing rate
β_2	Copepods predation rate
k_1	Half saturation constant
k_2	Half saturation constant
γ	Microzooplankton grazing efficiency
ϵ_P	Conversion efficiency- phytoplankton to copepods
ϵ_M	Conversion efficiency- microzooplankton to copepods

Units

d	Day
m	Metre
μg	Microgram
C	Carbon
L	litre

Abbreviation

Fig	Figure
Eq	Equation

2.2 Plankton model

We consider a tri-trophic planktonic food web which consists of phytoplankton P as primary producers, microzooplankton M as intermediate grazers and copepods Z as top predators. The variable h describes depth level of the water column. The trophic interactions take place in the euphotic zone between the surface ($h = 0$) and the base of the euphotic zone $h = H$ since the zone is adequately illuminated to permit photosynthesis by phytoplankton. The model equations follow as below

$$\begin{aligned}
\frac{\partial P}{\partial t} &= D\frac{\partial^2 P}{\partial h^2} + r\exp(-\phi h - \omega\int_0^h P dh)P(1-\frac{P}{K}) - mP \\
&\quad - f_{P_1}M - f_{P_2}\overline{Z}z, \\
\frac{\partial M}{\partial t} &= D\frac{\partial^2 M}{\partial h^2} + \gamma M f_{P_1} - \mu M - f_M\overline{Z}z, \\
\frac{d\overline{Z}}{dt} &= \frac{\overline{Z}}{H}\int_0^H (\epsilon_P f_{P_2} + \epsilon_M f_M)z dh - \delta\overline{Z},
\end{aligned} \tag{2.1}$$

where $P = P(h,t)$ and $M = M(h,t)$ are densities of phytoplankton and microzooplankton at depth h and at time t respectively. Phytoplankton and microzooplankton are exposed to turbulent diffusion since they have limited swimming abilities. D is the diffusion coefficient (suggested to be constant); $\overline{Z} = \overline{Z}(t)$ is the density of copepods averaged over the entire euphotic zone at time t; Copepods have good swimming abilities to resist vertical turbulence. $z = z(h,t)$ is the instantaneous relative local density of copepods depending on the density of prey: the density of copepods at depth h is given by the product of $\overline{Z}$ and z. The vertical distribution of $z = z(h,t)$ generally depends on the vertical distribution of both prey species and is mathematically determined by in Section 2.2.3.

The model parameters have the following meanings: r is maximum growth rate and K is carrying capacity of phytoplankton. Phytoplankton need light to photosynthesise so their growth rate is proportional to light intensity. When the depth of water increases, the amount of suitable light for phytoplankton expo-

Table 2.1: Parameters definitions, units, fixed values and possible ranges. The corresponding references are provided

	Parameters and Definition	**Units**	**Fixed values**	**Ranges**
r	Phytoplankton intrinsic growth rate	d^{-1}	1.5	$0.1 - 2$ [22]
K	Phytoplankton carrying capacity	μg C L^{-1}	2000	$50 -$ inf [81]
ϕ	Light attenuation coefficient	m^{-1}	0.05	$0.005 - 0.15$ [3]
ω	Self-shading coefficient	$1/(m\ \mu g\ C\ L^{-1})$	0.002	$0.0005 - 0.005$ [3]
g	Microzooplankton grazing rate	d^{-1}	7.5	$2 - 12$ [23]
β_1	Copepods grazing rate	d^{-1}	1.4	$0.6 - 1.4$ [40, 22]
β_2	Copepods predation rate	d^{-1}	1.4	$0.6 - 1.4$ [40, 81]
k_1	Half saturation constant	μg C L^{-1}	20	$20 - 100$ [40, 81]
k_2	Half saturation constant	μg C L^{-1}	60	$20 - 100$ [40, 81]
γ	Microzooplankton grazing efficiency	–	0.3	$0.15 - 0.64$ [23]
ϵ_P	Conversion efficiency- phytoplankton to copepods	–	0.35	$0.2 - 0.8$ [23, 38]
ϵ_M	Conversion efficiency- microzooplankton to copepods	–	0.7	$0.2 - 0.8$ [23, 38]
m	Phytoplankton mortality	d^{-1}	0.02	$0 - 0.3$ [33]
μ	Microzooplankton mortality	d^{-1}	0.05	$0.01 - 0.1$ [16]
δ	Copepods mortality	d^{-1}	0.01	$0.01 - 0.15$ [24, 16]
D	Diffusion coefficient	$m^2\ d^{-1}$	1	$1 - 10$ [3]

nentially decreases owing to absorption by the water and self-shading of light by phytoplankton located above the given depth. These can be formalised by $\exp(-\phi h)$ with ϕ being the light attenuation coefficient and by an integral term $\exp\left(-\omega \int_0^h P(h)dh\right)$ with the self-shading coefficient ω, respectively. We assume that the light irradiance is not very high and there is no growth inhibition, see [25]. Microzooplankton densities are also high in the surface since they graze on phytoplankton. The parameters m, μ and δ are mortality coefficients of phytoplankton, microzooplankton and copepods respectively. The function f_{P_1} is the functional response of microzooplankton; f_{P_2} and f_M describe copepods grazing on phytoplankton and feeding on microzooplankton respectively. The conversion of grazed phytoplankton into new biomass of microzooplankton is described by γ, whereas phytoplankton and microzooplankton conversion efficiency of copepods

are described by ϵ_P and ϵ_M, respectively.

The plankton model has zero-flux boundary conditions for phytoplankton and microzooplankton to prevent the plankton leaving the considered part of the water column such that

$$\begin{aligned} \frac{\partial P(0,t)}{\partial h} &= \frac{\partial P(H,0)}{\partial h} = 0, \\ \frac{\partial M(0,t)}{\partial h} &= \frac{\partial M(H,0)}{\partial h} = 0, \end{aligned} \tag{2.2}$$

The functional response of microzooplankton f_{P_1} depends only on phytoplankton density. Using conventional aproach (Holling type II disk equation), we shall assume the following parametrisation [36]

$$f_{P_1} = \frac{gP}{k_1 + P}, \tag{2.3}$$

where g is maximum grazing rate on phytoplankton by microzooplankton and k_1 is half saturation constant. To proceed further, we need to parameterise the functional responses of the zooplankton. We have three cases of functional responses for feeding copepods to analyse the model: Holling Type II functional response for copepods feeding on single resource (only microzooplankton in Fig 2.1(a)), Holling type II and type III functional responses for ceopepods feeding on two resources (phytoplankton and microzooplankton) in Fig 2.1(b).

2.2.1 Single resource food chain

We shall first consider the simplest scenario, in which copepods only graze on microzooplankton as in Fig 2.1(a) to compare with the model with an omnivorous top predator. In this case, single resource Holling Type II (disk equation) functional response (f_M) is used for feeding on microzooplankton by copepods as fallow

$$f_M = \beta_2 \frac{M}{k_2 + M}, \tag{2.4}$$

(a)

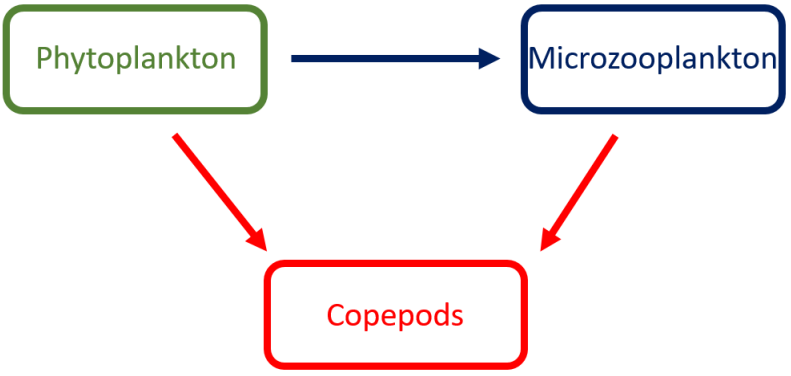

(b)

Figure 2.1: (a):Copepods prey on microzooplankton and microzooplankton graze on phytoplankton, (b): Copepods are fed by both microzooplankton and phytoplankton and microzooplankton graze on phytoplankton

where β_2 is maximal feeding rate and k_2 is half saturation constant. Besides, Copepods are carnivorous and don't graze on phytoplankton, thus the functional response f_{P_2} becomes zero. We call this model as *single resource food chain* or *linear feeding model*. There is no competition between the species in this model. Microzooplankton grazing plays important role in this plankton dynamics. It regulates the population rate of phytoplankton and it is a link between phytoplankton and copepods.

2.2.2 Multiple resource food chain

In the previous section, copepods were suggested to be carnivorous and they only feed one type of resources. Here we suppose herbivorous copepods which feed on both microzooplankton and phytoplankton as in Fig 2.1(b). Parameterization of the functional response of copepods depending on two food sources

(phytoplankton and microzooplankton) is more complicated issue. Overall, there exist a large number of possible parameterisations, each of which has its biological rationale (see [36, 83, 102]). Thus we firstly seek for a proper multi-prey functional response of copepods to obtain coexistence for all species. Also, these functional responses should be comparable with the single resource functional response. In this section, we consider two different types of multi-resources functional responses describing either that the top predator doesn't switch prey or that the predator preferentially consumes the most common species.

Proportion based functional response

Prey switching means that predator are able to select the most common type of resources to consume. The relative preference is constant in no prey switching model [36]. We construct the model with well known no-prey switching functional response for copepods feeding on two resources (phytoplankton in addition to microzooplankton). This response is derived by extending single resource Holling Type II (disk equation) functional response [32, 90] in the section 2.2.1 and show as follow

$$\begin{aligned} f_{P_2} &= \beta_1 \frac{\eta_1 P}{k_2 + \eta_1 P + \eta_2 M}, \\ f_M &= \beta_2 \frac{\eta_2 M}{k_2 + \eta_1 P + \eta_2 M}, \end{aligned} \tag{2.5}$$

where β_1 and β_2 are copepods predation rates, k_2 is half saturation coefficient. η_1 and η_2 are non-negative control parameters and their values are assumed 0 or 1. Notice that the single resource parametrisation of functional response is obtained as Eq (2.4) if we say that η_1 is zero and η_2 is one. Let suppose that both η_1 and η_2 are one. Then, we obtain simplified no-switching functional responses as below

$$\begin{aligned} f_{P_2} &= \beta_1 \frac{P}{k_2 + P + M}, \\ f_M &= \beta_2 \frac{M}{k_2 + P + M}, \end{aligned} \tag{2.6}$$

Functional response with switching: kill the winner (KTW)

In the functional response with active prey switching, the food preference is not constant and the predator selects foods depending on their abundance or fewness of resources. Prey switching might be defined that the predator's preference for prey increases if that prey increases. On the other hand, if prey is rare then the preference of predator is weak [42, 91, 94]. Therefore, the selecting active prey switching functional response is more rational and realistic. We use the recently suggested parametrisation called as "Kill-The-Winner" (KTW) functional response [116] given by

$$\begin{aligned} f_{P2} &= \beta_1 \frac{\eta_1 P^2}{\eta_1 P^2 + \eta_2 M^2} \frac{\eta_1 P + \eta_2 M}{k_2 + \eta_1 P + \eta_2 M}, \\ f_M &= \beta_2 \frac{\eta_2 M^2}{\eta_1 P^2 + \eta_2 M^2} \frac{\eta_1 P + \eta_2 M}{k_2 + \eta_1 P + \eta_2 M}, \end{aligned} \tag{2.7}$$

where parameters are the same meaning as in Eq (2.5). The model (2.7) can switch to the single resource functional response in Section (2.2.1) for $\eta_1 = 0$ and $\eta_2 = 1$. On the other hand, we assume that both η_1 and η_2 are 1 and then we attain the simplest KTW functional responses as below

$$\begin{aligned} f_{P2} &= \beta_1 \frac{P^2}{P^2 + M^2} \frac{P + M}{k_2 + P + M}, \\ f_M &= \beta_2 \frac{M^2}{P^2 + M^2} \frac{P + M}{k_2 + P + M}, \end{aligned} \tag{2.8}$$

It can be found more detail and the formal derivation of parametrization (2.8) in [116]. The main differences between the functional responses (2.6) and (2.8) is that active switching causes a substantial drop in resource consumption when the relative abundance of this resource is low.

2.2.3 Finalising the model equations

We define three different models called as Model I, Model II and Model III in regard to the functional responses of copepods as follows. Model I: copepods are not grazer and they feed only on microzooplankton. Thus the model has the functional response in (2.4). Model II: the copepods are omnivorous but they do not have the ability for selecting abundant resources. Thus, the model has the functional response in (2.6). Model III: copepods are also omnivorous and they are able to actively prefer abundant foods to less foods. The model is constituted with the KTW functional response in (2.8).

Copepods follow the ideal free distribution function $z(h,t)$. This function is defined with the densities of immobile species which are phytoplankton and microzooplankton. Since active movement of copepods occurs on a fast scale compared to their demographic scale, we cannot assign the density of copepods to a fixed horizontal layer in the water column. In the following, we describe the spatial distribution of copepods based on the relative distribution $z(h,t)$, which is the local density of copepods divided by their average density $\overline{Z}$. Based on previous empirical demonstrations [27, 57, 86, 81], we can assume that the relative distribution of copepods follows the ideal free distribution of the densities of immobile species which are phytoplankton and microzooplankton across the space, i.e.

$$z(h,t) = \frac{\eta_1 P(h,t) + \eta_2 M(h,t)}{\eta_1 \overline{P}(t) + \eta_2 \overline{M}(t)}, \tag{2.9}$$

where $\overline{P}$ and $\overline{M}$ are the space average densities of P and M, respectively. They are computed by

$$\overline{P} = \frac{1}{H}\int_0^H P(h,t)dh,$$

$$\overline{M} = \frac{1}{H}\int_0^H M(h,t)dh,$$

Note that for simplicity, the weights in Eq (2.9) are chosen to be the same as in

the above functional responses to reduce the number of independent parameters. This assumption is not critical and one can replace η_i with some independent parameters. For model I; the values of η_1 is 0 and η_2 is 1 as in the single resources functional response (2.4) and the function is given below

$$z(h,t) = \frac{M(h,t)}{\overline{M}(t)}, \tag{2.10}$$

As seen the function above, there is no P expression since according to assumption of this model, copepods don't graze on the phytoplankton. For Model II and Model III, both η_1 and η_2 are assumed 1 since both lower levels are resources for copepods.

$$z(h,t) = \frac{P(h,t) + M(h,t)}{\overline{P}(t) + \overline{M}(t)}, \tag{2.11}$$

Note that there is some indication in the literature that the conversion efficiency of copepods feeding on microzooplankton is often higher than when feeding on phytoplankton [38, 112]. However, the precise ratio between ϵ_P and ϵ_M is generally unknown. In this paper, we assume that $\epsilon_P = 0.5\epsilon_M$ in most of simulations. We also consider the scenario when $\epsilon_P = \epsilon_M$. Note that variation of the ratio ϵ_P/ϵ_M does not greatly affect the main qualitative results of the paper.

The dynamical system includes partial integro-differential equations. The parameter values and ranges considered here are taken from the literature; they are summarized in Table 2.1. The unit of plankton density is chosen as μgCL^{-1}. The models were analysed numerically using the explicit integration method (forward difference for the time derivative and the second order central difference for the space derivative):

$$\begin{aligned}
\frac{P_i^{j+1} - P_i^j}{\Delta t} &= D\frac{P_{i+1}^j - P_i^j + P_{i-1}^j}{\Delta h^2} + f_1(P, M, Z, t, h) \\
\frac{M_i^{j+1} - M_i^j}{\Delta t} &= D\frac{M_{i+1}^j - M_i^j + M_{i-1}^j}{\Delta h^2} + f_2(P, M, Z, t, h) \\
\frac{Z^{j+1} - Z^j}{\Delta t} &= f_3(P, M, Z, t, h)
\end{aligned}$$

where $P_i^j \Rightarrow P(h_i, t_j)$, $M_i^j \Rightarrow M(h_i, t_j)$ and $Z^j \Rightarrow \overline{Z}(t_j)$. We consider the size of euphotic zone to be $H = 80$ m and it is discretised in 300 levels which gives the space step $\Delta h \approx 0.2676$. We find that the optimal time resolution in terms of numerical stability Δt should be smaller than $(\Delta h)^2/2D \approx 0.0358$ and we generally select Δt as 0.001 or smaller. We compute linear system of 300 equations with 300 unknowns at each time step for the first and second equation in the system. The integrals in the system are evaluated using the trapezoidal rule [50]. Zero flux boundary condition can be expressed by

$$\frac{\partial P(0,t)}{\partial h} = 0 \Rightarrow \frac{P_2^j - P_1^j}{\Delta h} = 0 \Rightarrow P_2^j = P_1^j$$

similarly, $P_{299}^j = P_{300}^j$, $M_2^j = M_1^j$ and $M_{299}^j = M_{300}^j$. The initial conditions are assumed to be spatially uniform distributions of phytoplankton and microzooplankton. The accuracy of our numerical computation was checked by decreasing the step size in space by half (with the corresponding by decreasing the time step) to check whether or not the numerical results were close to each other. Some results were checked as well by an implicit numerical scheme (including the Crank-Nicolson scheme). On the other hand, we computed the non-spatial (the system of ODEs) model via the classical 4^{th} order Runge Kutta (RK4) method [77]. The accuracy of the numerical simulation was again checked by decreasing the time step and comparing the results of simulations consecutive smaller steps. Technically, all coding and simulations were done using MATLAB software.

2.3 Results

2.3.1 Non-spatial model

In this section, we briefly consider Models I, II and III in the case of a well-mixed system, i.e. assuming the ecosystem to be homogeneous. This will allow us to better understand the role of spatial heterogeneity in persistence and stability. The model equations of the corresponding well-mixed systems are formally

obtained by removing the diffusion terms and setting $\phi = 0$, $\omega = 0$ and $z(h) = 1$ from Model (2.1). We assume that $\epsilon_M = \epsilon_P = \epsilon$ for the simplicity. The resultant model without vertical distribution then becomes a system of ODEs as below

$$\begin{aligned}
\frac{d\overline{P}}{dt} &= r\overline{P}(1 - \frac{\overline{P}}{K}) - m\overline{P} - \frac{g\overline{P}}{k_1 + \overline{P}}M - f_{P_2}\overline{Z}, \\
\frac{d\overline{M}}{dt} &= \gamma\overline{M}\frac{g\overline{P}}{k_1 + \overline{P}} - \mu\overline{M} - f_M\overline{Z}, \\
\frac{d\overline{Z}}{dt} &= \epsilon\overline{Z}(f_{P_2} + f_M) - \delta\overline{Z}.
\end{aligned} \tag{2.12}$$

The system in (2.12) depends only on time and it is spatially homogeneous. The equilibrium states of the model can be analytically found by the solution of the system below:

$$\begin{aligned}
F_1(\overline{P}, \overline{M}, \overline{Z}) &= r\overline{P}(1 - \frac{\overline{P}}{K}) - m\overline{P} - \frac{g\overline{P}}{k_1 + \overline{P}}M - f_{P_2}\overline{Z}, \\
F_2(\overline{P}, \overline{M}, \overline{Z}) &= \gamma\overline{M}\frac{g\overline{P}}{k_1 + \overline{P}} - \mu\overline{M} - f_M\overline{Z}, \\
F_3(\overline{P}, \overline{M}, \overline{Z}) &= \epsilon\overline{Z}(f_{P_2} + f_M) - \delta\overline{Z}.
\end{aligned} \tag{2.13}$$

The non-negative roots of equation system (2.13) with variable $\overline{P},\ \overline{M},\ \overline{Z}$ give the steady states $(\overline{P}^*, \overline{M}^*, \overline{Z}^*)$ such as:

$$\begin{aligned}
F_1(\overline{P}^*, \overline{M}^*, \overline{Z}^*) &= 0, \\
F_2(\overline{P}^*, \overline{M}^*, \overline{Z}^*) &= 0, \\
F_3(\overline{P}^*, \overline{M}^*, \overline{Z}^*) &= 0.
\end{aligned} \tag{2.14}$$

After finding the steady states of the systems, we can analyse their stabilities by calculating Jacobian matrices as below

$$J = \begin{bmatrix} \frac{\partial F_1}{\partial P} & \frac{\partial F_1}{\partial M} & \frac{\partial F_1}{\partial Z} \\ \frac{\partial F_2}{\partial P} & \frac{\partial F_2}{\partial M} & \frac{\partial F_2}{\partial Z} \\ \frac{\partial F_3}{\partial P} & \frac{\partial F_3}{\partial M} & \frac{\partial F_3}{\partial Z} \end{bmatrix}.$$

The Jacobian matrix is $J^* = J(\overline{P}^*, \overline{M}^*, \overline{Z}^*)$ evaluated at the steady states. Then, the eigenvalues are calculated from $\det(J^* - \lambda I) = 0$. According to sign of λ, the stability of the states are determined. If all eigenvalues (or their real parts if complex) are negative, then the equilibrium state is stable. If not, it is unstable. In this study, We have three models related to functional responses of copepods. We call them "non-spatial model I, II, III" respectively.

Non-spatial model I: single resource food source

Let's start with non-spatial Model I. For this, we substitute the functional response (2.4) to system (2.14) and we get the following ODE system:

$$r\overline{P}^*(1 - \frac{\overline{P}^*}{K}) - m\overline{P}^* - \frac{g\overline{P}^*}{k_1 + \overline{P}^*}\overline{M}^* = 0, \tag{2.15}$$

$$\gamma\overline{M}^*\frac{g\overline{P}^*}{k_1 + \overline{P}^*} - \mu\overline{M}^* - \beta_2\frac{\overline{M}^*}{k_2 + \overline{M}^*}\overline{Z}^* = 0, \tag{2.16}$$

$$\epsilon\overline{Z}^*\beta_2\frac{\overline{M}^*}{k_2 + \overline{M}^*} - \delta\overline{Z}^* = 0. \tag{2.17}$$

One of the steady states is $(0, 0, 0)$, trivial. Secondly, we look for semi-trivial steady states. If $\overline{P}^* = 0$, then $\overline{M}^*$ can be only zero (the parameters and $\overline{Z}^*$ cannot be negative) from Eq (2.16), so $\overline{Z}^*$ is also zero from Eq (2.17). If we say $\overline{M}^* = 0$, then $\overline{Z}^* = 0$ from Eq (2.17) and $\overline{P}^* = \frac{Kr - mK}{r}$ from Eq (2.15). Lastly, suppose $\overline{Z}^* = 0$, then we substitute it to Eq (2.16), cancel some positive common factor $\overline{M}^*$, and find $\overline{P}^* = \frac{\mu k_1}{\gamma g - \mu}$. Thereafter, we find $\overline{M}^* = (r(1 - \frac{\overline{P}^*}{K}) - m)\frac{k_1 + \overline{P}^*}{g\overline{P}^*}$

from Eq (2.15). To find the non-trivial equilibrium, we can firstly cancel some common factors in the system above and obtain the system below:

$$0 = r(1 - \frac{\overline{P}^*}{K}) - m - \frac{g}{k_1 + \overline{P}^*}\overline{M}^*, \tag{2.18}$$

$$0 = \gamma\frac{g\overline{P}^*}{k_1 + \overline{P}^*} - \mu - \beta_2\frac{1}{k_2 + \overline{M}^*}\overline{Z}^*, \tag{2.19}$$

$$0 = \epsilon\beta_2\frac{\overline{M}^*}{k_2 + \overline{M}^*} - \delta. \tag{2.20}$$

$\overline{M}^*$ can be easily found from Eq (2.20) as follow.

$$\overline{M}^* = \frac{k_2\delta}{\epsilon\beta_2 - \delta}, \tag{2.21}$$

Then $\overline{M}^*$ is substituted to Eq (2.18) and it is arranged

$$A\overline{P}^* + B\overline{P}^* + C = 0, \tag{2.22}$$

where $A = r$, $B = k_1 r - Kr + mK$ and $C = -k_1 rK + mk_1 K + gK\overline{M}^*$. $\overline{P}^*$ can be calculated from the quadratic Eq (2.22)

$$\overline{P}^* = \frac{-B \mp \sqrt{B^2 - 4AC}}{2A}, \tag{2.23}$$

and then $\overline{Z}^*$ is found by substitution (2.21) and (2.23) to Eq (2.19) as the following:

$$\overline{Z}^* = (\frac{\gamma g\overline{P}^*}{k_1 + \overline{P}^*} - \mu)\frac{k_2 + \overline{M}^*}{\beta_2}, \tag{2.24}$$

Thus, the Jacobian matrix J^* is as the following

$$J^* = \begin{bmatrix} r - \frac{2\overline{P}^*}{K} - m - \frac{g\overline{M}^* k_1}{(k_1+\overline{P}^*)^2} & -\frac{g\overline{P}^*}{k_1+\overline{P}^*} & 0 \\ \frac{\gamma\overline{M}^* g k_1}{(k_1+\overline{P}^*)^2} & \frac{\gamma g\overline{P}^*}{k_1+\overline{P}^*} - \mu - \frac{\beta_2\overline{Z}^* k_2}{(k_2+\overline{M}^*)^2} & -\frac{\beta_2\overline{M}^*}{k_2+\overline{M}^*} \\ 0 & \frac{\epsilon\overline{M}^*\beta_2 k_2}{(k_2+\overline{M}^*)^2} & 0 \end{bmatrix}, \tag{2.25}$$

and the eigenvalues are calculated by its determinant with $\det(J^* - \lambda I) = 0$. We numerically computed the non-zero steady state since the analytical solution will be too cumbersome and we found only one non-trivial steady state in this system $(\overline{P}^*, \overline{M}^*, \overline{Z}^*) = (1967.8, 1.1, 95)$ using the default parameter values from Table (2.1). We also calculated the eigenvalues using MATLAB built in functions to obtain $\lambda_1 = -1.471$, $\lambda_{2,3} = 0.019 \pm 0.145i$. Since the real part of the eigenvalue is positive, the steady state is unstable. The steady states and their stabilities for different growth rates of phytoplankton are presented in Table (2.2). The non-trivial equilibria are unstable for any values of r as seen in the table. The model has stable equilibrium states only for small values of K and r (e.g. $K = 50$ and $r = 0.4$) but this is not much realistic.

According to large carrying capacity K, Eq (2.15) would be such that

$$0 = r - m - \frac{g}{k_1 + \overline{P}^*}\overline{M}^*, \tag{2.26}$$

$$r - m = \frac{g}{k_1 + \overline{P}^*}\overline{M}^*. \tag{2.27}$$

On the other hand, the first element of the Jacobian matrix (2.25) would be

$$r - m - \frac{g\overline{M}^* k_1}{(k_1 + \overline{P}^*)^2}, \tag{2.28}$$

$$\Rightarrow \quad r - m - \frac{g\overline{M}^*}{k_1 + \overline{P}^*}\frac{k_1}{k_1 + \overline{P}^*}. \tag{2.29}$$

Then we substitute Eq (2.27) to the term above and rearrange it:

$$\Rightarrow \quad r - m - (r - m)\frac{k_1}{k_1 + \overline{P}^*}, \tag{2.30}$$

$$\Rightarrow \quad (r - m)\Big(1 - \frac{k_1}{k_1 + \overline{P}^*}\Big), \tag{2.31}$$

$$\Rightarrow \quad (r - m)\Big(\frac{\overline{P}^*}{k_1 + \overline{P}^*}\Big). \tag{2.32}$$

Since $r - m > 0$ and $\frac{\overline{P}^*}{k_1 + \overline{P}^*} > 0$, the first element of the matrix (2.25) is positive.

Table 2.2: $(\overline{P}^*,\ \overline{M}^*,\ \overline{Z}^*)$ and λ of steady states for variable values of parameter r and fixed values of all other parameters in non-spatial Model I.

r	$(\overline{P}^*,\ \overline{M}^*,\ \overline{Z}^*)$	λ	stability
0.1	$(88.243,\ 1.1,\ 77.86)$	$(0.023,\ 0.033 \pm 0.206i)$	unstable
	$(1491.8,\ 1.1,\ 94.70)$	$(-0.07,\ 0.02 \pm 0.145i)$	unstable
0.2	$(26.12,\ 1.1,\ 53.43)$	$(0.011,\ 0.055 \pm 0.33i)$	unstable
	$(1753.9,\ 1.1,\ 94.9)$	$(-0.171,\ 0.019 \pm 0.145i)$	unstable
0.3	$(9.368,\ 1.1,\ 29.137)$	$(0.04,\ 0.048 \pm 0.36i)$	unstable
	$(1837.3,\ 1.1,\ 94.9)$	$(-0.271,\ 0.019 \pm 0.145i)$	unstable
0.4	$(1.549,\ 1.1,\ 4.874)$	$(0.0005,\ 0.014 \pm 0.24i)$	unstable
	$(1878.5,\ 1.1,\ 95.0)$	$(-0.371,\ 0.019 \pm 0.15i)$	unstable
0.5	$(-2.981,\ 1.1,\ -19.379)$	–	–
	$(1903.0,\ 1.1,\ 95.0)$	$(-0.471,\ 0.019 \pm 0.15i)$	unstable
1	$(-11.701,\ 1.1,\ -140.6)$	–	–
	$(1951.7,\ 1.1,\ 95)$	$(-0.972,\ 0.019 \pm 0.15i)$	unstable
1.5	$(-14.512,\ 1.1,\ -261.81)$	–	–
	$(1967.8,\ 1.1,\ 95)$	$(-1.472,\ 0.02 \pm 0.15i)$	unstable

The determinant of the matrix is

$$\det(J^*) = -(r-m)\Big(\frac{\overline{P}^*}{k_1+\overline{P}^*}\Big)\Big(-\frac{\beta_2\overline{M}^*}{k_2+\overline{M}^*}\Big)\frac{\epsilon\overline{M}^*\beta_2 k_2}{(k_2+\overline{M}^*)^2}, \tag{2.33}$$

$$=(r-m)\Big(\frac{\overline{P}^*}{k_1+\overline{P}^*}\Big)\frac{\beta_2\overline{M}^*}{k_2+\overline{M}^*}\frac{\epsilon\overline{M}^*\beta_2 k_2}{(k_2+\overline{M}^*)^2}, \tag{2.34}$$

obviously positive and $\det(J^*) = \lambda_1\lambda_2\lambda_3 > 0$. That's why at least one of eigenvalues is positive and the equilibrium state is unstable.

Non-spatial model II: omnivorous copepods having functional response without switching

Model II is constructed by the rational based functional response (2.6). Then system (2.14) becomes as below to find equilibrium points and examine their

stabilities:

$$0 = r\overline{P}^*(1 - \frac{\overline{P}^*}{K}) - m\overline{P}^* - \frac{g\overline{P}^*}{k_1 + \overline{P}^*}\overline{M}^* - \beta_1\frac{\overline{P}^*}{k_2 + \overline{P}^* + \overline{M}^*}\overline{Z}^*, \tag{2.35}$$

$$0 = \gamma\overline{M}^*\frac{g\overline{P}^*}{k_1 + \overline{P}^*} - \mu\overline{M}^* - \beta_2\frac{\overline{M}^*}{k_2 + \overline{P}^* + \overline{M}^*}\overline{Z}^*, \tag{2.36}$$

$$0 = \epsilon\overline{Z}^*(\beta_1\frac{\overline{P}^*}{k_2 + \overline{P}^* + \overline{M}^*} + \beta_2\frac{\overline{M}^*}{k_2 + \overline{P}^* + \overline{M}^*}) - \delta\overline{Z}^*. \tag{2.37}$$

We firstly start with semi-trivial steady states. Let suppose $\overline{P}^* = 0$, then $\overline{M}^*$ is zero from Eq (2.36) and $\overline{Z}^*$ is zero from Eq (2.37). If we assume $\overline{M}^* = 0$ and substitute it to Eq (2.37), then we find $\overline{P}^* = \frac{\delta k_2}{\epsilon\beta_1 - \delta}$ by cancelling positive common factors $\overline{Z}^*$. Later, we substitute known $\overline{M}^*$ and $\overline{P}^*$ to Eq (2.36) and obtain $\overline{Z}^* = (r(1 - \frac{\overline{P}^*}{K}) - m)\frac{k_2 + \overline{P}^*}{\beta_1}$. Lastly, if we say $\overline{Z}^* = 0$, then we get $\overline{P}^* = \frac{k_1\mu}{\gamma g - \mu}$ from (2.36) and then $\overline{M}^* = (r(1 - \frac{\overline{P}^*}{K}) - m)\frac{k_1 + \overline{P}^*}{g}$ from (2.35). To find non-trivial steady states, the common factors $\overline{P}^*$ in Eq (2.35), $\overline{M}^*$ in Eq (2.36) and $\overline{Z}^*$ in Eq (2.37) are cancelled and the new system becomes such that

$$0 = r(1 - \frac{\overline{P^*}}{K}) - m - \frac{g}{k_1 + \overline{P^*}}\overline{M^*} - \frac{\beta_1}{k_2 + \overline{P}^* + \overline{M}^*}\overline{Z}^*, \tag{2.38}$$

$$0 = \gamma\frac{g\overline{P}^*}{k_1 + \overline{P}^*} - \mu - \frac{\beta_2}{k_2 + \overline{P}^* + \overline{M}^*}\overline{Z}^*, \tag{2.39}$$

$$0 = \epsilon(\beta_1\frac{\overline{P}^*}{k_2 + \overline{P}^* + \overline{M}^*} + \beta_2\frac{\overline{M}^*}{k_2 + \overline{P}^* + \overline{M}^*}) - \delta. \tag{2.40}$$

First, Let's rearrange Eq (2.40) to make it look simpler.

$$\begin{aligned} 0 &= \epsilon\beta_1\overline{P}^* + \epsilon\beta_2\overline{P}^* - \delta k_2 - \delta\overline{P}^* - \delta\overline{M}^* \\ &= (\epsilon\beta_1 - \delta)\overline{P}^* + (\epsilon\beta_2 - \delta)\overline{P}^* - \delta k_2, \end{aligned} \tag{2.41}$$

Secondly, multiplying Eq (2.38) by β_2 and Eq (2.39) by $-\beta_1$, summing up them

$$0 = \beta_2 r(1-\frac{\overline{P}^*}{K}) - \beta_2 m - \frac{\beta_2 g\overline{M}^*}{k_1+\overline{P}^*} - \beta_1\gamma\frac{g\overline{P}^*}{k_1+\overline{P}^*} - \beta_1\mu$$

$$\Rightarrow \quad \overline{M}^* = a\overline{P}^{*2} + b\overline{P}^* + c, \tag{2.42}$$

where $a = -\frac{r}{gK}$, $b = \frac{1}{\beta_2 gK}(-\beta_2 rk_1 - \beta_1\gamma gK + \beta_2 rK - \beta_2 mK + \beta_1\mu K)$ and $c = \frac{1}{\beta_2 gK}(\beta_2 rKk_1 - \beta_2 mKk_1 + \beta_1\mu Kk_1)$ then we substitute (2.42) to (2.41)

$$\begin{aligned} 0 =& (\epsilon\beta_1 - \delta)\overline{P}^* + (\epsilon\beta_2 - \delta)(a\overline{P}^{*2} + b\overline{P}^* + c) - \delta k_2 \\ 0 =& (\epsilon\beta_2 - \delta)a\overline{P}^{*2} + (\epsilon\beta_1 - \delta + (\epsilon\beta_2 - \delta)b)\overline{P}^* + (\epsilon\beta_2 - \delta)c - \delta k_2 \end{aligned}$$

we can call the equation such as

$$A\overline{P}^{*2} + B\overline{P}^* + C = 0 \qquad \Rightarrow \qquad \overline{P}^* = \frac{-B \mp \sqrt{B^2 - 4AC}}{2A}, \tag{2.43}$$

where $A = (\epsilon\beta_2 - \delta)a$, $B = (\epsilon\beta_1 - \delta + (\epsilon\beta_2 - \delta)b)$ and $C = (\epsilon\beta_2 - \delta)c - \delta k_2$. Later, $\overline{M}^*$ and $\overline{Z}^*$ can be found easily from (2.41) and (2.39) respectively as below

$$\overline{M}^* = \frac{\delta k_2}{\epsilon\beta_2 - \delta} - \frac{(\epsilon\beta_1 - \delta)\overline{P}^*}{\epsilon\beta_2 - \delta}, \tag{2.44}$$

$$\overline{Z}^* = (\gamma\frac{g\overline{P}^*}{k_1+\overline{P}^*} - \mu)\frac{k_2 + \overline{P}^* + \overline{M}^*}{\beta_2}, \tag{2.45}$$

Therefore, we have non-trivial steady state $(\overline{P}^*, \overline{M}^*, \overline{Z}^*)$ as in (2.43), (2.44), and (2.45) if they are positive. Existence of steady states and their stabilities depend on parameters. According to the values of parameters in Table 2.1, $(\overline{P}^*, \overline{M}^*, \overline{Z}^*)$ have two values: one of them is $(-3.313, 4.404, -21.672)$ and the other one is $(9023.3, -9022.2, 95.8)$. Thus, there doesn't exist equilibrium state for the fixed parameter values. There are some non-trivial steady states for small values of parameter r as seen in Table 2.3 and they are unstable.

Table 2.3: $(\overline{P}^*,\ \overline{M}^*,\ \overline{Z}^*)$ and λ of the steady states for variable values of parameter r and fixed values of all other parameters in non-spatial Model II.

r	$(\overline{P}^*, \overline{M}^*, \overline{Z}^*)$	λ	stability
0.1	$(1.038,\ 0.053,\ 2.661)$	$(0.003,\ 0.0005 \pm 0.051i)$	unstable
	$(107580,\ -107580,\ 0.001)$	–	–
0.2	$(0.654,\ 0.437,\ 0.926)$	$(0.001,\ 0.002 \pm 0.106i)$	unstable
	$(54779,\ -54778,\ 96)$	–	–
0.4	$(-0.074,\ 1.165,\ -2.545)$	–	–
	$(28380,\ -28379,\ 96)$	–	–
0.6	$(-0.752,\ 1.843,\ -6.018)$	–	–
	$(19581,\ -19580,\ 96)$	–	–
0.8	$(-1.386,\ 2.477,\ -9.494)$	–	–
	$(15181,\ -15180,\ 96)$	–	–
1	$(-1.980,\ 3.071,\ -12.971)$	–	
	$(12542,\ -12541,\ 96)$	–	–
1.2	$(-2.538,\ 3.629,\ -16.451)$	–	–
	$(10783,\ -10781,\ 96)$	–	–
1.5	$(-3.313,\ 4.404,\ -21.672)$	–	–
	$(9023.3,\ -9022.2,\ 95.8)$	–	–

$$J^* = \begin{bmatrix} r - \frac{2r\overline{P}^*}{K} - m - \frac{g\overline{M}^* k_1}{(k_1+\overline{P}^*)^2} - \frac{\beta_1 \overline{Z}^*(k_2+\overline{M}^*)}{(K_2)^2} & -\frac{g\overline{P}^*}{k_1+\overline{P}^*} + \frac{\beta_1 \overline{P}^* \overline{Z}^*}{(K_1)^2} & -\frac{\beta_1 \overline{P}^*}{K_2} \\ \frac{\gamma \overline{M}^* g k_1}{(k_1+\overline{P}^*)^2} + \frac{\beta_2 \overline{M}^* \overline{Z}^*}{(K_2)^2} & \frac{\gamma g \overline{P}^*}{k_1+\overline{P}^*} - \mu - \frac{\beta_2 \overline{Z}^* k_2 + \overline{P}^*}{(K_2)^2} & -\frac{\beta_2 \overline{M}^*}{K_2} \\ \epsilon \overline{Z}^* \frac{\beta_1 k_2 + (\beta_1 - \beta_2)\overline{M}^*}{(K_2)^2} & \epsilon \overline{Z}^* \frac{\beta_2 k_2 + (\beta_2 - \beta_1)\overline{P}^*}{(K_2)^2} & 0 \end{bmatrix}$$

where $K_1 = k_1 + \overline{P}^* + \overline{M}^*$ and $K_2 = k_2 + \overline{P}^* + \overline{M}^*$

Non-spatial model III: omnivorus copepods having functional response with switching

Substituting the KTW functional response to (2.12), we obtain non-spatial Model III. Semi-trivial steady states are the same as that of non-spatial Model II. Therefore, we just look non-trivial steady states. For this we cancel some common

factors (as each equilibrium is assumed positive) as below:

$$
\begin{aligned}
0 &= r(1-\frac{\overline{P}^*}{K}) - m - \frac{g}{k_1+\overline{P}^*}\overline{M}^* - \beta_1 \frac{\overline{P}^*}{\overline{P}^{*2}+\overline{M}^{*2}} \frac{\overline{P}^*+\overline{M}^*}{k_2+\overline{P}^*+\overline{M}^*}\overline{Z}^*, \\
0 &= \gamma \frac{g\overline{P}^*}{k_1+\overline{P}^*} - \mu - \beta_2 \frac{\overline{M}^*}{\overline{P}^{*2}+\overline{M}^{*2}} \frac{\overline{P}^*+\overline{M}^*}{k_2+\overline{P}^*+\overline{M}^*}\overline{Z}^*, \\
0 &= \epsilon(\beta_1 \frac{\overline{P}^{*2}}{\overline{P}^{*2}+\overline{M}^{*2}} \frac{\overline{P}^*+\overline{M}^*}{k_2+\overline{P}^*+\overline{M}^*} + \beta_2 \frac{\overline{M}^{*2}}{\overline{P}^{*2}+\overline{M}^{*2}} \frac{\overline{P}^*+\overline{M}^*}{k_2+\overline{P}^*+\overline{M}^*}) - \delta.
\end{aligned}
\tag{2.46}
$$

The zeros of the system of Eq (2.46) cannot be found analytically and we numerically solved the corresponding system using Newton's method via Matlab. We compute three different roots of the system according to the values of parameters in Table 2.1, but only one of them is positive: $(\overline{P}^*, \overline{M}^*, \overline{Z}^*) = (1.047, 0.044, 61.377)$ which is steady state of the system. The elements of the Jacobian matrix are

below

$$
\begin{aligned}
\frac{\partial F_1}{\partial \overline{P}} =& r - \frac{2\overline{P}^* r}{K} - m - \frac{g\overline{M}^* k_1}{(k_1+\overline{P}^*)^2} - \beta_1 \overline{Z}^* \left(\frac{2\overline{P}^*\overline{M}^{*2}}{(K_3)^2}\frac{\overline{P}^*+\overline{M}^*}{K_2} + \frac{\overline{P}^{*2}}{K_3}\frac{k_2}{K_2^2}\right),\\
\frac{\partial F_1}{\partial \overline{M}} =& -\frac{g\overline{P}^*}{k_1+\overline{P}^*} - \beta_1 \overline{Z}^* \left(-\frac{2\overline{M}^*\overline{P}^{*2}}{(K_3)^2}\frac{\overline{P}^*+\overline{M}^*}{K_2} + \frac{\overline{P}^{*2}}{K_3}\frac{k_2}{K_2^2}\right),\\
\frac{\partial F_1}{\partial \overline{Z}} =& -\beta_1 \frac{\overline{P}^{*2}}{K_3}\frac{\overline{P}^*+\overline{M}^*}{K_2},\\
\frac{\partial F_2}{\partial P} =& \frac{\gamma\overline{M}^* g k_1}{(k_1+\overline{P}^*)^2} - \beta_2 \overline{Z}^* \left(-\frac{2\overline{P}^*\overline{M}^{*2}}{(K_3)^2}\frac{\overline{P}^*+\overline{M}^*}{K_2} + \frac{\overline{M}^{*2}}{K_3}\frac{k_2}{K_2^2}\right),\\
\frac{\partial F_2}{\partial \overline{M}} =& \frac{\gamma g\overline{P}^*}{k_1+\overline{P}^*} - \mu - \beta_2 \overline{Z}^* \left(\frac{2\overline{M}^*\overline{P}^{*2}}{(K_3)^2}\frac{\overline{P}^*+\overline{M}^*}{K_2} + \frac{\overline{M}^{*2}}{K_3}\frac{k_2}{K_2^2}\right),\\
\frac{\partial F_2}{\partial \overline{Z}} =& -\beta_2 \frac{\overline{M}^{*2}}{K_3}\frac{\overline{P}^*+\overline{M}^*}{K_2},\\
\frac{\partial F_3}{\partial \overline{P}} =& \epsilon \overline{Z}^* \left(\frac{2\beta_1\overline{P}^*\overline{M}^{*2} - 2\beta_2\overline{P}^*\overline{M}^{*2}}{(K_3)^2}\frac{\overline{P}^*+\overline{M}^*}{K_2} + \frac{\beta_1\overline{P}^{*2}+\beta_2\overline{M}^{*2}}{K_3}\frac{k_2}{K_2^2}\right),\\
\frac{\partial F_3}{\partial \overline{M}} =& \epsilon \overline{Z}^* \left(\frac{2\beta_2\overline{M}^*\overline{P}^{*2} - 2\beta_1\overline{M}^*\overline{P}^{*2}}{(K_3)^2}\frac{\overline{P}^*+\overline{M}^*}{K_2} + \frac{\beta_1\overline{P}^{*2}+\beta_2\overline{M}^{*2}}{K_3}\frac{k_2}{K_2^2}\right),\\
\frac{\partial F_3}{\partial \overline{Z}} =& 0,
\end{aligned}
\tag{2.47}
$$

where $K_2 = k_2 + \overline{P}^* + \overline{M}^*$, $K_3 = \overline{P}^{*2} + \overline{M}^{*2}$. The eigenvalues of the Jacobian matrices with regard to the system in (2.47) can be found by being substituted the non-trivial steady state $(\overline{P}^*, \overline{M}^*, \overline{Z}^*)$:

$$
\begin{bmatrix} \lambda_1 \\ \lambda_2 \\ \lambda 3 \end{bmatrix} = \begin{bmatrix} 0.042 - 0.178i \\ 0.042 + 0.178i \\ -0.069 \end{bmatrix}.
$$

The real part of λ_1 and λ_2 are positive ($R(\lambda_{1,2}) > 0$) which means the steady state is unstable. We vary the values of r, K, and ϵ, but there is no stable steady states in non-spatial model.

Table 2.4: $(\overline{P}^*,\ \overline{M}^*,\ \overline{Z}^*)$ and λ of steady states for variable values of parameter r and fixed values of all other parameters in non-spatial Model III.

r	$(\overline{P}^*,\ \overline{M}^*,\ \overline{Z}^*)$	λ	Stability
0.2	-	–	–
0.3	$(0.893,\ 0.196,\ 7.832)$	$(-0.042,\ 0.008 \pm 0.190i)$	unstable
0.4	$(0.943,\ 0.148,\ 12.630)$	$(-0.054,\ 0.017 \pm 0.187i)$	unstable
0.5	$(0.971,\ 0.120,\ 17.216)$	$(-0.060,\ 0.023 \pm 0.185i)$	unstable
0.8	$(1.012,\ 0.079,\ 30.613)$	$(-0.066,\ 0.031 \pm 0.182i)$	unstable
1	$(1.027,\ 0.064,\ 39.437)$	$(-0.067,\ 0.035 \pm 0.181i)$	unstable
1.5	$(1.047,\ 0.044,\ 61.378)$	$(-0.069,\ 0.042 \pm 0.178i)$	unstable

2.3.2 Model I: single resource food chain in space

In model I, stable coexistence of the three species is possible for the default parameter values from Table 2.1. The conversion efficiency of copepods ϵ_M is a key parameter determining the system stability and small changing in ϵ_M affects the dynamics of the system. Variation of the average densities of plankton species are shown in the bifurcation diagrams in Fig 2.2 for variable ϵ_M and other all parameters are fixed ($\epsilon_P = 0.5 \times \epsilon_M$, actually, there is no influence of ϵ_P in Model I since $f_{P_2} = 0$). The shown diagrams are constructed numerically, by plotting averaged population densities over the euphotic zone for large time $t \geqslant 2000$ after the initial transients died out. We set species densities with magnitude smaller than 10^{-5} to zero. The lower bound of ϵ_M and other critical values of parameters are found numerically taking into account the cutting threshold of 10^{-5}.

The bifurcation diagrams say that copepods cannot establish in the system and the phytoplankton density is kept low by microzooplankton grazing at very small ϵ_M ($\epsilon_M < 0.058$). The semi logarithmic plot in Fig 2.2(b) shows clearly that phytoplankton species can survive at low density. The stable semi-trivial steady state is obtained as $(\overline{P}^*, \overline{M}^*, \overline{Z}^*) = (0.4207, 0.9365, 0)$ where $\overline{P}^*$ and $\overline{M}^*$ are spatially average steady states of phytoplankton and microzooplankton as in Fig 2.3(a). Lower values of ϵ_M than the critical values 0.058 is impotence

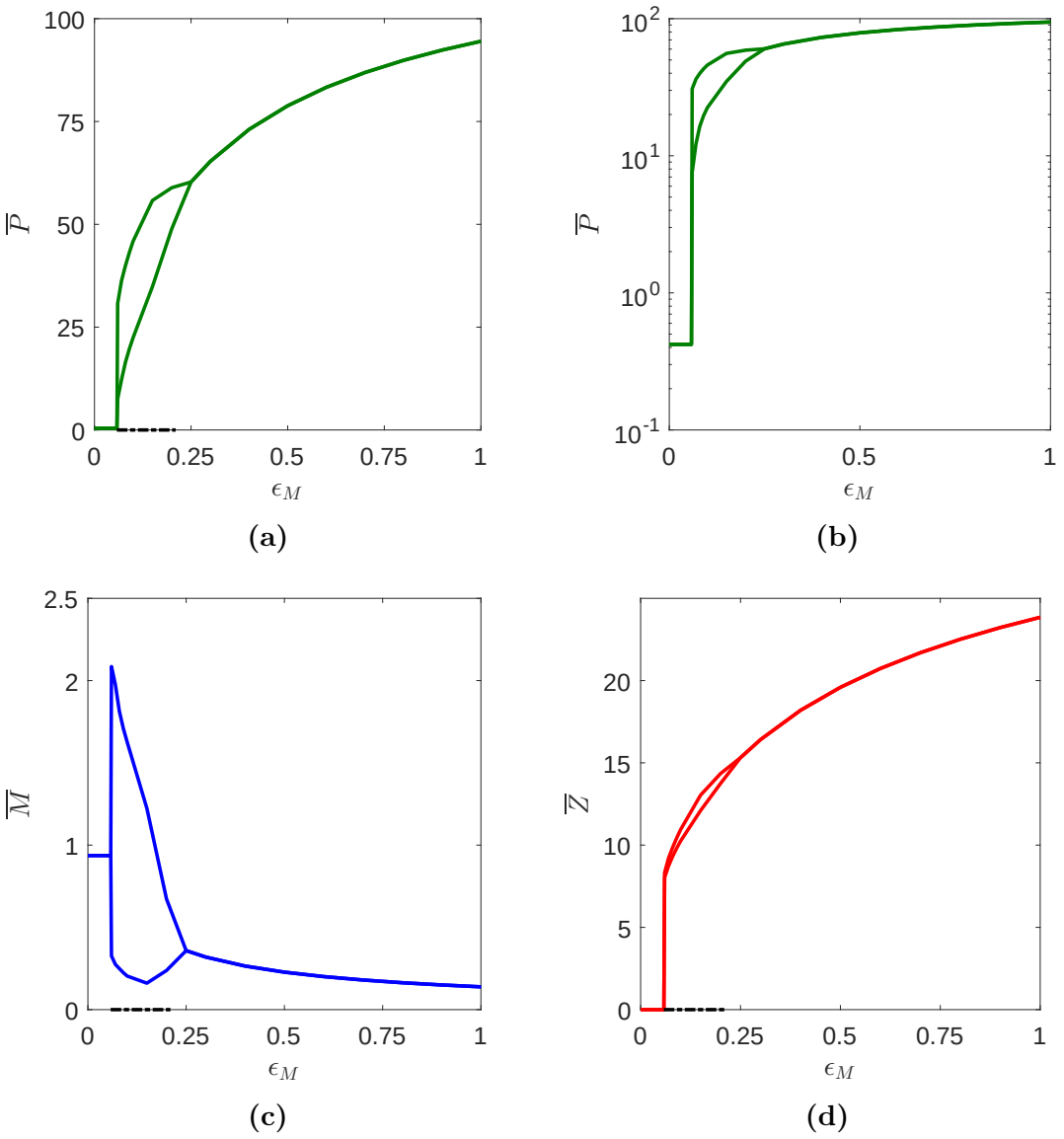

Figure 2.2: (Spatially average densities of phytoplankton (a), microzooplankton (c) and copepods (d) in Model I plotted against microzooplankton conversion efficiency to copepods ϵ_M. The other parameters are given in table 2.1 (fixed values). In the case of periodic oscillations, the maximal and the minimal densities are shown in the figure. The dashed segment on the horizontal axis denotes the range of bistability, where copepods establishment depends on initial density. Small values of ϵ_M leads to death of all copepods.

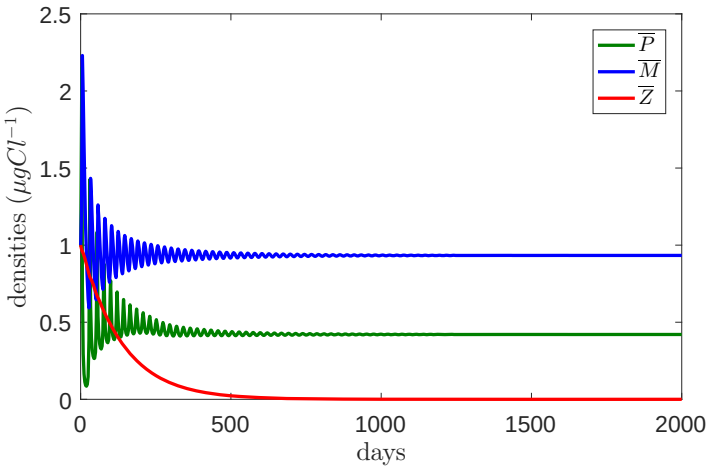

(a)

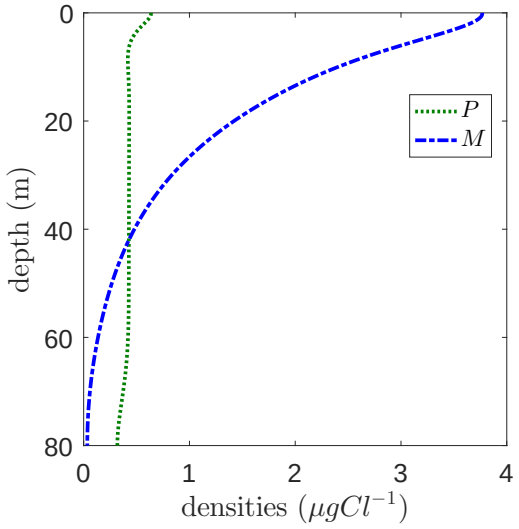

(b)

Figure 2.3: As ϵ_M is 0.05, the initial densities of species are 1 and the other all parameter values are as in Table 2.1. (a): Time series of spatially averaged densities of species in Model I. The average density of Copepods goes zero for small values of ϵ_M. (b): Vertical distribution of phytoplankton and microzooplankton in absence of copepods. Copepods may go extinct in all three models for small values of ϵ_M.

for the densities of phytoplankton and microzooplankton since copepods cannot survive. The vertical distributions of phytoplankton and microzooplankton are as in Fig 2.3(b). Phytoplankton density is very low even in the near surface of water and it doesn't change much with depth. However, microzooplankton density is higher than phytoplankton density near surface until around 40 metres. It decreases with depth and becomes almost zero at base of euphotic zone.

For higher values of ϵ_M than 0.058, the system dynamic depends on initial value of copepods densities until 0.21. Copepods may also go extinct with low initial value of copepods density in this ranges of ϵ_{M}. The system dynamic behaves as in Fig 2.3(a) which is obtained for $\epsilon_M = 0.16$ and the initial values of the copepods density as 1.

Another condition is for large enough initial values of copepods, all plankton species can coexist for larger ϵ_M values than 0.058 which reveals bistability in the system. The densities of species exhibit temporal oscillations for the values of ϵ_M between 0.058 and 0.25. The oscillations and the limit cycle shown in Fig 2.4 for $\epsilon_M = 0.16$ when initial value of copepods density is 14. The steady states of average densities of species in these figures are around 50, 0.62 and 13 μgCL^{-1}, respectively. For larger values of ϵ_M than 0.25, stable coexistence of all species become possible. This is shown with the simulation of average densities of all three trophic levels in Fig 2.5 for $\epsilon_M = 0.4$. In this dynamic, the average densities $\overline{P}$, $\overline{M}$ and $\overline{Z}$ go to around 87, 0.26 and 18, respectively. The spatial distributions of phytoplankton and microzooplankton in euphotic zone across the water column are shown in Fig 2.6 for $\epsilon_M = 0.4$ and the values of other parameters from Table 2.1. One can see from the figure that the local density of the primary producers may achieve very high values near the surface because of abundant sunlight and carbon dioxide in surface although the overall system is stabilized. This signifies an intensive plankton bloom. In this case, microzooplankton can also find plenty of resources (phytoplankton) for grazing.

In the diagram of Fig 2.2(d), larger values of ϵ_M naturally make copepods density higher. Microzooplankton are consumed much more by copepods with increasing their density, so microzooplankton density decreases. This makes phytoplankton density higher as expected. Realistically, conversion efficiency cannot be 1, which means 100% efficiency, but we run theoretically from 0 to 1 to see how it influences the dynamics of species.

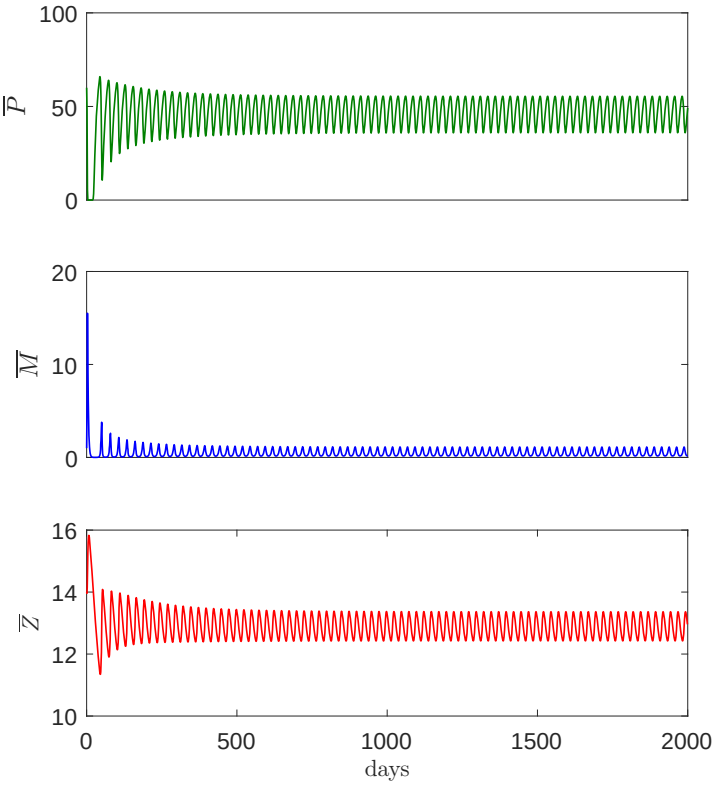

(a)

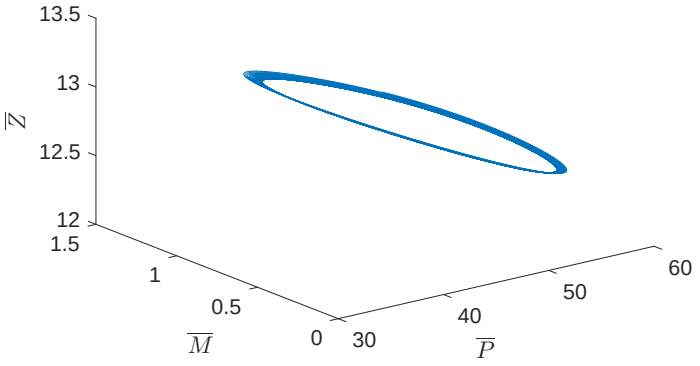

(b)

Figure 2.4: Time series of species (a) shows the temporal oscillations of the average densities of the species for $\epsilon_M = 0.16$ and the initial values are $P(h,1) = 60$, $M(h,1) = 1$ and $\overline{Z}(1) = 14$ in Model I. All the other parameters are as in Table 2.1. The limit cycle is also presented by phase-space trajectory (b).

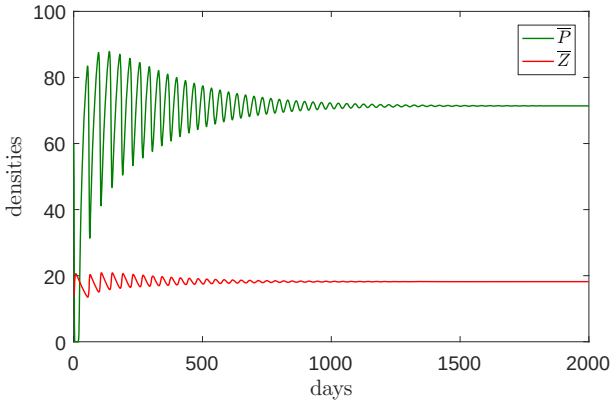

(a)

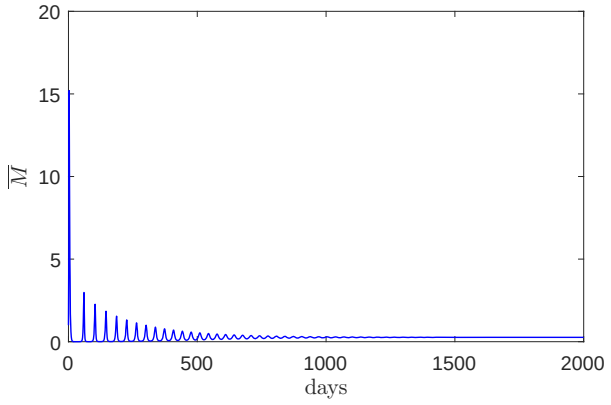

(b)

Figure 2.5: Temporal dynamics of spatially average phytoplankton, microzooplankton and copepod densities respectively in Model I in terms of $\epsilon_M = 0.4$ and the other parameters are fixed in Table 2.1 .

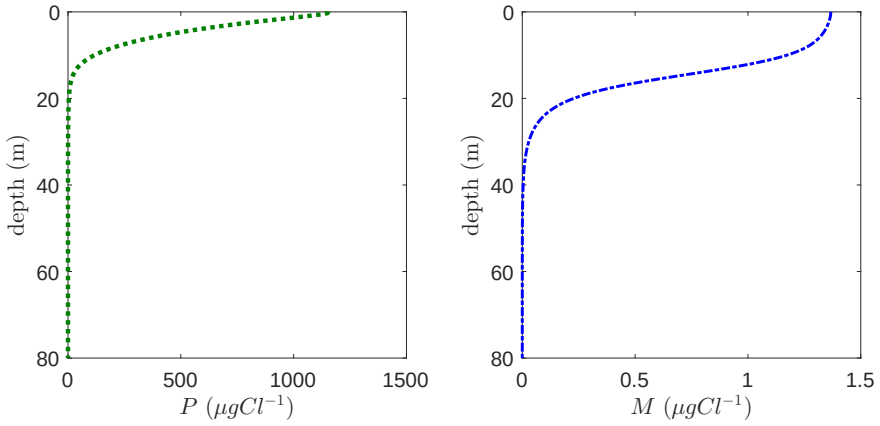

(a) **(b)**

Figure 2.6: Vertical distribution of phytoplankton (a) and microzooplankton (b) for fixed values of parameters and $\epsilon_M = 0.4$ in Model I.

2.3.3 Multiple resource food chain in space

In this section, we examine two models with different feeding habits of the top predator. They are assumed to be omnivorous, with grazing phytoplankton in addition to feeding on microzooplankton. There will be competition between microzooplankton and copepods to graze on phytoplankton associated with this feeding. This competition may cause extinction of some species or decreasing of their densities. Copepods grazing on phytoplankton decreases the density of phytoplankton, thereby, this indirectly affects density of microzooplankton.

Model II: omnivorous copepods with a non-switching functional response

For Model 2.1 with the functional responses 2.6, the time series of average densities of species in Fig 2.7(a),(b) shows that phytoplankton and copepods can survive, but microzooplankton go extinct for the fixed parameter values as in Table 2.1 and $2\epsilon_P = \epsilon_M = 0.7$. We see here that the densities of species are much lower than in the previous model. Especially, the steady state of average density of phytoplankton decreases to 0.6 μgCL^{-1} from 70 μgCL^{-1} and the microzooplankton density goes zero. Vertical distribution of phytoplankton is also presented by Fig 2.7(c). It shows each level steady states of phytoplankton. The surface density of phytoplankton is around 2 μgCL^{-1} and it decreases to zero with depth. On the other hand, we ignore vertical distribution of microzooplankton since the density is too low. The distribution of copepods follows that of only P since there is no microzooplankton.

Actually, we found that the coexistence of the three trophic levels to be very restricted. Variation of the copepods conversion efficiency shows that the coexistence of all species is possible only for some very small values of ϵ_M. This small range is shown by the bifurcation diagram in Fig 2.8. Notice that we usually consider that ϵ_P is half of ϵ_M. At low ϵ_M, copepods cannot get established in the

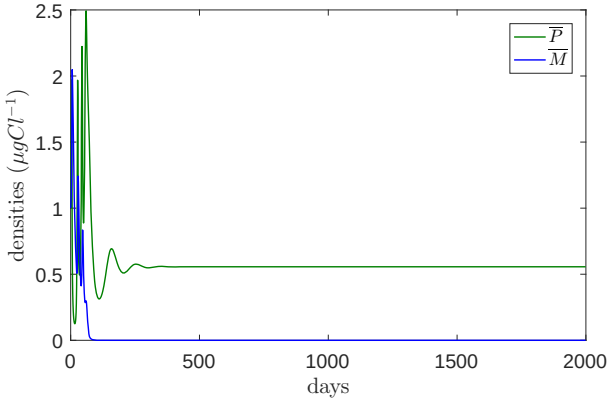

(a)

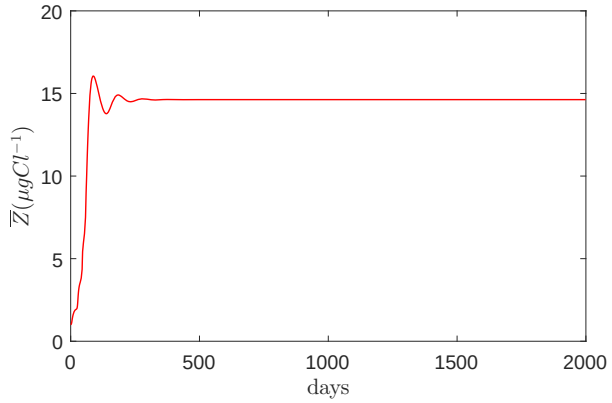

(b)

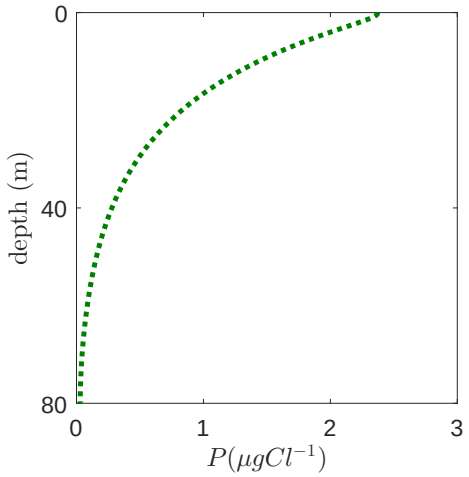

(c)

Figure 2.7: (a),(b): The average densities of phytoplankton (green line) and micro-zooplankton (blue line) in (a) and copepods in (b) across 2000 days show that the intermediate grazer (M) cannot survive in Model II. (c): The vertical distribution of phytoplankton is with depth of water. The parameters are fixed as in the table 2.1 and $\epsilon_M = 0.7$. The copepods have the functional response with no switching

system and the primary production is controlled by microzooplankton as Model I and Fig 2.3(a). The corresponding vertical distributions of the species are shown in Fig 2.3(b) which is same as Model I.

The model also exhibits a bi-stability (i.e. the coexistence of two stable equi-

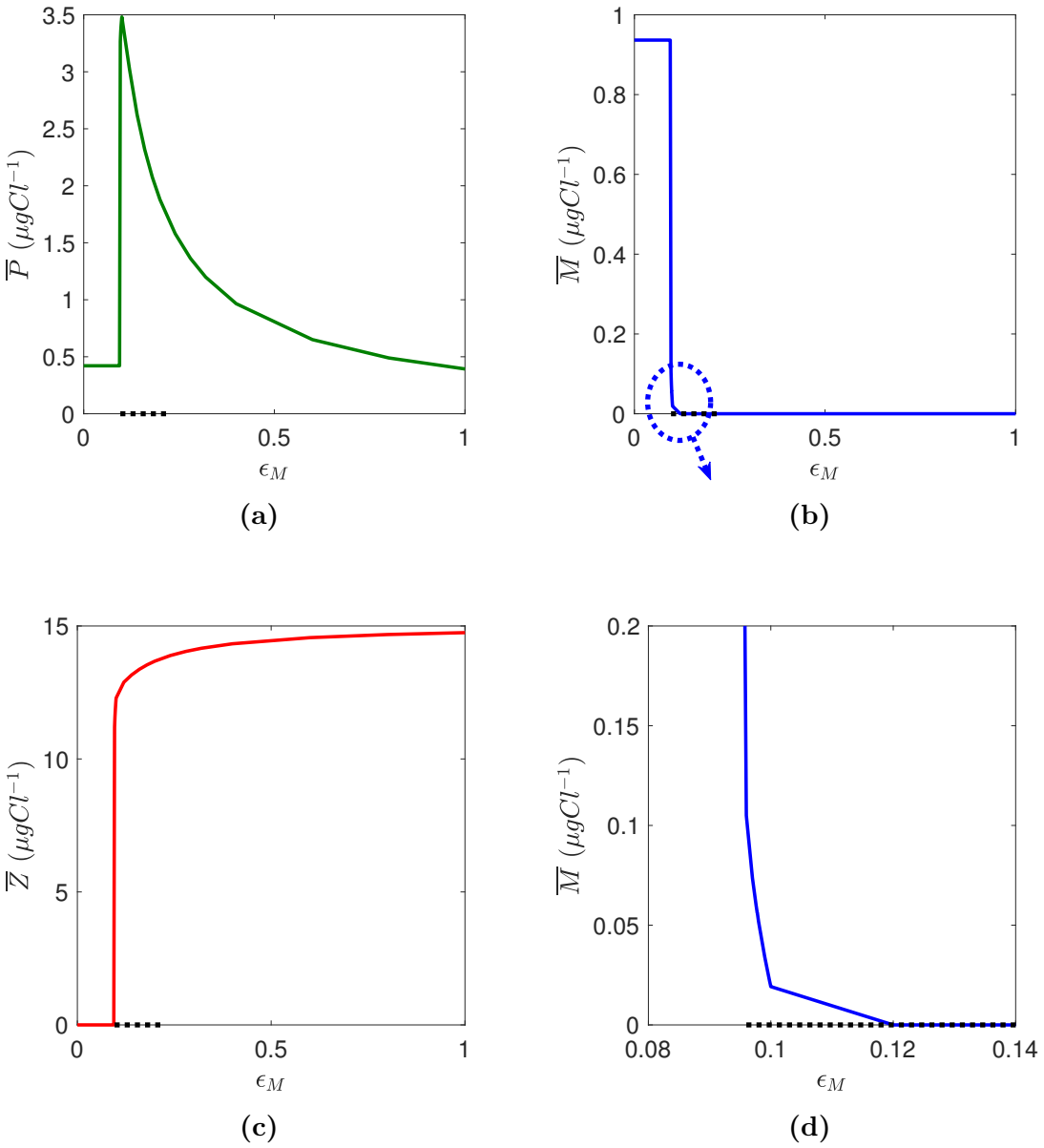

Figure 2.8: Spatially average densities of phytoplankton (a), microzooplankton (b) and copepods (c) in Model II are plotted against conversion efficiency of microzooplankton to copepods ϵ_M. Diagram (d) is a zoom of diagram (b). $\epsilon_P = 0.5\epsilon_M$ and the other all parameters are given in Table 2.1. The dashed segment on the horizontal axis denotes the range of bistability, where copepods establishment depends on initial density.

librium states) in the values of ϵ_{M} between 0.096 and 0.22 depending on the initial values of species. The range of ϵ_{M} is shown by the thick black dot line in the same figure. The system exhibits two different dynamical regimes for this interval of the parameter. One of them is as shown in the bifurcation diagrams for initial densities of copepods higher than 12. The second dynamical regime is possible for low initial densities of copepods, e.g. $\overline{Z}_0 = 1\ \mu\mathrm{gCL}^{-1}$. In this case, copepods cannot survive for the mentioned range of ϵ_{M}. The dynamics of system become mono-stable for the smaller ϵ_{M} than 0.096.

The coexistence of all three plankton species is possible within only small range of parameters centred at $\epsilon_M = 0.11$ on the interval between 0.094 and 0.12 (see Figs 2.8(b),(d)). Small increase or decrease in the parameter values will result in the extinction of either microzooplankton or copepods. Notice here that the initial values of species are also important to obtain coexistence of all species. To obtain coexistence for all species, we select very small initial values of microzooplankton as 0.2 and large initial values of copepods as 12. The spatial average densities of the species over time are shown in Figs 2.9(a),(b) for fixed parameters and critical values of ϵ_M and ϵ_P ($\epsilon_M = 0.1 = 2\epsilon_P$). The figure shows that the average density of microzooplankton is very low where the coexistence is possible for all species. The vertical spatial distribution of phytoplankton and microzooplankton are presented in Figs 2.9(c),(d). The corresponding ideal free distribution of copepods is presented in Fig 2.9(e).

Larger values of ϵ_M than 0.12 results in the extinction of the intermediate trophic level while the primary producer and the top predator can survive in the long term (Microzooplankton lose the competition against copepods). Indeed, there is no influence of ϵ_M after dying microzooplankton completely. However, ϵ_P is also variable in the bifurcation diagram since $\epsilon_M = 0.5\epsilon_P$ as we mentioned above. The type of dynamics is the same as in Fig 2.7 for large conversion efficiency to copepods. The bifurcation diagram demonstrates that increase in $\epsilon_M - \epsilon_P$ supports copepods density and it causes the density of phytoplankton to decrease

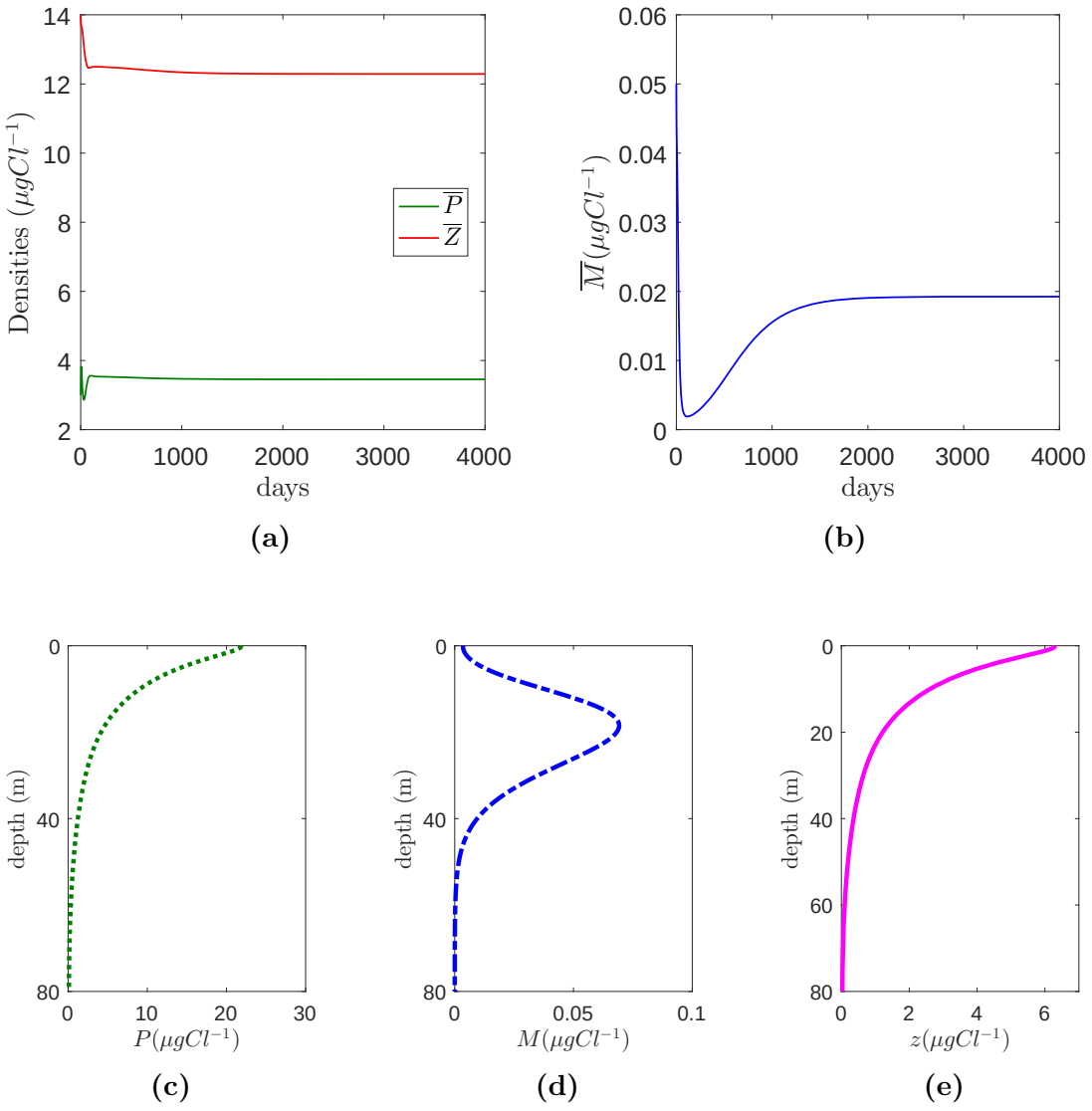

Figure 2.9: Model II analyse for small values of ϵ_M such that $\epsilon_M = 0.1 = 2\epsilon_P$. The other parameter values are fixed in Table 2.1. The average densities of species over time are shown in (a) and (b). Vertical distribution of phytoplankton and microzooplankton are shown in (c), (d). (e) shows the relative distribution of copepods.

for $\epsilon_M > 0.12$.

On the other hand, a particular interesting feature here is in the vertical profile of microzooplankton, with a maximum density at h = 18m in Fig 2.9(d), whereas the density of phytoplankton decreases monotonously with depth in Fig 2.9(c). This is because copepods density (predator and competitor for microzooplankton) is very high in near the surface due to high concentration of phytoplankton. The

vertical distribution followed by copepods is in Fig 2.9(e). The grazing pressure by copepods decreases with depth by decreasing in their own density due to decrease in phytoplankton density. Thus, microzooplankton can survive a little bit deep of water. Secondly, phytoplankton (resource of microzooplankton) don't exist much in deep of water. Therefore, microzooplankton find more appropriate condition at some intermediate sea level instead of surface or deep of water.

To verify that omnivorous top predator largely hinders the coexistence of all species in the given tri-trophic food web, we have constructed a set of bifurcation diagrams in respect to variable copepods grazing (β_1) and predation (β_2) coefficient in the range between 0.6 and 1.4 for both parametes. The diagrams have been constructed for $\epsilon_M = 0.1$, 0.12, 0.14, 0.2 and $\epsilon_P = \epsilon_M/2$ in Fig 2.10.

One can see that the coexistence of all species in the given tri-trophic levels (denoted by green circle in Fig 2.10) is only possible within a rather narrow domain in the (β_1, β_2) plane. Otherwise, a small fluctuation in parameters would eventually result in extinction of a trophic level, either the intermediate or the top predator. According to those diagrams, copepods predation efficiency is inversely proportional to copepods predation rate to obtain coexistence. If both parameters increase, then the density of copepods increases faster. Conversely, copepods cannot survive for both parameters is low. For larger values of ϵ_M than 0.24, microozoplankton die out for any condition.

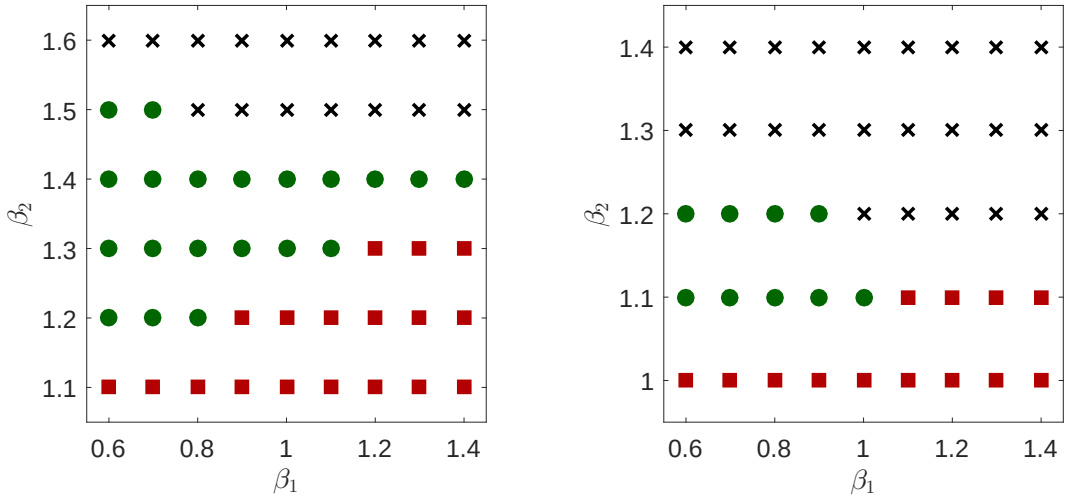

(a) $\epsilon_M = 0.1$

(b) $\epsilon_M = 0.12$

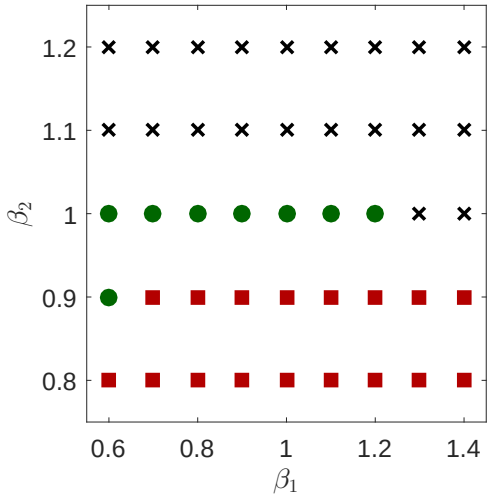

(c) $\epsilon_M = 0.14$

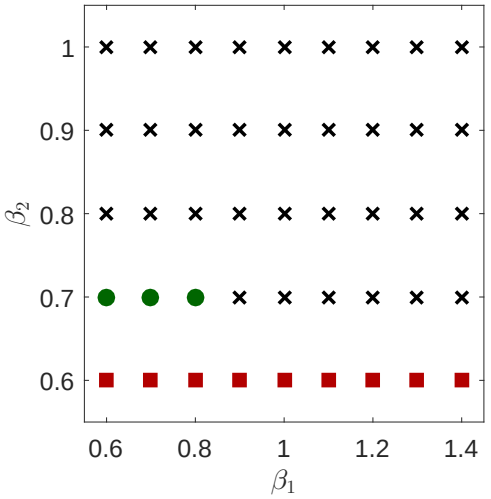

(d) $\epsilon_M = 0.2$

Figure 2.10: Bifurcation diagrams in the β_1 - β_2 plane show the outcome of interaction between the trophic levels for values $\epsilon_M = 0.1,\ 0.12,\ 0.14$ and 0.2 respectively. $\epsilon_P = 0.5\epsilon_M$ and the other all parameters are fixed in Table 2.1. Different coexistences are shown by different symbols. Green circles shows the coexistence of all species. Crosses correspond to the coexistence of phytoplankton and copepods, with microzooplankton being extinct. Red squares denote the coexistence of phytoplankton and microzooplankton, with copepods being extinct.

Model III: omnivorous copepods with a functional response with switching

In Model III, the coexistence of all three trophic levels is restored where the copepods are omnivorous with active prey switching. According to the fixed values of parameters in Table 2.1 and $\epsilon_M = 0.7$ ($\epsilon_P = 0.5\epsilon_M$), the spatially average densities of species and phase-space trajectory are shown in Fig 2.11. The traject-

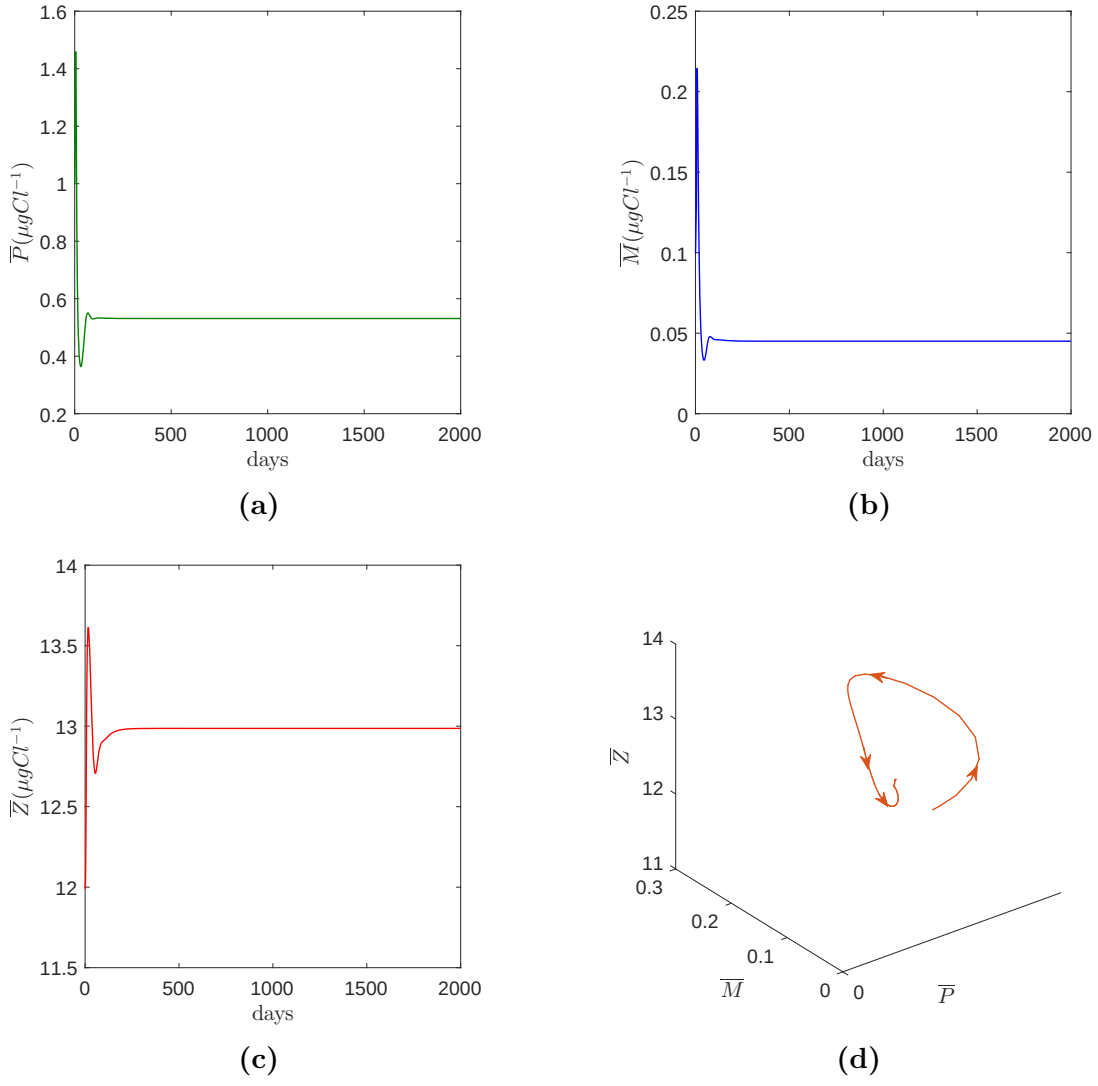

Figure 2.11: (a),(b) and (c) show the average densities of phytoplankton, microzooplankton and copepods across 2000 days in Model III, respectively. (d) shows phase-space trajectory of average densities. Coexistence of the all species is possible with the fixed parameters in Table 2.1 and $\epsilon_M = 0.7$.

ory goes the spatially average steady state $(0.476, 0.033, 13.336)$ in Fig 2.11(d). High initial values of copepods makes the densities of the other two species almost zero for around 500 days. Then, they rise and keep the same stationary states as above. The vertical distribution of primary producer shows us in Fig 2.12 that phytoplankton densities are interestingly much lower near the surface as compared to Model I since copepods graze on them in addition to microzooplankton.

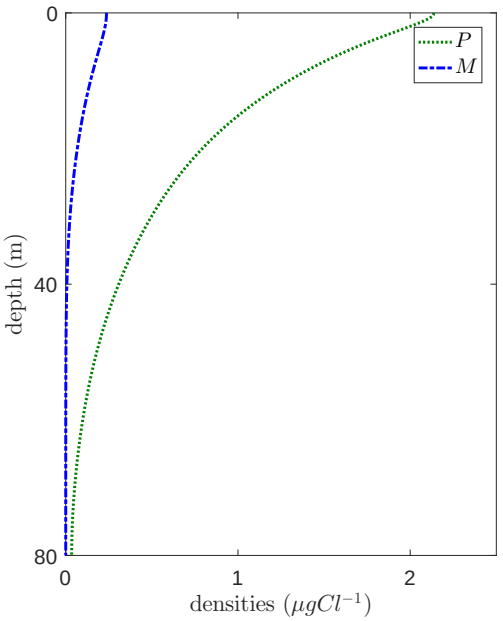

Figure 2.12: Vertical distribution of phytoplankton and microzooplankton densities in Model III are shown for $\epsilon_M = 0.7 = 2\epsilon_P$ and the other parameters as given by the fixed parameters in Table 2.1.

A Typical bifurcation diagram is shown in Fig 2.13 for variable ϵ_M where $\epsilon_P = 0.5\epsilon_M$. Copepods go extinct for the smaller values of ϵ_M than 0.17 while phytoplankton and microzooplankton are able to stably coexist. In that case, we obtain the same vertical distribution with no copepods dynamics in Fig 2.3(b) of the previous model.

In the case where ϵ_M is large enough ($\epsilon_M > 0.17$), it allows the copepods to survive and the coexistence for all species becomes possible in a stable mode. There is no oscillation for any values of ϵ_M. Copepods show logarithmic growth whereas phytoplankton and microzooplankton decrease exponentially in increase

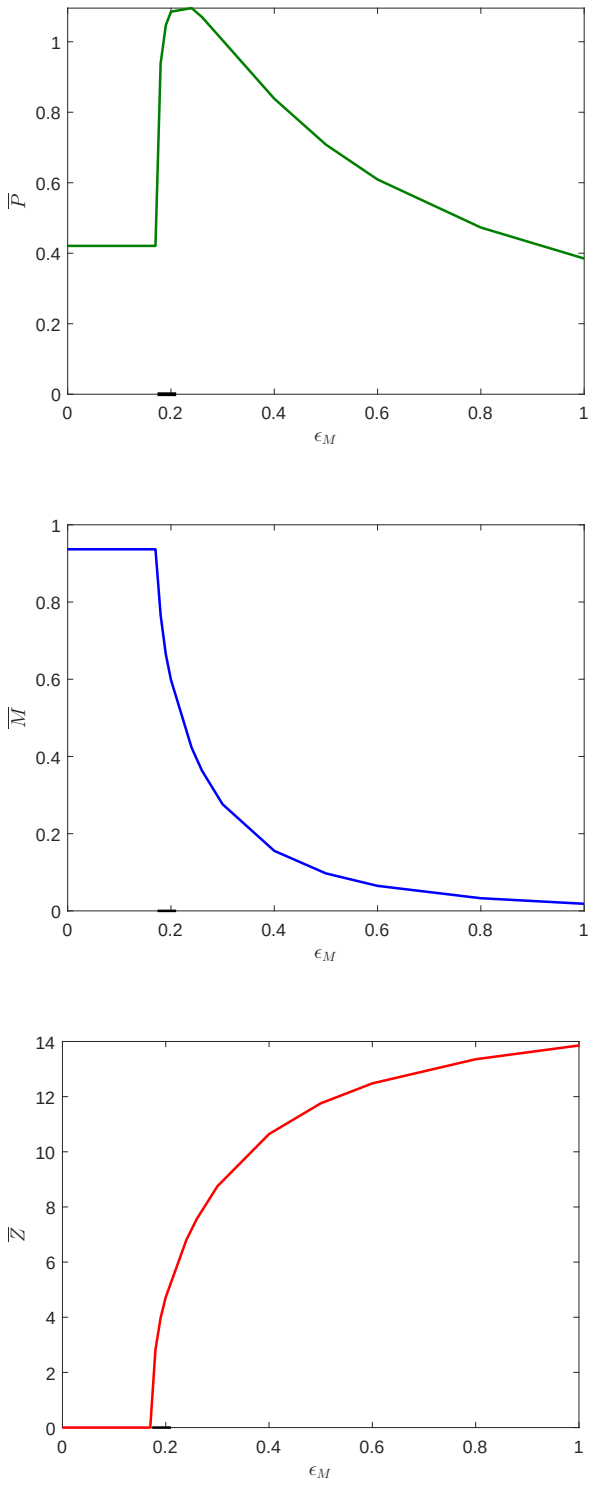

Figure 2.13: Spatially average densities of phytoplankton, microzooplankton and copepods for Model III are respectively plotted against the copepods conversion efficiency ϵ_M ($\epsilon_P = 0.5\epsilon_M$) for the fixed parameters in Table 2.1. The dashed segment on the horizontal axis denotes the range of bistability, where copepods establishment depends on initial density.

ϵ_M values starting with 0.17 to 1 in the diagram. In addition to this, the system has the bi-stabilities which is shown by the black thick line on the horizontal axis of the bifurcation diagram. This says that two distinct dynamics are obtained with the same parameter values by different initial values of species.

Our extensive numerical simulations show that stable coexistence of all species is observed within a wide range of parameters. In particular, variation of (β_1, β_2) within the same ranges as in Fig 2.10 will not result in extinction of any of the trophic level which is showed with bifurcation diagrams in Fig 2.14. It can be seen that increasing copepods grazing rate (β_1) causes to decrease the average densities of the species. On the other hand, increasing copepods predation rate leads to increase of the average densities of phytoplankton and copepods while decrease of the microzooplankton average density.

Similarly, we also explored the effect of the key parameters in Model III on the equilibrium species densities. The average densities of species $\overline{P}$, $\overline{M}$, and $\overline{Z}$ on the parameters δ, ϕ and ω, which are the mortality rate of copepods, the water absorption coefficient and the self-shading coefficient, respectively in Fig 2.15. A gradual increase of δ (due to predation by fish, for instance) would weaken the copepods and decreased their density. Thus, the densities of the two lower level species will increase. For the critical values of δ ($\delta = 0.03$), copepods cannot survive and the model becomes two speices system consisting of the primary producer and intermediate grazer as in Fig 2.3(b). On the other hand, an increase of water absorption rate (e.g. due to turbidity of water) or the self shading coefficient depending on plankton position would result in decreases of the densities of the primary producers. Correspondingly, the densities of microzooplankton and copepods drop. A gradual increase of ϕ and ω decrease the average densities of all species. This behaviour can be explained by the fact that an increase in water absorption or the densities of total species results in a drop of the density of the primary producer, which in turn results in a drop of the density of top predator. Due to a decrease of the trophic pressure exserted by the copepods and

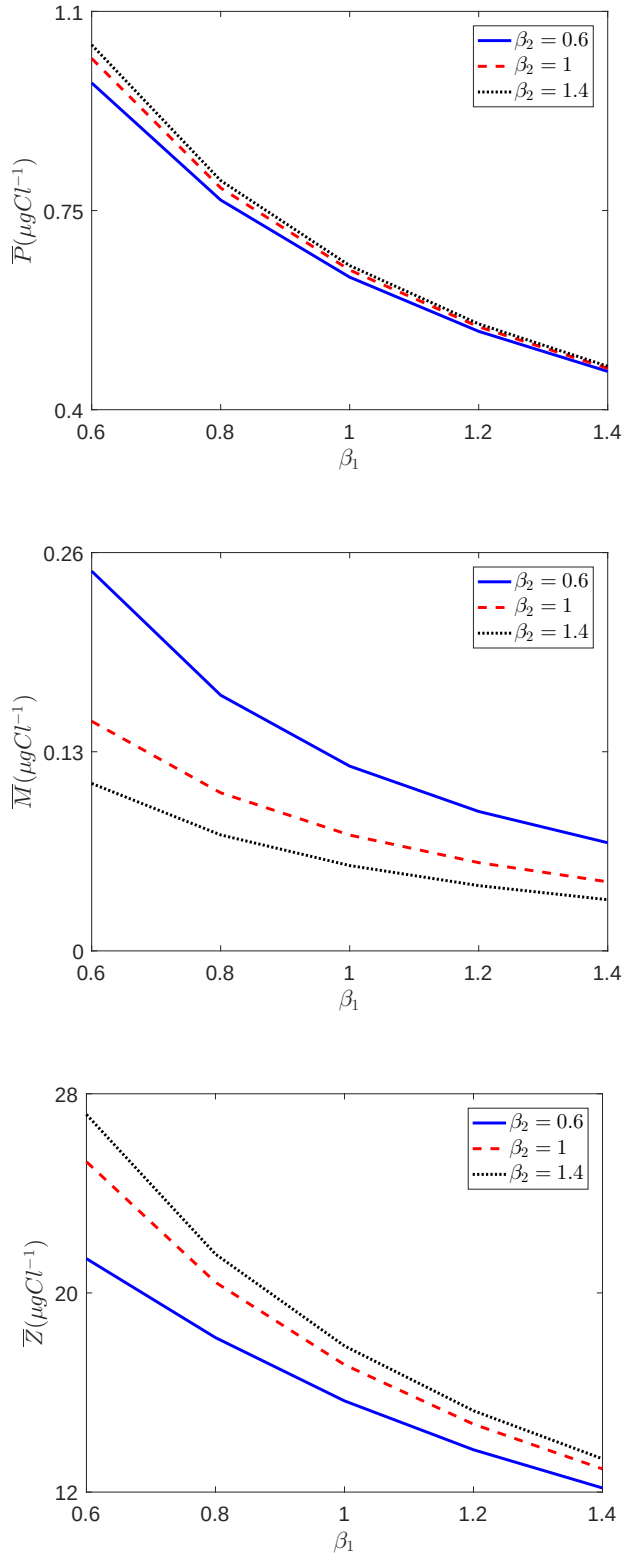

Figure 2.14: The diagrams show the space averaged densities of species for β_1 between 0.6 and 1.4 constructed for different β_2 =0.6, 1, 1.4. All the other parameters are fixed as in Table 2.1.

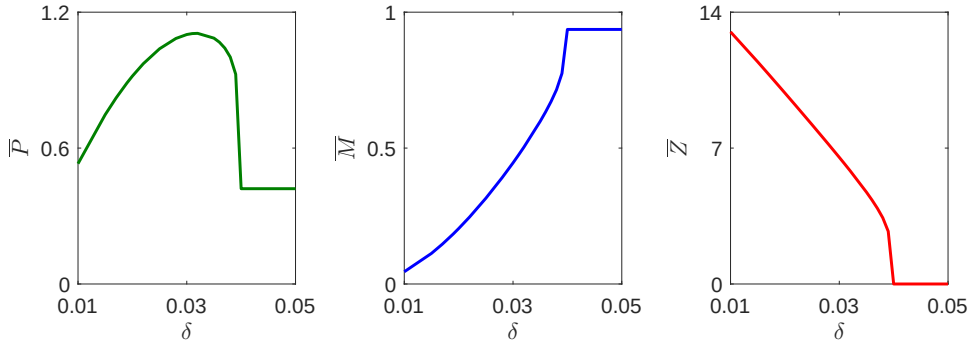

(a)

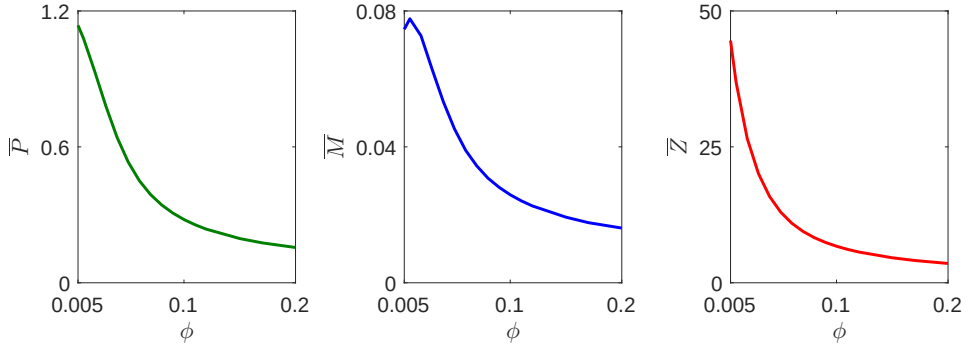

(b)

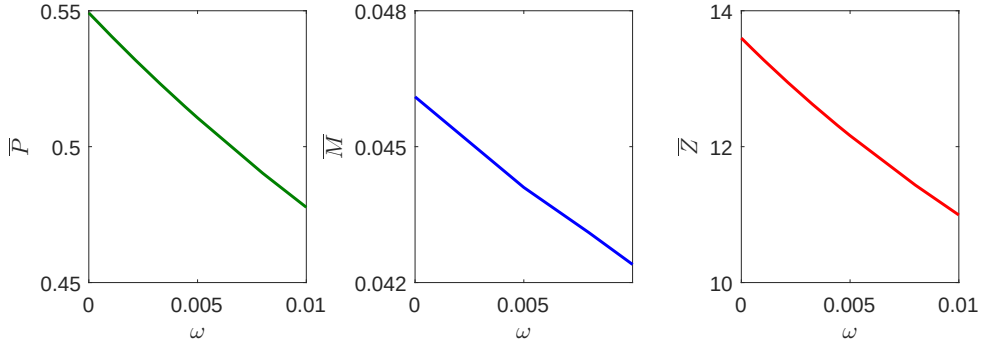

(c)

Figure 2.15: Bifurcation diagrams showing the average densities of species in Model III as functions of key parametes: (a): δ between between 0.01 and 0.05, (b): ϕ between 0.005 and 0.15, (c): ω between 0 and 0.01. The other parameters are fixed as indicated in Table 2.1.

microzooplankton.

2.3.4 Comparison between the functional responses in the spatial model I, II and III

The question of why a particular copepods genera follows a particular type of functional response is fundamental to zooplankton ecology, with several different approaches proposed. For instance, based on the generic principles of evolution theory, one can suggest that the current functional responses are the result of long term natural selection. For instance, a functional response with active switching could be more beneficial for the entire population of copepods than a simple Monod-like (Holling type II) response, and the individuals using the more efficient response should over-compete the other copepod individuals. In this section, we try to gain some preliminary insight into this complicated problem by modelling the outcome of the competition between two copepods species having different types of functional response. That is, we considered the main tri-trophic model (2.1), where copepods population $\overline{Z}$ consists of two subpopulations $\overline{Z}_i$, $\overline{Z}_j$ with different functional responses. We considered the three following combinations:(i) $\overline{Z}_1$ is non-omnivorous and $\overline{Z}_2$ is omnivorous with a non-switching functional response; (ii) $\overline{Z}_1$ is non-omnivorous and $\overline{Z}_3$ is omnivorous having a functional response with switching; (iii) $\overline{Z}_2$ is omnivorous with a non-switching functional response and $\overline{Z}_3$ is omnivorous having a functional response with switching. In each case, we assumed the same half saturation constants and the maximum consumption rates for the functional responses of both subpopulations of copepods.

Numerical simulations in Fig 2.16 show the following competition outcomes. Populations of omnivorous copepods (with or without active switching) always over-compete the population with a single source functional response. Thus, to have a supplementary food source seems to be beneficial for copepods. On the other hand, competition between omnivorous copepods with and without active switching results in the coexistence of both populations. This occurs mainly be-

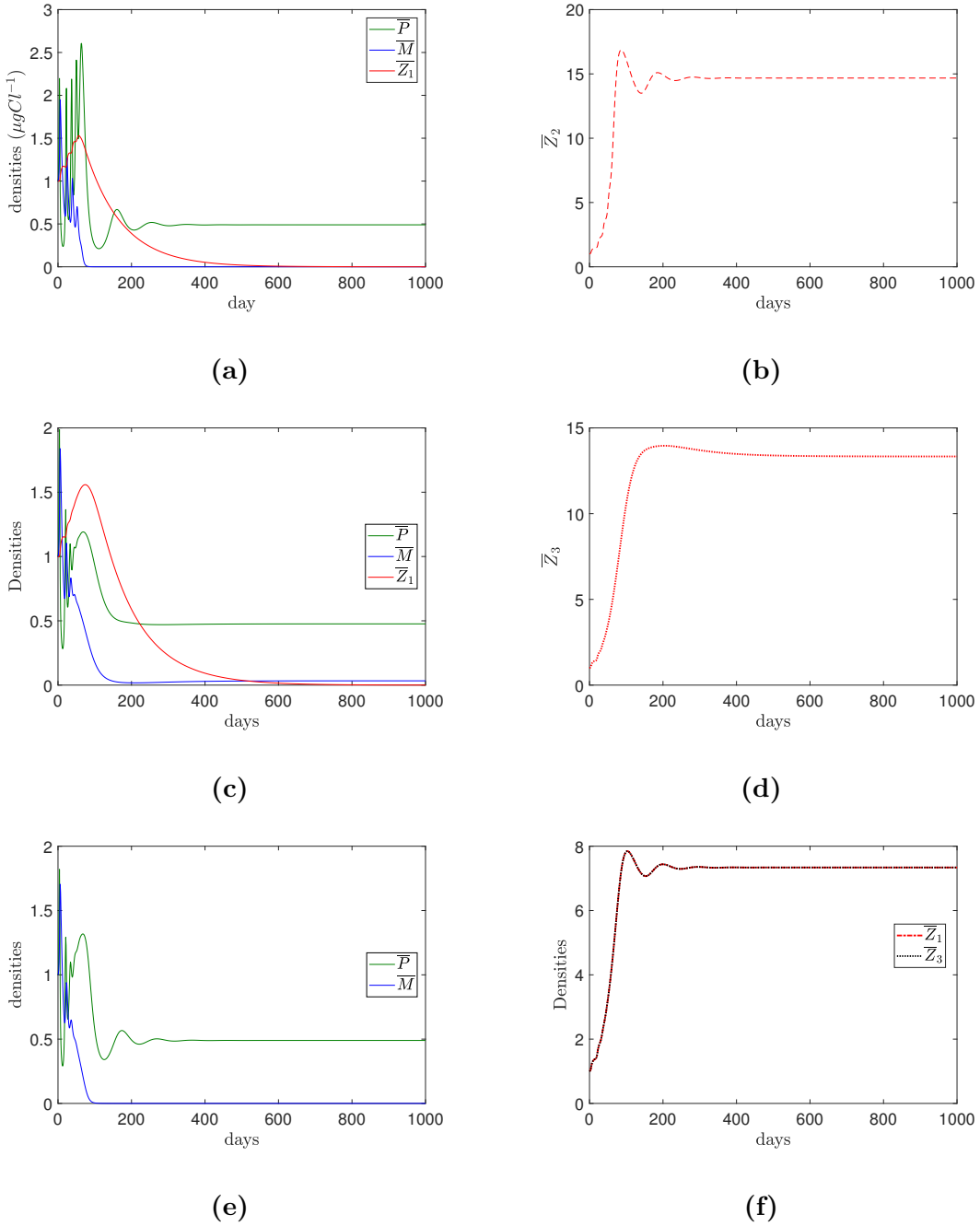

Figure 2.16: The same tri-trophic model 2.1, where the top predator population $\overline{Z}$ consists of two subpopulations with different functional responses such that $\overline{Z}_1$ is carnivorous, $\overline{Z}_2$ is omnivorous with a non-switching functional response and $\overline{Z}_3$ is omnivorous with having a functional response with switching. Competition between the top predators shows between $\overline{Z}_1$ and $\overline{Z}_2$ in (a,b); $\overline{Z}_1$ and $\overline{Z}_3$ in (c,d); $\overline{Z}_2$ and $\overline{Z}_3$ in (e,f) across the time.

cause intensive grazing by the subpopulation with the non switching functional response eradicates the intermediate trophic level (microzooplankton) and the resultant system becomes a two-level one. In the case where the maximal consumption rates are different, the winner will be the subpopulation of the copepods having the largest β_1 and β_2. Thus, our preliminary results indicate that a functional response either with or without switching may be selected. Note that in our simple competition analysis we neglected any potential cost of active switching, and morphological aspects which may not allow certain species to use different strategies. A more thorough analysis should be done elsewhere.

2.4 Summary for chapter 2

Plankton communities possess a very rich and complicated population dynamics which is reflected in the corresponding mathematical models. There exists a large number of publications to solve the paradox of enrichment [99]. The main idea is that the original predator prey model presented by Rosenzweig was too simple and it should be improved by more realistic and adequate features as spatial dimension or/and complicated trophic structure. Here we contribute to the solution of the enrichment paradox.

In this chapter, we revisited the dynamics of a generic tri-trophic plankton model in eutrophic environment. The aim of this chapter was to show the importance of the functional response parameterisation in heteregeneous environment for the plankton dynamics which includes omnivorous copepods. We pay attention to the light gradient for the primary producers with self-shading. Also we consider highly mobile copepods in the vertical direction. Another key point of this chapter is the copepods feeding habits which might be carnivorous (only feeding on microzooplankton) or omnivorous (consuming both intermediate grazers and primary producers).

Our results show that stable coexistence of all species is impossible in a well-mixed system for all three types of functional response parameterisations. This demonstrates that heterogeneity of space is imperative for a successful top-down control and stabilization of the system. However, the spatial model is still not enough for the coexistence for all species including omnivorous top predator. This is proven with Model II which result in one of the grazers (copepods or microzooplankton) dying out. We obtained a stable coexistence for only small range of some parameter values, which are unrealistic (see Fig 2.8 and Fig 2.10). In the case, where copepods are not omnivorous but only feed on microzooplankton, the average steady states of species in the system may exhibit oscillations for some values of parameters Fig 2.5. Also, vertical distributions of lower population levels

show that phytoplankton bloom occurs near the surface (see Fig 2.6).

One of the main findings of this chapter is that the functional response with active switching can provide coexistence of all species in the model in Figs 2.12, 2.11 whereas a Holling type II functional result cannot guarantee such a coexistence. Our results are broadly consistent with empirical observations and this contributes to solving the paradox of enrichment in the plankton system. The coexistence is observed for large parameters ranges but phytoplankton density remain low in Fig 2.13, Fig 2.14 and Fig 2.15. We also found bi-stability for some values of copepods efficiency $\epsilon_{M,P}$, which has not be found earlier. According to this, copepods can survive (for a sufficiently large initial density of copepods) or die out depending on initial values of the densities (see Fig 2.2, Fig 2.8 and Fig 2.13).

Chapter 3

Modelling seasonal dynamics of bacteria-phage interactions with a temperature-dependent lysogeny

3.1 Introduction

Here, we build and explore two non-spatial conceptual mathematical models (ODEs and DDEs based) to describe and predict daily and seasonal dynamics of the size and composition of B. pseudomallei population controlled by its temperature-dependent phages. The models are suggested to mimic host-parasite interactions in the surface water at the top of a typical rice field in South-eastern countries. The practical importance of our modelling follows from the fact that the pathogenic bacteria B. pseudomallei causes a severe disease Melioidosis resulting in a high human mortality: it is thus important to be able to understand the factors controlling the disease and to make some predictions regarding its seasonal dynamics. The parameters for the models are taken from either the experimental researches or from relevant scientific publications which are cited in the text. As a particular ecological case study, we consider seasonal bacteria dynamics in two

endemic regions of Thailand (Sa Kaeo and Nakhon) by using the historic data on temperature variation and intensity of solar ultraviolet radiation. Our simulation results using both models are in agreement with higher risk of melioidosis acquisition during the "warm and wet" season reported in Southeast Asia [7]. We explore the dependence of bacteria-phage dynamics on the key model parameters such as the carrying capacity of the environment (quantifying the degree of eutrophication), the phage burst size and the binding rate of phages to be able to explain the observed difference in the disease acquisition rate for different environmental conditions. Our study emphasizes the role of the interplay between the variation of temperature and UV radiation on the seasonal patterns of bacterial numbers.

A version of this chapter has been submitted in "Scientific Reports" with the title "Temperature-dependent virus lifecycle choices may reveal and predict facets of the biology of opportunistic pathogenic bacteria".

Notations related to chapter 3

t	Time
T	Temperature ($^{\circ}C$)
u	Ultraviolet index
$S(t)$	Density of susceptible bacteria at time t
$I_1(t)$	Density of infected bacteria in lysogenic cyle at time t
$I_2(t)$	Density of infected bacteria in lytic cyle at time t
$N(t)$	Total density of bacteria at time t
$P(t)$	Density of bacteriophage at time t
C	Carrying capacity
$\alpha(T)$	Growth rate of susceptible bacteria at temperature T
$\overline{\alpha}(T)$	Growth rate of lysogenic bacteria at temperature T
$\alpha_{\max}$	Maximum intrinsic birth rate of bacteria
$\lambda_1(T)$	Lysogenic process rate to lytic cycle at temperature T
$\lambda_{1\max}$	Maximum lysogenic process rate (transition rate from lysogenic cycle to lytic cycle)
λ_2	Lysis (bacteria death) constant
K	Phage adsorption rate
K_{S}	Effective per bacteria contact rate
ϵ	Adsorption efficiency
$K_1(T)$	Transition rate from susceptible to lysogenic cycle at temperature T
$K_2(T)$	Transition rate from susceptible to lytic cyle at temperature T
T_0	Optimum temperature for growth and lysis ($^{\circ}C$)
T_1	Optimum transition temperature ($^{\circ}C$)
$\mu(u)$	Mortality rate at UV index u
b	Burst size of phages
τ	Constant delay time

Units

$^{\circ}C$	The degree celsius
ml	Millilitre

Abbreviation

Fig	Figure
Eq	Equation

3.2 The model

In previous mathematical models of the bacteria-phage interaction the main focus was mostly on the lytic type of infection, where penetration of a phage into the bacterial cell would signify an eventual lysis (breaking down of the membrane of a bacterium) and cell death. Moreover, the model parameters were assumed to be constant. In our model we consider the possibility in existence of lytic or lysogenic (the adsorbed phages do not immediately lyse the infected bacteria since they need time for replication) outcome of infection which is determined by the ambient temperature. In other words, there can be either lysogenic or lytic cycles in our model and the temperature is crucial to determine the transitions from susceptible to lysogenic or lytic cycles (Fig 3.1).

We model bacteria-phage interactions in the stagnant water of an agricultural

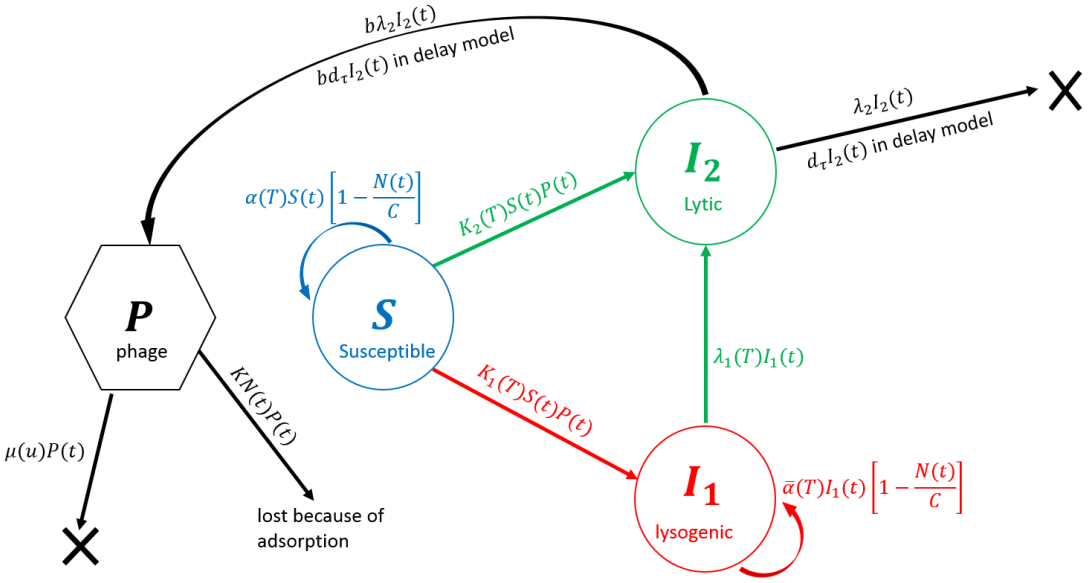

Figure 3.1: Schematic diagram explaining the bacteria-bacteriophage interactions given by **Models I** and **II**. The system consists of four compartments: Susceptible bacteria (S), infected bacteria in lysogenic (I_1) and lytic (I_2) state and the free bacteriophages (P). Arrows show loses in some compartments or transitions between compartments. The function denoted by d_τ in the figure is given by $d_\tau = K_2(T(t-\tau))S(t-\tau)P(t-\tau) - \lambda_1(T(t-\tau))I_1(t-\tau)$

land. We consider the spatially homogeneous environment (for simplicity ignoring bacteria in the soil). The phage-bacteria interaction with two possible infection cycles consists of four main compartments: phage-free bacteria (S) which are healthy but susceptible to phage, infected bacteria through the lysogenic (I_1) or the lytic (I_2) cycles as well as free phage (P). The total density of the host bacterial population is denoted by $N = S + I_1 + I_2$.

The flowchart to illustrate the model is shown in Fig 3.1 for both approaches in terms of reproduction of phages by lysing bacteria. The first one is based on the ordinary differential equations framework where the bacterial cell disintegration is expressed by the multiplication of the lysing coefficient λ_2 and the number of infected bacteria in lytic cycle with the term $\lambda_2 I_2$ in the equation of I_2 [4, 105, 54]. The number of newly released free phages can be calculated by multiplying the lysis term $\lambda_2 I_2$ and the average burst size b which gives $b\lambda_2 I_2$. The overall model equations are

$$\begin{aligned}
\frac{dS(t)}{dt} &= \alpha(T(t))S(t)\left[1 - \frac{N(t)}{C}\right] - K_S S(t)P(t),\\
\frac{dI_1(t)}{dt} &= \overline{\alpha}(T(t))I_1(t)\left[1 - \frac{N(t)}{C}\right] + K_1(T(t))S(t)P(t) - \lambda_1(T(t))I_1(t),\\
\frac{dI_2(t)}{dt} &= K_2(T(t))S(t)P(t) + \lambda_1(T(t))I_1(t) - \lambda_2 I_2(t),\\
\frac{dP(t)}{dt} &= -KN(t)P(t) - \mu(u(t))P(t) + b\lambda_2 I_2(t).
\end{aligned} \tag{3.1}$$

where α and $\overline{\alpha}$ are growth rates of susceptible and lysogenic bacteria; C is carrying capacity of total bacteria; K is phage adsorption rate; K_S is effective per bacteria contact rate; K_1 and K_2 are transition rate from susceptible to lysogenic and lytic cycle, respectively; λ_1 is transition rate from lysogenic to lytic cycle; and μ is mortality rate of phages.

The growth of susceptible phage-free bacteria is described by a standard logistic function parameterisation [55], where $\alpha(T)$ is the maximal per capita growth rate and C is the carrying capacity of the environment. This gives the maximal

possible number of bacteria which the environment can sustain. This number gives the maximal possible number of bacteria which the environment can sustain. We assume that the carrying capacity for a given area is constant and accounts for all other (non-phage) factors affecting B. pseudomallei existence (i.e. the growth rate and phage non-related mortality) in the environment.

Infection of susceptible bacteria results in lysogeny at low temperatures. This means the transition from S to I_2. At low temperatures, the growth rates of both lysogenic ($\overline{\alpha}(T)$) and susceptible bacteria are considered to be logistic with the same carrying capacity. However, it is different for high temperatures due to transition from the lysogenic to the lytic cycle (for details see the next section).

The infection of susceptible bacteria lyses (the bacterial cell are killed by bursting) at high temperatures. Thus, the cells firstly become infected in the lytic cycle and then eventually results in cell lysis and death. This is shown by the transition from S to I_2 in Fig 3.1. Moreover, an increase in temperature would interrupt the normal lysogenic cycle of I_1 and the infection becomes lytic: this is described by transition from I_1 to I_2 and it is mathematically modelled by the term $\lambda_1(T)I_1$. The term KNP describes phage binding to not only susceptible but also infected bacteria. This causes the density of phages to decrease since each adsorbed phages will die. Note that adsorption of phages to already infected bacteria results in a loss of phage. Also, the phages experience natural mortality due to various reasons which is expressed with the term μP. The density P increases due to release of new b phages at the lysis; where b is known as the burst size. The mortality rate of bacteriophages (μ) strongly depends on solar ultraviolet radiation (UVR) exposure; this quantity is denoted by u.

The probability of adsorption of a single phage to a single bacterium is proportional to K but not all of the adsorbed phages are successful in infecting bacteria. This might be because of two reasons. The first is that, for a multiple infection of a bacterium by several phages, only one of them (the first one) will be successful. The other is that bacteria can become resistant to phages by modifying

themselves. Therefore, the efficient adsorption rate (or viral infection rate) can be expressed with by $K_S = \epsilon K_P$ and the infection of susceptible bacteria is calculated by the term "$-K_S SP$" in the first equation of (3.1). We call the above system of ODEs **Model I**.

The other method of modelling bacterial lysis and viral replications is based on delay differential equations (DDEs) which we refer to as **Model II** in this chapter. The delayed-based approach is somewhat more frequent in the literature as compared to the ODEs based modelling approach [5, 39, 108, 14, 54] [3, 31, 94, 10, 44]. The equations of Model II read as follows

$$\begin{aligned}
\frac{dS(t)}{dt} =& \alpha(T(t))S(t)\Big[1 - \frac{N(t)}{C}\Big] - K_S S(t)P(t),\\
\frac{dI_1(t)}{dt} =& \overline{\alpha}(T(t))I_1(t)\Big[1 - \frac{N(t)}{C}\Big] + K_1(T(t))S(t)P(t) - \lambda_1(T(t))I_1(t),\\
\frac{dI_2(t)}{dt} =& K_2(T(t))S(t)P(t) + \lambda_1(T(t))I_1(t) - d_\tau,\\
\frac{dP(t)}{dt} =& - KN(t)P(t) - \mu(u(t))P(t) + bd_\tau,
\end{aligned} \tag{3.2}$$

where $d_\tau = K_2(T(t-\tau))S(t-\tau)P(t-\tau) + \lambda_1(T(t-\tau))I_1(t-\tau)$ is the delay terms in the third and the last equations and τ is delay time (between infection and lysis). In the equation for I_2 , the delay term $K_2(T(t-\tau))S(t-\tau)P(t-\tau)$ says that those bacterial cells which were infected τ minutes ago are experiencing lysis at the current moment of time. In the same concerns, the term $\lambda_1(T(t-\tau))I_1(t-\tau)$ describes the lysis of those former lysogenic cells I_1 which were converted to the lytic cycle τ minutes ago due to an increase of the ambient temperature. In the equation for P, the mentioned above terms are multiplied by the burst size b to give the number of released free phages.

Using each of Models I and II has its advantages and disadvantages for modelling bacteria-phage interaction (for example, the replication time τ may be variable). Thus, in this study we will explore both models. Note also one can make the above models of bacteria-phage interaction more complicated to make them more

biologically realistic. For instance, the phages attached to the susceptible bacteria are often released after non-fixed lysis time depending on some factors such as temperature. However, here we intentionally prefer to keep our models of temperature dependent lysogeny as simple as possible (e.g. assuming constant lysis time) to be able to understand the generic behaviour of such systems including the dependence of the dynamics on key parameters.

3.2.1 Model parameterisation

Most parameters used in our models were obtained either from the original experimental data [19] or the relevant experimental literature sources. The parameters describing bacteria-phage interactions are generally temperature dependent but we assume that some of the parameters are constant or independent on temperature. We suppose that only two processes would be temperature dependent which are bacterial (susceptible and lysogenic bacteria) growth rates and the type of infection (lysogenic or lytic), including the transition from the lysogenic to the lytic cycle. The temperature dependence of the bacterial growth rate of susceptible B. pseudomallei has been evaluated using experimental results of Chen et al (2003) [18]. They presented the growth constant of 12 different strains of the bacteria at temperature 4, 22, 25, 30, 37, 42, 45 °C. We fitted the average values of growth rate using 7 different strains from the mentioned paper to exclude negative values by using the non-linear regression techniques from GraphPad Prism[1] based on minimisation of the sum of the squares. We find that the resulting temperature dependence of $\alpha(T)$ can be well approximated by a Gaussian function (see Fig 3.2(a) and the average experimental growth rates at each temperature are shown by dots):

$$\alpha(T) = \exp\Big(-\frac{(T-T_0)^2}{2\sigma^2}\Big)\alpha_{\max}. \tag{3.3}$$

[1] Scientific 2D graphing and statistics software [1]

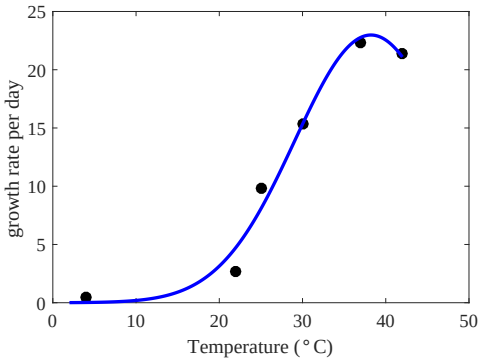

(a)

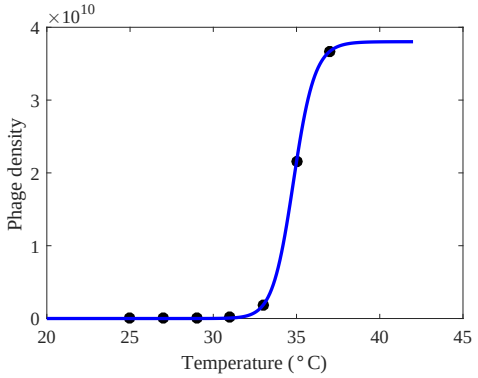

(b)

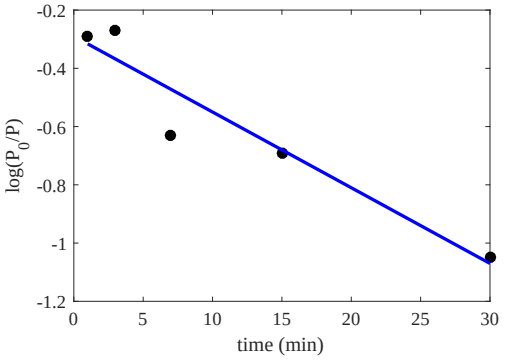

(c)

Figure 3.2: Experimental estimation of the key model parameters. (a) Dependence of the growth rate of B. pseudomallei on temperature. (b) Bacteria-phage interactions depending on temperature. Appearance of a large number of phages at approximately 34 $^{\circ}C$ signifies a switch between lysogenic and lytic infection types; (c) Binding of phages to bacterial cells. The graph shows the natural log of the ratio of the initial number of free phages and the density of phages at time t. For each experiment, fitting of curves was done using the GraphPad Prism software. For details, see the main text.

Our non-linear regression fitting using the GraphPad Prism software gives the following estimates of the parameters: $\sigma = 9.1 \pm 2.3\ ^\circ C$; $T_0 = 38.22 \pm 2.4\ ^\circ C$; $\alpha_{\max} = 23 \pm 2.5\ \text{day}^{-1}$. Thus the maximal bacterial growth occurs at about $38\ ^\circ C$.

The per capita growth rate of lysogenic bacteria is considered to be given by the following function

$$\overline{\alpha}(T) = \alpha(T)\Big[1 - \frac{T^n}{T_1^n + T^n}\Big] = \alpha_{\max} \exp\Big(-\frac{(T-T_0)^2}{2\sigma^2}\Big)\Big[1 - \frac{T^n}{T_1^n + T^n}\Big]. \qquad (3.4)$$

According to this expression, the growth rate of lysogenic bacteria at low temperatures is the same as that of susceptible bacteria, whereas the normal cell division of I_1 stops and bacteria become lytic at higher temperatures as in Fig 3.3(b). The

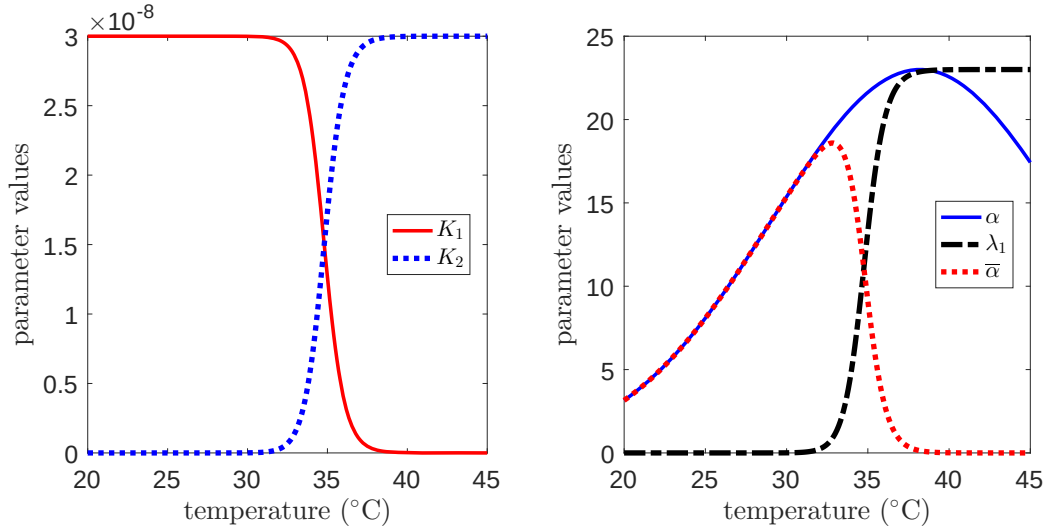

Figure 3.3: (a) shows transition rates from suceptible bacteria to lysogenic and to lytic cycles depending on temperatures as in Eq 3.5, Eq 3.6. (b) presents growth rates of susceptible and lysogenic bacteria and transition rate from lysonec cycle to lytic cycle.

switch between lysogenic and lytic infection scenarios occurs at the critical temperature T_1. We consider that the switching process can be described via a sharp S-shape curve $T_1^n/(T_1^n + T^n)$ which - for a large parameter n - is close to zero for $T < T_1$ and close to one for $T > T_1$.

The use of the S-shaped curve to describe the lysogenic-lytic switch is confirmed by experimental results [19] presented in Fig 3.2(b). The graph shows

Table 3.1: Definitions, units, ranges and the fixed values of constant Parameters

Symbol	**Meaning**	**Unit**	**Range**	**Default Value**
$\alpha_{\max}$	maximum growth rate of bacteria	day^{-1}	$19 - 27$	23 [18]
C	bacteria carrying capacity	ml^{-1}	–	2×10^6
K	phage adsorption rate	$\text{ml}^{-1}\text{day}^{-1}$	–	1×10^{-7}
ϵ	adsorption efficiency	–	–	0.3
$\lambda_{1\max}$	maximum lysogenic process rate	day^{-1}	$19.1 - 27.2$	23 [18]
λ_2	constant lysis rate	day^{-1}	–	20 [18]
b	burst size of phages	–	158 ± 54	100 [34]
T_0	Optimum temperature for growth and lysis	°C	$35.6 - 50.6$	38.2 [18]
T_1	optimum transition temperature	°C	$34.81 - 34.84$	34.8
σ	standard deviation of growth rate	°C	$6.7 - 17.4$	9.1
u	ultraviolet index	–	$8 - 12$	–
μ_c	constant mortality rate with UV	day^{-1}	–	0.1
n	transition width	–	$53.7 - 56.3$	55

the density of free phages after infecting bacterial culture of B. pseudomallei depending on the ambient temperature. One can see that the number of phages is extremely low for $25\ ^\circ C < T < 32\ ^\circ C$ which signifies the infection resulting in lysogeny. For higher temperatures $T > 34\ ^\circ C$, the viral infection becomes lytic and it results in a substantial increase of phage reproduction. Our model fitting of the S-shaped curve gives the following estimates for the parameters $T_1 = 34.8 \pm 0.02\ ^\circ C$ and $n = 54 \pm 1$. Thus the switch between lysogenic and lytic infections occurs at approximately $35\ ^\circ C$, which is an important biological result for temperature-dependent lysogeny of B. pseudomallei. Also, the figure shows that the temperature-dependent lysogeny is a gradual process, i.e. at $T = T_1$ approximately 50% bacteria are lysogenic and 50% still follow the lytic cycle. Using this experimental result, we can parameterise the dependence of the phage

adsorption constant on the temperature as

$$K_1(T) = (1 - \frac{T^n}{T_1^n + T^n})K_S, \tag{3.5}$$

$$K_2(T) = \frac{T^n}{T_1^n + T^n}K_S, \tag{3.6}$$

where K_S is the phage adsorption constant, which we assume to be temperature independent. Note that the sum of K_1 and K_2 equals K_S. Using the same temperature dependence for the switch rate λ_1 between lysogenic and lytic state we obtain

$$\lambda_1(T) = \frac{T^n}{T_1^n + T^n}\lambda_{1\max}, \tag{3.7}$$

where the maximal transition rate $\lambda_{1\max}$ is assumed to be equal to the maximal growth rate of the susceptible bacteria. All temperature dependent parameter functions are shown in Fig 3.3.

The overall adsorption rate K of phages was estimated from another unpublished experiment [19] which is represented in Fig 3.2(c). This figure shows the natural logarithmic ratio between the initial number of phages at the start of the experiment and the number of phages at time t. Then we can calculate the adsorption rate of phages to bacteria by the rate of its change as

$$\frac{dP}{dt} = -KNP \Rightarrow \ln(\frac{P}{P_0}) = -KNt,$$

where $N = N_0 = 1.5 \times 10^8$ and $\ln(P_0/P(t_1)) = 1.05$; P_0 is initial values of the density of phages and t_1 is 30 minutes or $30/(60 \times 24)$ day according to the

experimental diagram in Fig 3.2(c). Thus, K can be calculated as follow:

$$\begin{aligned} K &= -\frac{1}{N_0 t_1}\ln\left(\frac{P(t_1)}{P_0}\right)\frac{\text{ml}}{\text{minute}} \\ &= -\frac{60\times 24}{N_0 t_1}\ln\left(\frac{P(t_1)}{P_0}\right)\frac{\text{ml}}{\text{day}} \\ &= 3.36\times 10^{-7}\ \text{ml day}^{-1}. \end{aligned}$$

The fitting of the points with a straight line gives $K = (33.6\pm 5.7)\times 10^{-8}$ ml day^{-1}. This value is within the reported values from the literature; however, since other sources report a wide range of K, we will vary its value to reveal dependence of model outcome on this parameter. The efficient adsorption rate or viral infection rate is calculated by $K_S = \epsilon K$ where the phage infection efficiency coefficient ϵ is not well known, here we assume it to vary within $0.2 - 0.6$.

The other model parameters are taken from the literature. In particular, the burst size of phage b is estimated to vary in range of 100 and 212 [34]. We consider it to be temperature-independent. The value of carrying capacity C of B. pseudomallei in rice fields is not well known since different sources provide different estimates [113, 120, 93]. It is also likely that C highly varies from field to field since it largely depend on pH, iron concentration, fertilisers, carbon/nitrogen ratio, etc [120]. In this chapter, we explore a wide range of C to be able to model nutrient poor and nutrient rich environment and the effect of fertilises even though we consider the default value of $C = 2\times 10^6$ cell/ml, which is located in the middle of the reported values. The lysis rate of bacteria λ_2 in Model I is assumed to be constant. Since the average latent period of infection is approximately $\tau = 50$ min [34], we may assume that averagely 50% of lytic bacteria die in 50 minutes after infection. Therefore, λ_2 can be estimated by the rate of change of I_2 as

$$\frac{dI_2}{dt} = -\lambda_2 I_2 \quad \Rightarrow \quad \ln\left(\frac{I_2(t)}{I_2(0)}\right) = -\lambda_2 t \tag{3.8}$$

where for $t_1 = 50$ minutes $\frac{I_2(t_1)}{I_2(0)} = 1/2$ and so λ_2 becomes

$$\begin{aligned}\lambda_2 &= -\frac{\ln(1/2)}{50} = 0.0139 \text{ min}^{-1} \\ &= 0.0139 \times 60 \times 24 = 20.0160 \text{ day}^{-1}.\end{aligned} \tag{3.9}$$

The mortality of free phages μ is a key parameter of the model. Such mortality can be caused by exposure to ultraviolet (UV) solar radiation [106], adsorption to particles other than bacterial cells, consumption by flagellates or amoebas [111]. In particular, we examined the interaction on the surface of water so they are directly exposed to sun radiation. It is reported that phages suffer $90-95\%$ mortality over a day due to exposure to sun radiation in summer and 50% mortality in winter [106]. The mortality rate in day can be found through the following equation:

$$\begin{aligned}&\frac{dP}{dt} = -\mu P, \\ \Rightarrow \quad &P(t) = P_0 \exp(-\mu t)\end{aligned}$$

where $P_0 = P(0)$. We assume that duration of the UV radiation exposure is $t_1 = 12$ hours $= 1/2$ day,

$$\Rightarrow \quad \mu = -\ln\Big(\frac{P(t_1)}{P_0}\Big)\frac{1}{t_1}$$

$P(t_1)/P_0 = 5/100 = 1/20$ for 95% of death in phages; and $P/P(0) = 50/100 = 1/2$ for 50% of death in phages. Therefore, mortality rate of phages μ is between 1.39 day^{-1} and 5.99 day^{-1} in day time due to the influence of UV. We assume that in Thailand the summer time corresponds to the UV index equal $u = 12$ whereas the winter time would correspond to $u = 8$. This is actually in good agreement with the historical data (see Fig 3.4). In this chapter, we consider the phage mortality to be given by

$$\mu(u) = \begin{cases} \mu_c + Y_0 \exp(ku) & \text{in day} \\ \mu_c & \text{at night} \end{cases} \tag{3.10}$$

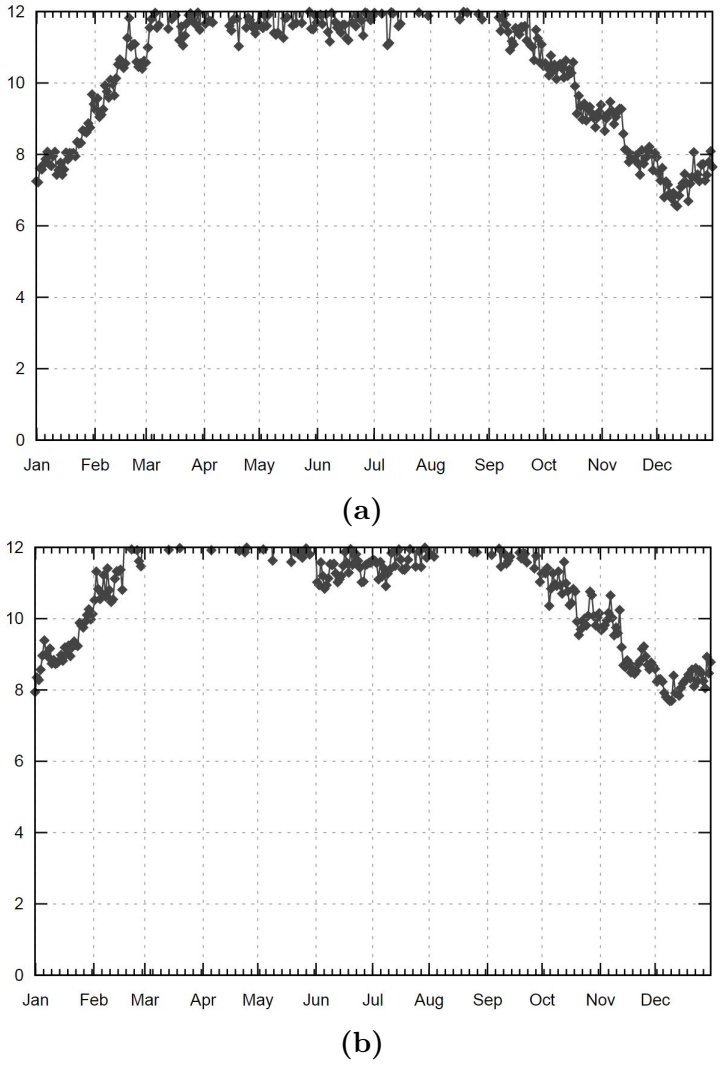

Figure 3.4: (a) Nakhon Phanom and (b) Sa Kaeo UV index history in 2015 is from the website "www.weatheronline.co.uk"

where μ_c is the background (light-independent) mortality; u is the ultraviolet (UV) index value which varies from 0 (minimum and especially at night) to 12 (maximum exposure) [30]. As we see that the mortality rate of phages is exponentially proportional to the variable u (Fig 3.5). Thus, we can estimate the values of $Y_0 = 0.073$ day^{-1} and $k = 0.367$ by neglecting the background mortality in experiments of [106].

The background mortality parameter μ_c is extremely hard to estimate (e.g. it may depend on the abundance of flagellates), so we consider the default value of $\mu_c = 0.1$ day^{-1}. We also vary this parameter to check the sensitivity of model

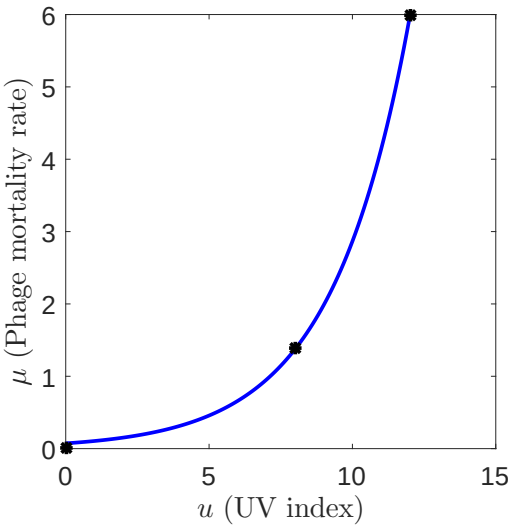

Figure 3.5: Black star signs show the values of mortality related to variable u such that $\mu(u = 0) = 0$, $\mu(u = 8) = 1.39$ and $\mu(u = 12) = 5.99$ while the exponential function is the estimation of this values.

predictions to μ_c. In this chapter, we apply modelling to describe bacteria-phages interactions in two important provinces of Thailand: Nakhon Phanom and Sa Kaeo, and we use the average historical data on UV radiation from the weather website [2]. Variation of UV index across the year in the considered areas is shown in Fig 3.4. We take monthly average of UV index and use interpolation to describe UV variation each day of the year. We also take into account the variation of the length of day time and night across the year to calculate the exposure of phages to UV. For this purpose we use sunset-sunrise time reports from the website[3].

Finally, we consider daily and seasonal variation of temperatures in the mentioned provinces of Nakhon Phanom and Sa Kaeo in Thailand to parameterise Models I and II. Using the information on historical temperatures from the website[4], we computed the 4 years average $(2013 - 2016)$ of the mean monthly air temperatures. To obtain the highest surface temperature, we multiply the maximal temperatures by an empirical coefficient $\eta = 1.15$ (it is assumed between 1 and 1.3 [46]) which allows to provide realistic surface temperatures. The temper-

[2] `www.weatheronline.co.uk`: enter city name, history, UV index respectively
[3] `www.sunrise-and-sunset.com`
[4] `www.worldweatheronline.com`

ature variation across the year is found by piecewise cubic spline interpolation of monthly average values for two provinces (see Fig 3.6(a)). The daily temperat-

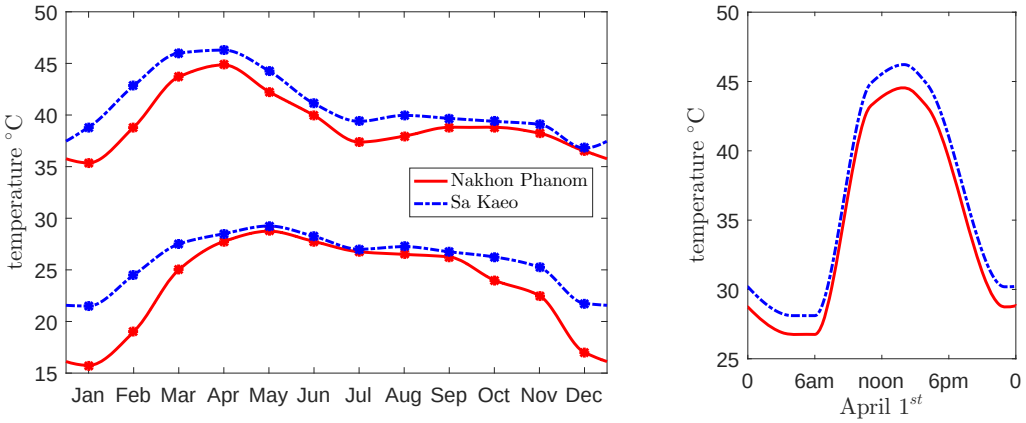

Figure 3.6: (a) Seasonal variation of the maximal and minimal surface temperatures in two endemic provinces in Thailand: Nakhon Phanom and Sa Kaeo. (b): Hourly temperature values within day of April 1st (2016). for the same provinces in Thailand. The temperatures are averaged over 4 years: 2013-2016. The data is obtained from the website www.worldweatheronline.com.

ure variation for each day was approximated using the minimal and the maximal temperatures in Fig 3.6(a) and shape temperature variation at the start of each month (for the other days of the month the shape of the temperature variation was considered to be the same). An example of daily temperature variation on 1st April is shown in Fig 3.6(b) for both Sa Kaeo and Nakhon; one can see the shapes of the curves are close to each other.

We used 4th order explicit Runge-Kutta (RK4) method to simulate the system of ODEs in Model I. We used the second order finite difference method with a smaller step size to simulate the delay differential equations (DDEs) in Model II [77]. Some results have been checked using a more advanced Runge-Kutta method of order 4 in the delay terms. Applying RK4 to a system of DDE is more complicated. We need to find for this method the midpoints of each two grids. Let us consider a simple example:

$$y' = f(t, y, z),\ y(t_0) = y_0,\ z(t) = y(t - \tau)$$

where τ is the delay. Then the RK4 method with delay becomes

$$\begin{aligned} K_1 &= f(t_n, y_n, z_n); \\ K_2 &= f(t_n + \Delta t/2, y_n + 0.5 * \Delta t * K_1, z_{n+1/2}); \\ K_3 &= f(t_n + \Delta t/2, y_n + K_2 * \Delta t/2, z_{n+1/2}); \\ K_4 &= f(t_n + \Delta t, y_n + K_3 * \Delta t, z_{n+1}); \\ y_{n+1} &= y_n + \Delta t/6 * (K_1 + 2 * K_2 + 2 * K_3 + K_4); \\ z_{n+a+1} &= y_{n+1}; \\ t_{n+1} &= t_n + \Delta t \end{aligned}$$

where a is the step size in delay as $\tau/\Delta t$ and $z_{n+1/2}$ is a midpoint between z_n and z_{n+1}. We compute this midpoints with higher degree polynomial interpolation. The summary of model parameters as well using Lagrangian polynomial interpolation. To check the numerical accuracy of the results, we ran our simulations for smaller time steps ($1/5^{\text{th}}$ of the basic time step) and compared the simulation results for the different time steps (which remained close to each other). The summary of model parameters as well their values are provided in Table 3.1. The unit of the densities of bacteria and phages are taken as cell/ml.

3.3 Modelling results

A typical pattern of population dynamics of bacteria-phage interactions across the year is shown in Fig 3.7. First year simulations are removed to get rid of transient dynamics and come closely to model attractors. The curves in the figure are based on Model I and are constructed for the temperature and UV variation corresponding to Nakhon Phanom province. The seasonal variations of the densities of free phages and susceptible bacteria are shown in addition to those of infected bacteria. The phage density decreases during the period of warm days between March and September and it is higher in winter days. On the contrary, the number of susceptible bacteria is dangerously high level in spring and summer.

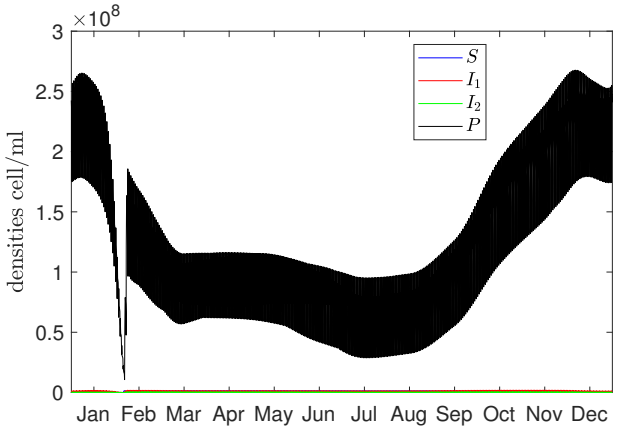

(a)

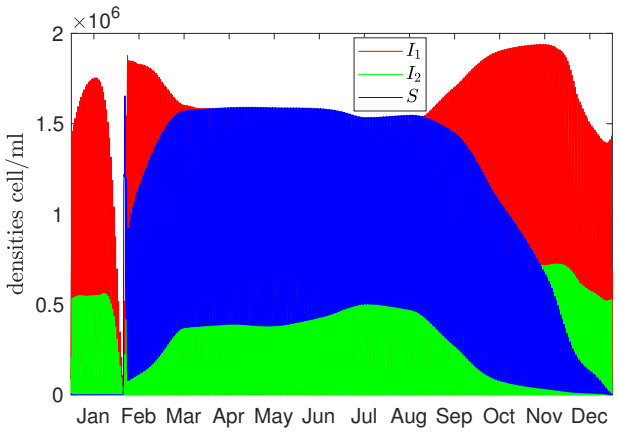

(b)

Figure 3.7: Seasonal and daily dynamics of the bacteria-phage system predicted by **Model I** for the temperature and solar radiation records corresponding to the **Nakhon Phanom** province. (a) Seasonal variation of free phage density (CFU/ml). (b) Seasonal variation of phage-free bacteria (blue curve), lysogenic bacteria (red curve) and bacteria in the lytic state (green curve). The model parameters are taken from Table 3.1 as default values.

Interestingly, the density of infected bacteria in lytic cycle I_2 does not much change with seasonal variations throughout the whole year. This is possible because of the ranges of daily temperature variations. Each day in Thailand, the difference in temperature variation is very high. Also its low temperature is below the critical values for the transition (T_1) and the high temperature is above it (see Fig 3.6(a)). Thus, lytic and lysogenic infection appear each day of the year. The observed permanent presence of I_2 explains the fact that free phages P can persist

across the whole year since their number always replenishes through lysis of I_2. The density of susceptible bacteria is close to zero and I_1 is very high around January since the temperature couldn't reach above the optimum temperature (T_1) of transition. After January, susceptible density suddenly increases and lysogenic decreases. Also, the free phage density decreases at first since they are adsorbed by susceptible bacteria, then it again increases with released new phages.

One can also see that all four densities exhibit high amplitude daily oscillations. The dynamics on April 1^{st}, which is the warmest month of the year, are shown for the densities of susceptible bacteria, infected bacteria and phages (Fig 3.8(a)). This figure shows that the dominance of lysogenic and lytic bacteria is highly variable across the day: at night the infected bacteria are mostly lysogenic whereas day time infection is mostly lytic. The density of susceptible bacteria is maximal in the evening (around 8pm) and it is minimal in the morning (around 9am). This pattern changes in winter because temperatures main remain lower than the critical transition temperature T_1 (see Figs 3.8(b),(c)).

To reduce the complexity caused by high frequency daily oscillations, we plot the seasonal variation of daily averaged densities[5] of the bacteria S, I_1, I_2 in Fig 3.9(b) and all species in Fig 3.9(a) (mostly shown phage density). The population size of susceptible bacteria S is higher during warm season whereas the phages numbers are higher during cooler seasons according to these results. Now it can be clearly seen that the highest numbers of S occur in March−September. This is a period of a higher infection risk. However, there might be high risk time within each day in winter as well. This detail can be seen with daily variations as we mentioned above.

We also investigated the bacteria-phages dynamics for temperature and solar variation corresponding to Sa Kaeo province. All parameters are the same as that of the table 3.1. The temperature variation and ultraviolet index across the year for Sa Kaeo is given by the historical data in Figs 3.6, 3.4(b), respectively. The

[5] We compute daily averaged values by the left Riemann sum.

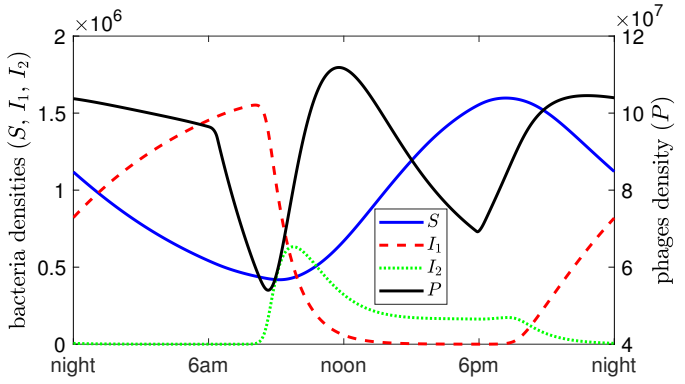

(a)

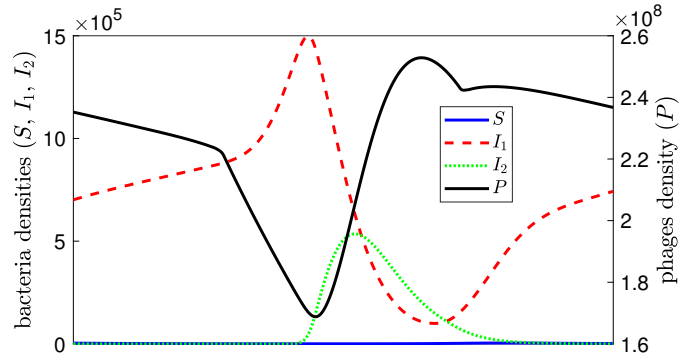

(b)

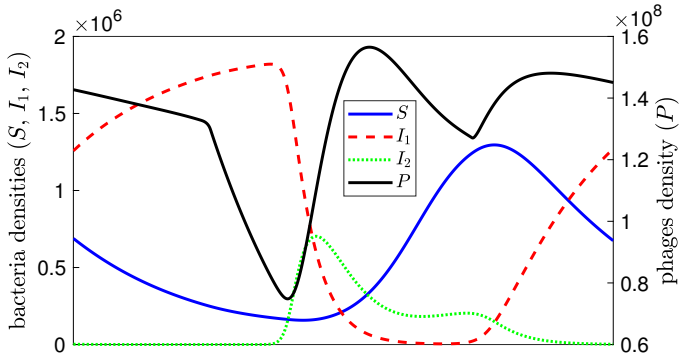

(c)

Figure 3.8: Daily dynamics of the bacteria-phage system predicted by **Model I** for the temperature and solar radiation records corresponding to the **Nakhon Phanom** province. Daily variation of viral (black curve) and bacterial components (phage-free bacteria "blue curve", lysogenic bacteria "red curve" and bacteria in the lytic state "green curve") of the system corresponding on (a) April 1^{st}, (b) January 1^{st} and (c) October 1^{st}. The model parameters are taken from Table 3.1 as default values.

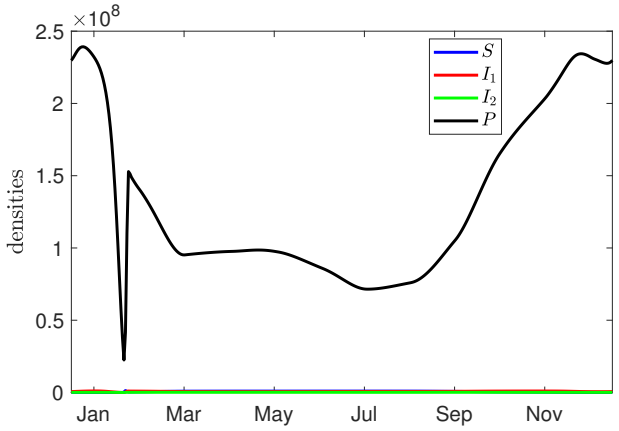

(a)

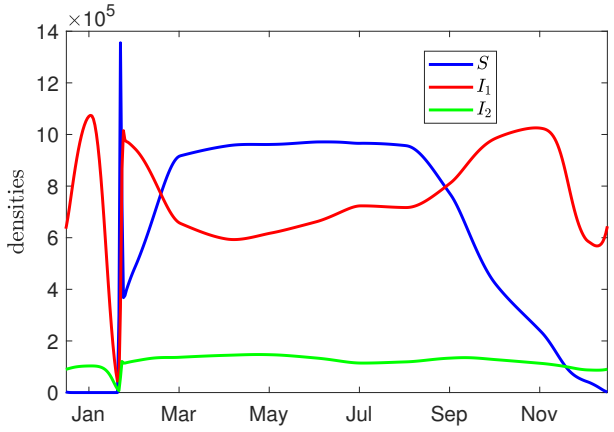

(b)

Figure 3.9: Seasonal dynamics with daily average densities of the bacteria-phage system predicted by **Model I** for the temperature and solar radiation records corresponding to **Nakhon Phanom** province. The model parameters are taken from Table 3.1 as default values.

temperatures in Sa Kaeo are higher than in Nakhon Phanom. In addition, the UV index in winter in Sa Kaeo is slightly higher than in Nakhon Phanom in winter. This is the main reason of why even in the coldest days, susceptible bacteria can survive in Sa Kaeo (see Fig 3.10(a),(c)). Also, the densities variation within day in Fig 3.10(b),(d) and daily average densities of species in Fig 3.10(e),(e) are shown. Weather of Sa Kaeo is warmer than Nakhon Phanom. In addition, its UV index is a little bit higher than Nakhon Phanom in winter. That's why even in the coldest days, susceptible bacteria can survive in Sa Kaeo (see Figs 3.10(c),(f)).

In Model I, λ_2 is constant and equals to 20 day^{-1}: this corresponds to 50

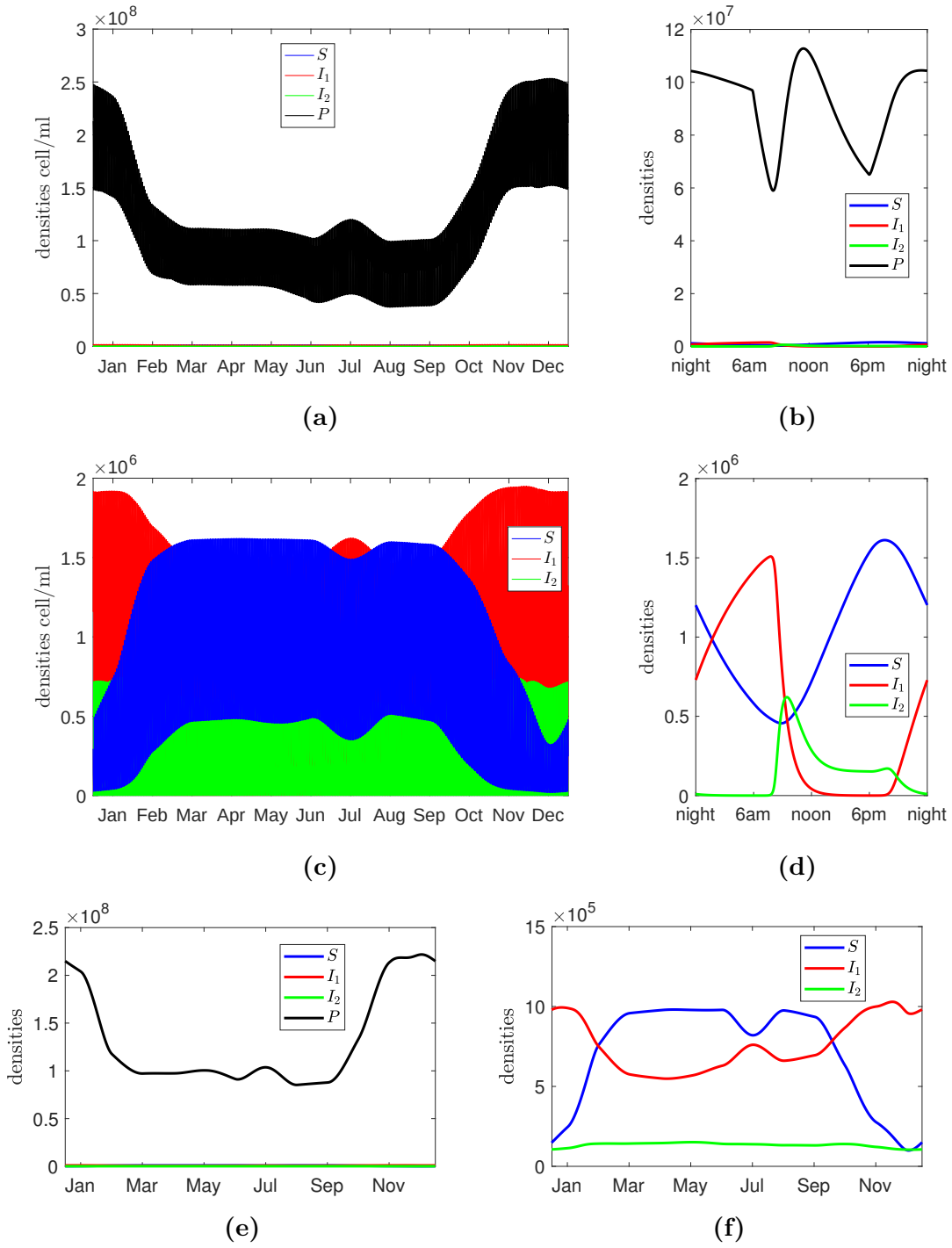

Figure 3.10: Seasonal and daily dynamics of the bacteria-phage system predicted by **Model I** for the temperature and solar radiation records corresponding to the **Sa Kaeo** province. (a) Seasonal variation of free phage density (CFU/ml). (c) Seasonal variation of phage-free bacteria (blue curve), lysogenic bacteria (red curve) and bacteria in the lytic state (green curve). (b),(d) Daily variation of viral and bacterial components of the system corresponding on April 1^{st}. (e),(f) Seasonal dynamics with daily average densities of the bacteria-phage system. The model parameters are taken from Table 3.1 as default values.

minutes lysing (delay) time in Model II. Implementation of Model II (i.e. DDEs framework) provides similar predictions about seasonal and daily variation of bacteria and phage densities in Nakhon Phanom for the same model parameters. The corresponding graphs are shown in Fig 3.11. More simulations related to Model II for Sa Kaeo Province can be found in Fig 3.12. Therefore, Model I (based on ODEs) and Model II (based on DDEs) give similar results both in terms of quantitative and qualitative behaviour.

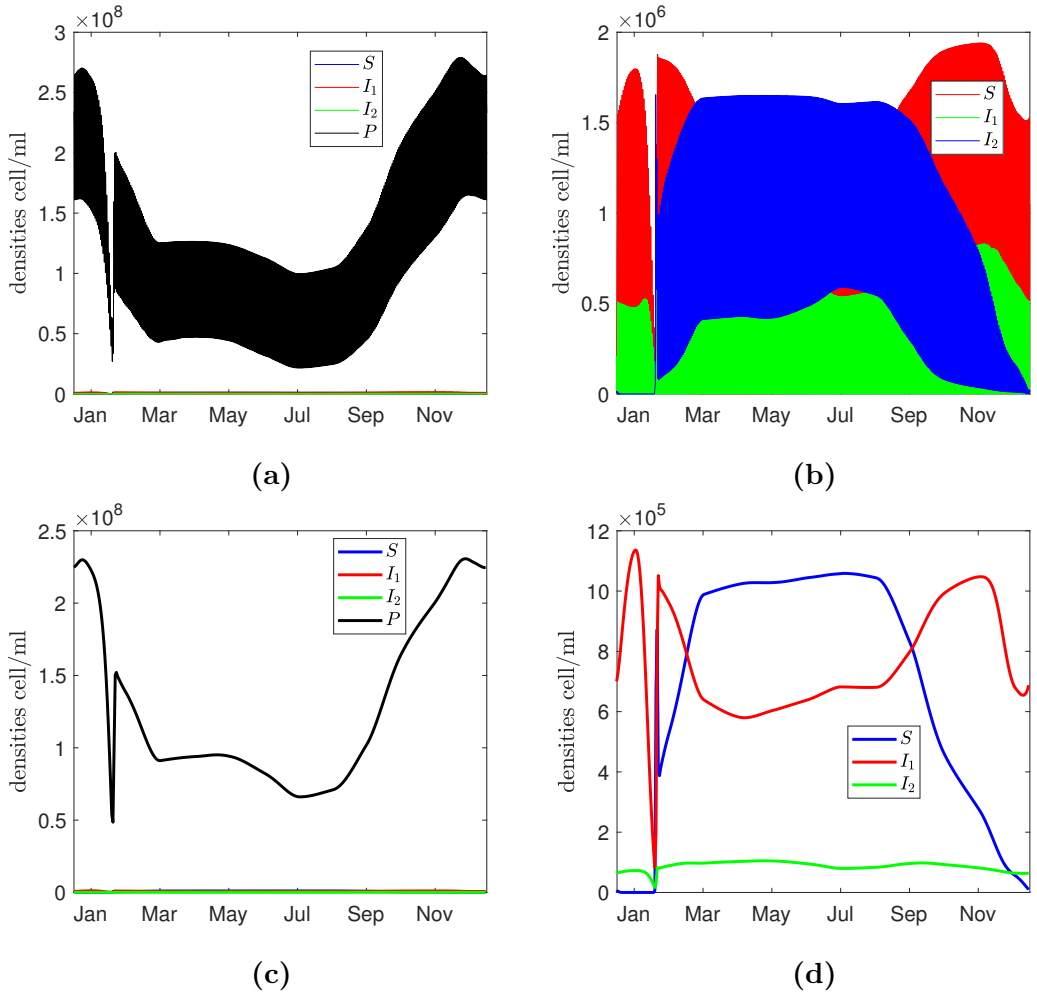

Figure 3.11: Seasonal and daily dynamics of the bacteria-phage system predicted by **Model II** for the temperature and solar radiation records corresponding to the **Nakhon Phanom** province. (a) Seasonal variation of free phage density (CFU/ml). (b) Seasonal variation of phage-free bacteria (blue curve), lysogenic bacteria (red curve) and bacteria in the lytic state (green curve). (c,d) Daily average densities of viral and bacterial components of the system through the year. The model parameters are taken from Table 3.1 as default values.

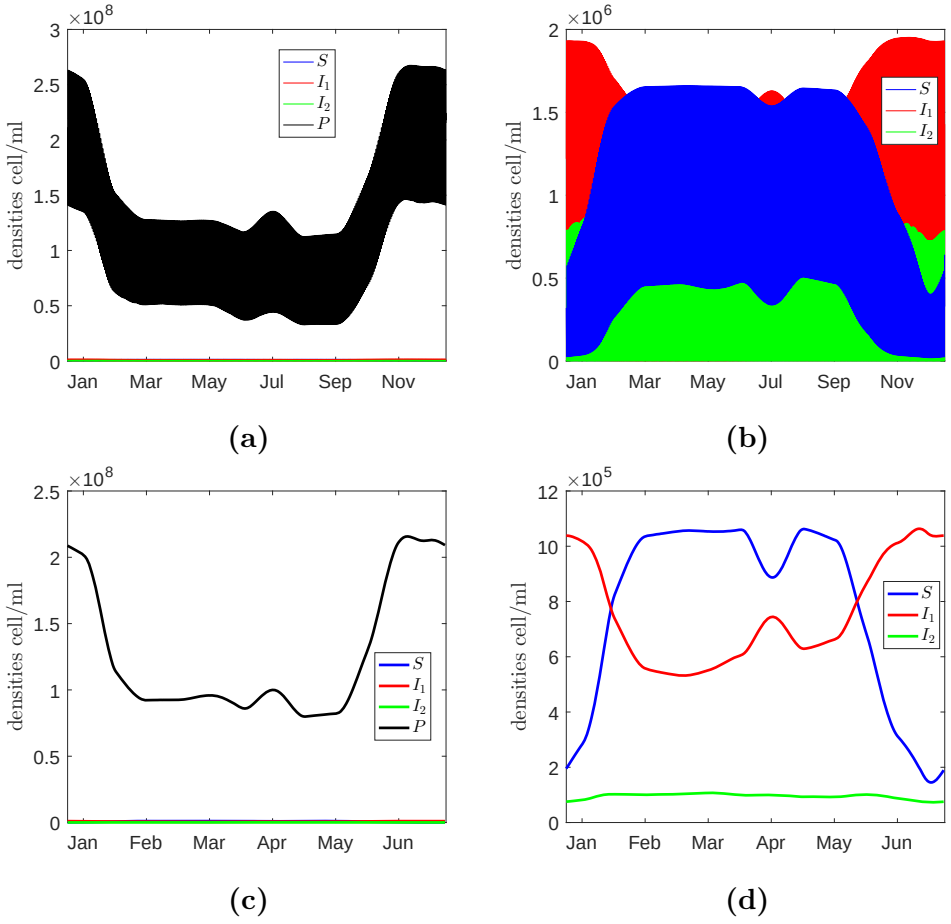

Figure 3.12: Seasonal and daily dynamics of the bacteria-phage system predicted by **Model II** for the temperature and solar radiation records corresponding to the **Sa Kaeo** province in Chapter 3. (a) Seasonal variation of free phage density (CFU/ml). (b) Seasonal variation of phage-free bacteria (blue curve), lysogenic bacteria (red curve) and bacteria in the lytic state (green curve). (c,d) Daily average densities of viral and bacterial components of the system through the year. The model parameters are taken from Table 3.1 as default values.

It is of practical interest to investigate the dependence of bacteria-phage dynamics on the nutrient status of the environment. For instance, bacteria populations can be largely affected by nutrient enrichment via the use of fertilises. This is described by the parameter C. We observe a phenomenon which is close to the paradox of enrichment, i.e. large-amplitude oscillations occur by increasing C. The outcomes of two different values of the carrying capacity on bacteria-phage interaction are shown in Fig 3.13. A $4-$fold increase of C compared to the default value would result in the appearance of a large outbreak of S in March (see

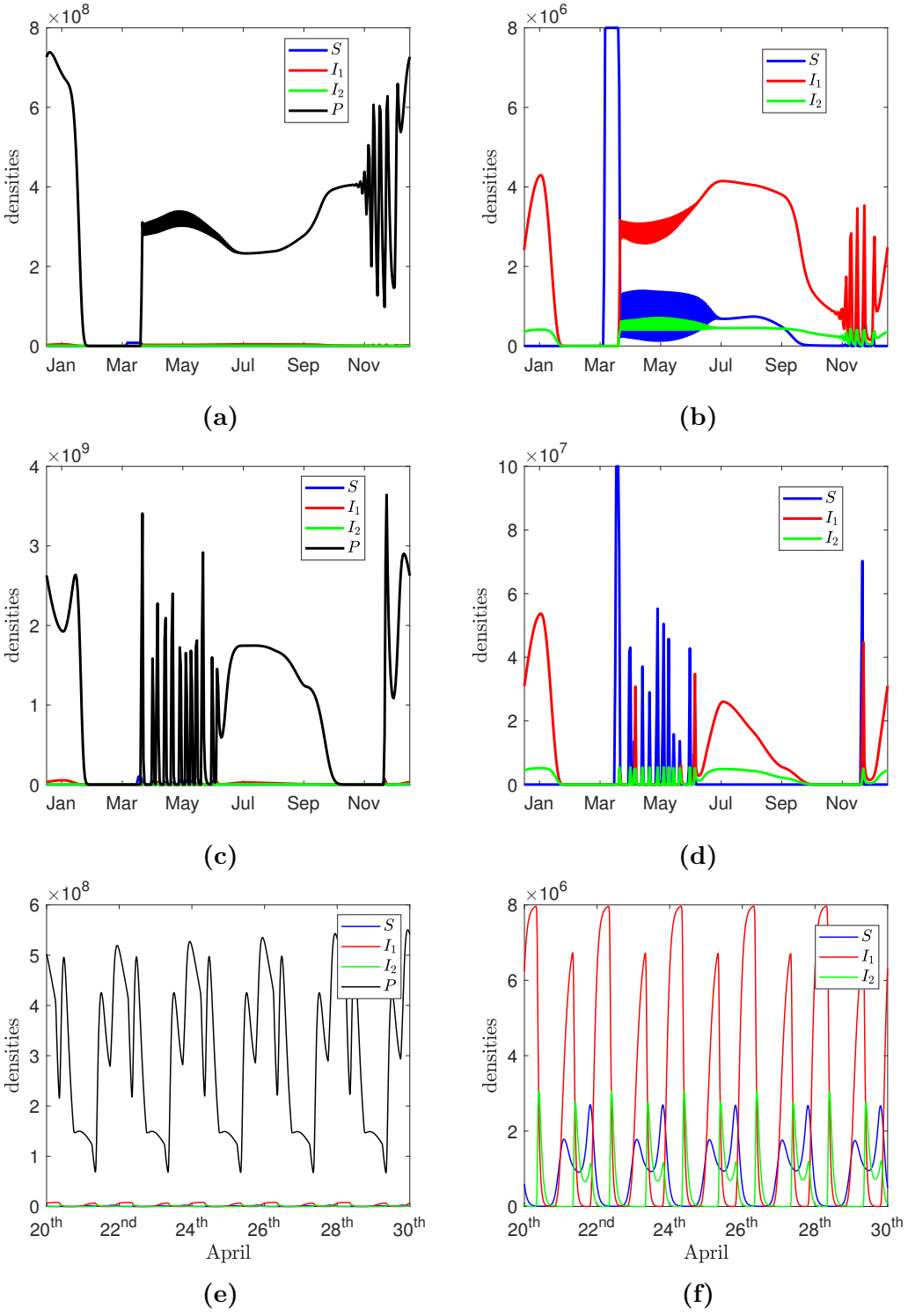

Figure 3.13: Variation of daily average densities of bacteria across the year for different values of the carrying capacity C (**Nakhon Phanom** province): $C = 8 \times 10^6$ cell/ml in (a),(b) and $C = 1 \times 10^8$ cell/ml in (c),(d). (e),(f) show daily variation of phages and bacterial components of the system corresponding on April $1^{st} - 9^{th}$ in the case of $C = 8 \times 10^6$. Simulations are based on **Model I**, the other parameters are taken from Table 3.1 as default values.

Fig 3.13(b)). The bacterial density in this outbreak is close to C. This half month-long outbreak is followed by almost periodical oscillations of species densities until early July. Note that unlike in Fig 3.7(b), pronounced oscillations in bacterial densities in Fig 3.13(b) are not daily periodic oscillations but have a period of around two days. To show detail in variation independently from daily oscillation is given by Fig 3.13(e),(f). Another pattern in the oscillations of species densities is observed in late autumn; however it is characterized by a smaller amplitude of S.

A further increase in C leads to a more irregular dynamics shown in Fig 3.13(c),(d). The outbreaks of S occur within March-July and a single peak in November. The small period of high species densities are separated by periods where the density is very low ($>$ 103cells/ml). Interestingly, similar dependence on the carrying capacity is observed in Model II and for the temperature variations corresponding to the Sa Kaeo province which are shown in Figs 3.14 and 3.15, respectively. However, Model I in Sa Kaeo province predicts the existence of irregular oscillations throughout the whole year with only slight degree of seasonality for high values of C (Fig 3.15(c),(d)).

We saw above that different carrying capacity produce different dynamics in the bacteria-phages models. We thoroughly explored the dependence of dynamical regimes on the combination of key parameters b (burst size) and K (adsorption rate) in addition to C (carrying capacity). The results are presented in the form of bifurcation diagrams shown in Fig 3.16. With the variable parameters in the diagrams, we obtain four different dynamical regimes which are: Regime (I) signifies extinction of phages in the system and only phage-free bacteria S can survive (no viral infection); Regime (II) expresses the type of dynamics in terms of fixed parameters given by Fig 3.9(b) and Regime (III) and Regime (IV) correspond to the patterns of dynamics shown in Fig 3.13(a),(b) and Fig 3.13(c),(d), respectively. In Regimes (II)-(IV), all four compartments coexist though the year. Note that it is hard to trace the exact boundary between them. Our classification of

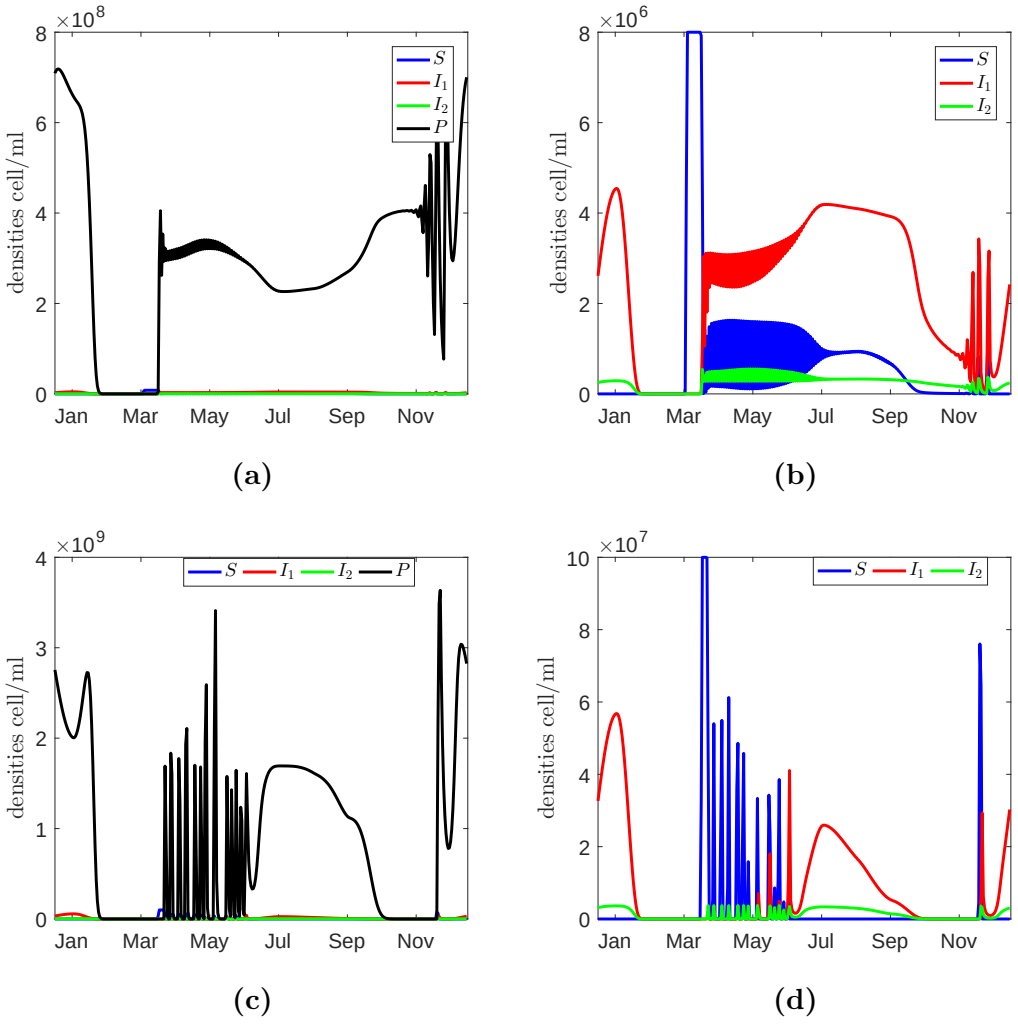

Figure 3.14: Variation of daily average densities of bacteria across the year for different values of the carrying capacity C (**Nakhon Phanom** province): $C = 8 \times 10^6$ cell/ml in (a),(b) and $C = 1 \times 10^8$ cell/ml in (c),(d). Simulations are based on **Model II**, the other parameters are taken from Table 3.1 as default values.

Regime (III) is based on the requirement that there should be species oscillations in summer with a period > 1 day with species densities staying below a certain threshold (here we use $S_0 = 10^3$ cells/ml as a threshold), whereas for regime IV the minimal density of S through oscillations in summer should be smaller than a certain threshold. One can see from the diagrams that an increase in the carrying capacity of bacteria or the adsorption rate of phages would result in phage extinction, whereas high values of these parameters will cause irregular oscillations of species densities. Increasing of burst size would result in persistence of phages; however it has less effect on the system dynamics as compared to the other para-

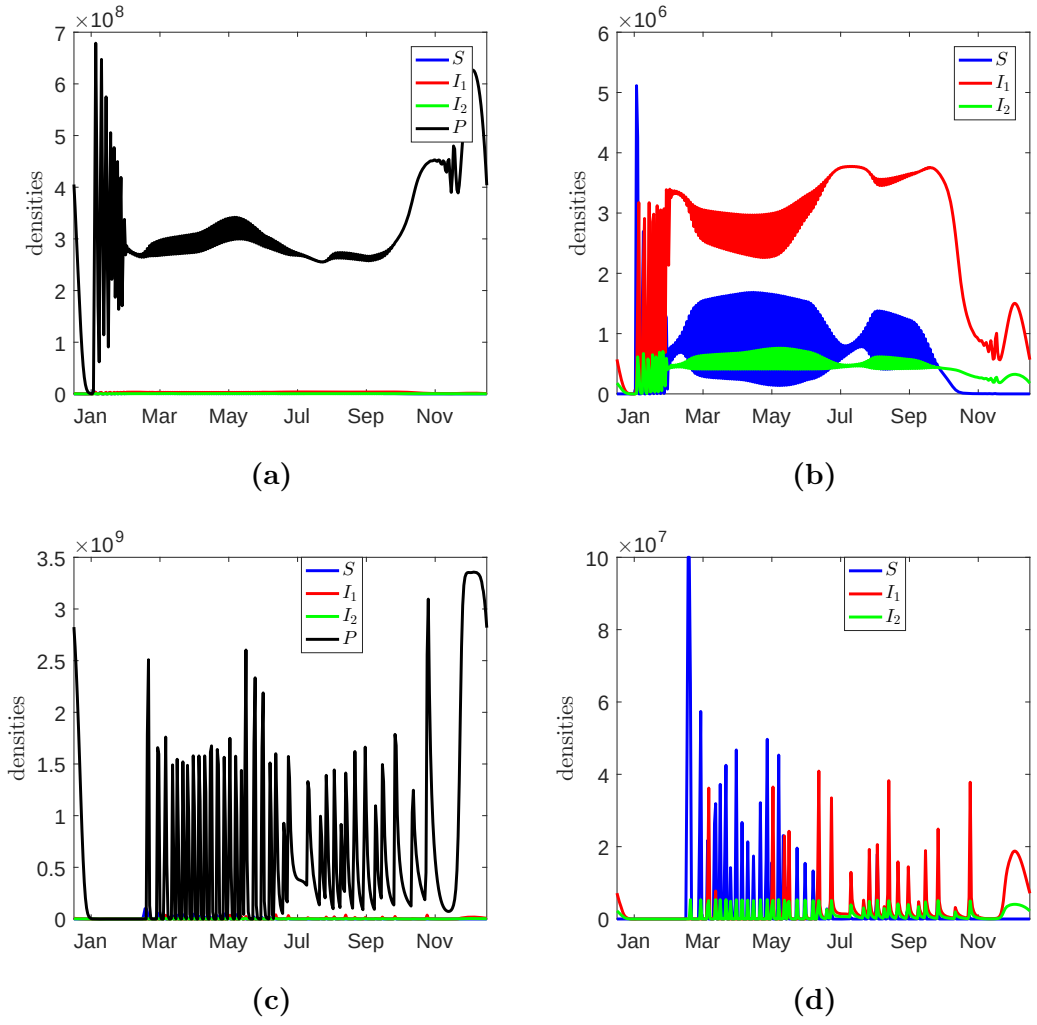

Figure 3.15: Variation of daily average densities of bacteria across the year for different values of the carrying capacity C (**Sa Kaeo** province): $C = 8 \times 10^6$ cell/ml in (a)(b) and $C = 1 \times 10^8$ cell/ml in (c),(d). Simulations are based on **Model I**, the other parameters are taken from Table 3.1 as default values.

meters. Finally, we find that variation of μ_c the background mortality of phages within the region of $0.1 - 0.5$ day^{-1} shows the dynamics is not sensitive to this parameter.

3.3.1 Separate effects of temperature variation and UV index

It is of importance to understand the mechanisms controlling the dynamical patterns observed in the models. We check the separate variation impact of the

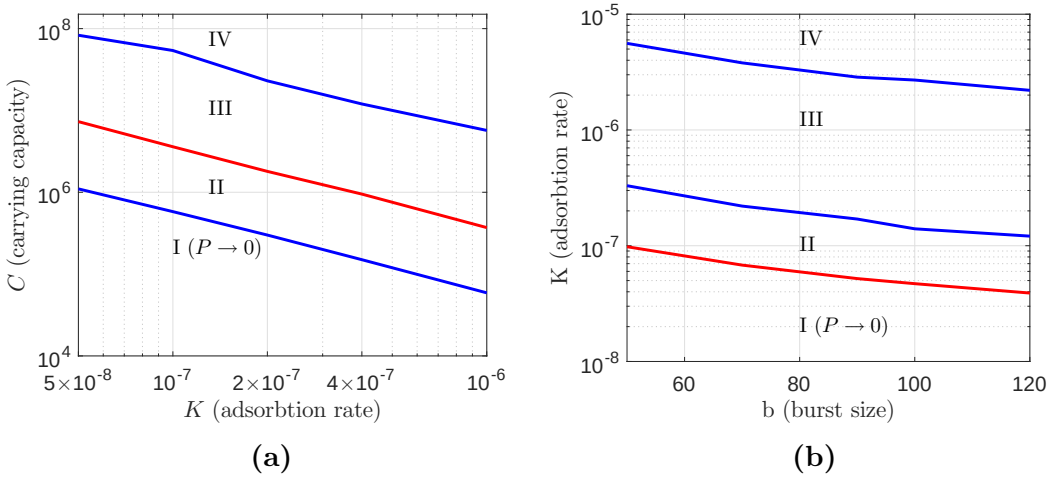

Figure 3.16: Bifurcation diagrams showing possible dynamical regimes in **Model I** (**Nakhon Phanom** province) depending on the parameters K (overall phage adsorption rate); C (carrying capacity of bacteria) and b (burst size of phages). The classification of regimes I-IV is explained in the text. Other parameters are taken from Table 3.1 as default values.

UV intensity level (given by u) across the year and that of the ambient temperature T. We firstly artificially keep the maximal and the minimal temperatures to be constant and only vary u following the historic data. We find that the seasonal dynamics of bacterial numbers remains similar as in the complete model with variable temperature for the default value of the carrying capacity $C = 2\times10^6$ cell/ml (Fig 3.17(a),(b)). This signifies that the phages are mainly controlled by the solar radiation and their high mortality during the period of March-September is caused by a high UV index (u), thus S would increase during that period due to reduction of free phage numbers. This suggestion is confirmed by the fact that in simulations with a seasonal variation of temperature but a constant u, pronounced seasonal patterns are not observed (for high constant UV index as $u = 11$ in Fig 3.17(c),(d) and low constant UV index as $u = 8$ in Fig 3.17(e),(f). On the other hand, in a highly eutrophic environment (e.g. $C = 1\times10^8$ cell/ml), keeping the UV intensity constant does not strongly affect model dynamics, whereas variation of temperature is important for observing seasonal patterns (see Fig 3.18). This signifies that in nutrient rich environment the driving force is host-pathogen (internal) interaction which is promoted by seasonal variation of daily temperature ranges: during

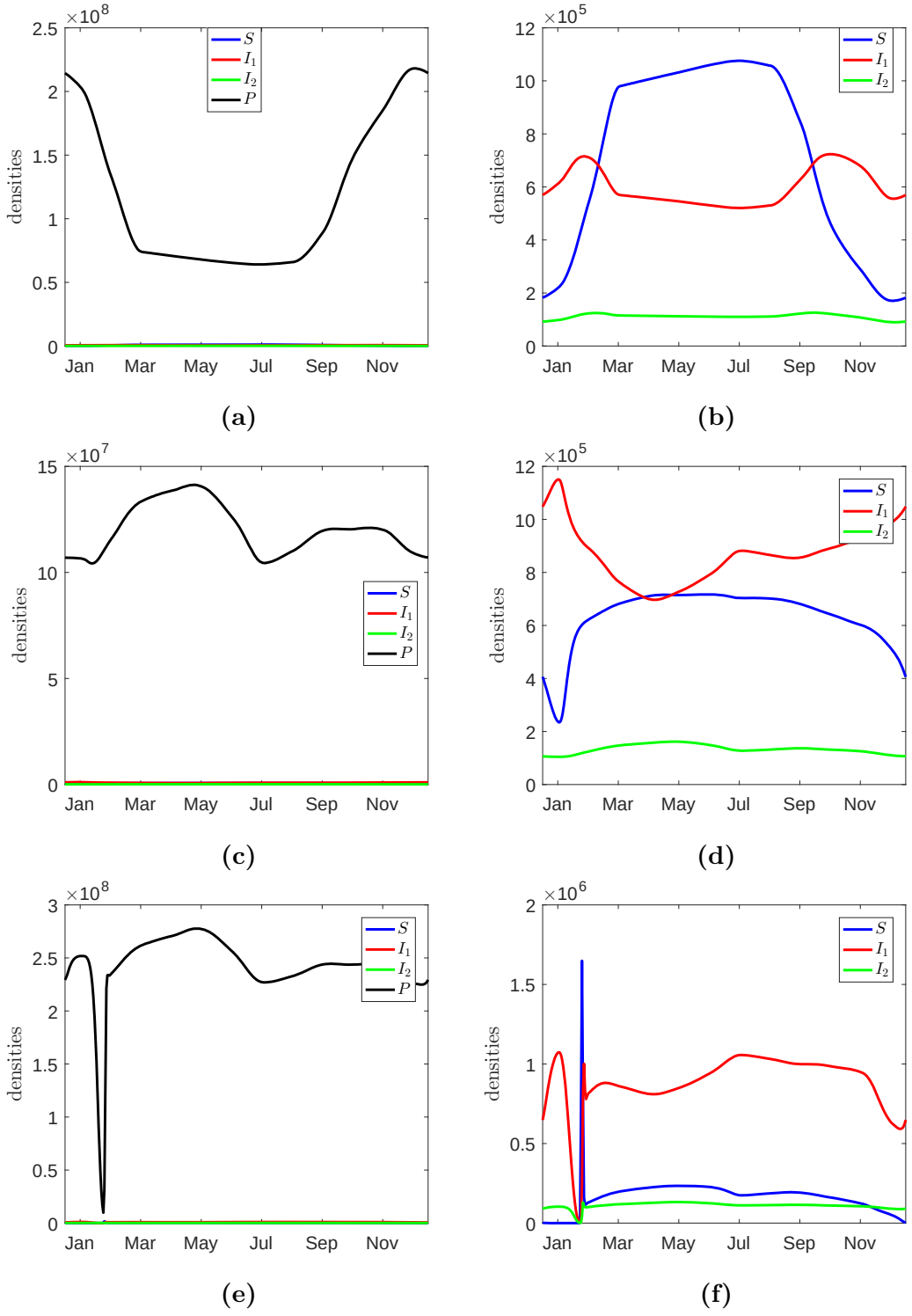

Figure 3.17: Variation of daily average densities of bacteria across the year for $C = 2 \times 10^6$ cell/ml (**Nakhon Phanom** province): Simulations are based on **Model I**, the other parameters are taken from Table 3.1. (a),(b) simulate the scenario that each day high and low weather temperature are kept constant (41 and 15 $^\circ C$) and they don't change with season. (c),(d) and (e),(f) simulate the model for seasonal variable temperature but constant UV index for $u = 11$ and $u = 8$ respectively.

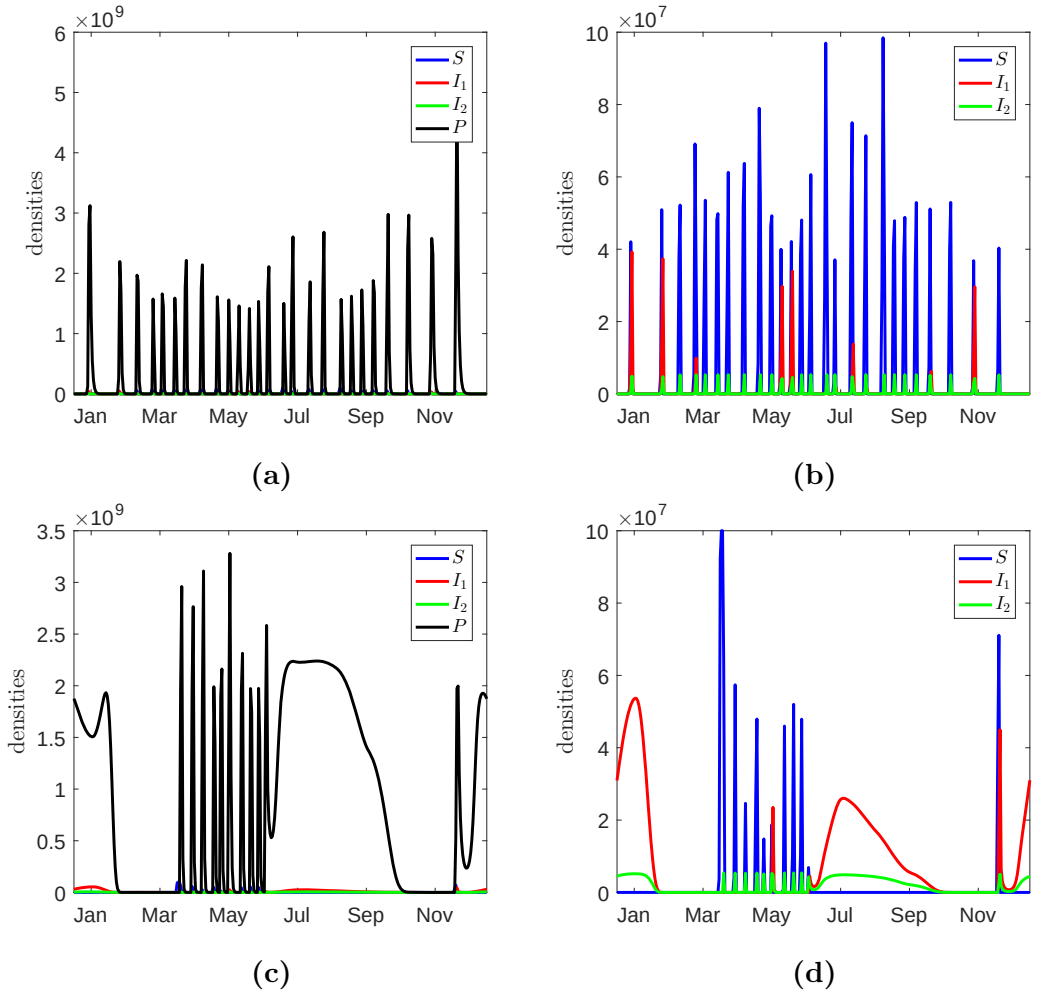

Figure 3.18: Variation of daily average densities of bacteria across the year for $C = 1 \times 10^8$ cell/ml (**Nakhon Phanom** province): Simulations are based on **Model I**, the other parameters are taken from Table 3.1. (a),(b) simulate the scenario that each day high and low weather temperature are kept constant (41 and 15 $^\circ C$) and they don't change with season. (c),(d) simulate the model for seasonal variable temperature but constant UV index for $u = 11$ and $u = 8$ respectively.

warm seasons a large part of the day would correspond to lytic infection cycle with a release of a large number of free phages. The above results hold for both models I and II.

3.3.2 Mathematical analysis of the system for particular temperature values

Here we briefly explore the particular case where the model parameters are constant. In particular, we will consider the cases of constant temperature and independent mortality rate of phage from UV ray. This can be helpful to understand the laboratory experiments which normally conducted under the same conditions. Also, such studies can help to understand what happens in the case where some amount of bacteria and phages are introduced into a living organism of a human or a mammal.

For the sake of simplicity we consider Model I (i.e. non-delayed model). The model equations become:

$$\frac{dS}{dt} = \alpha S\left(1 - \frac{N}{C}\right) - K_S SP, \tag{3.11}$$

$$\frac{dI_1}{dt} = \overline{\alpha} I_1\left(1 - \frac{N}{C}\right) + K_1 SP - \lambda_1 I_1, \tag{3.12}$$

$$\frac{dI_2}{dt} = K_2 SP + \lambda_1 I_1 - \lambda_2 I_2, \tag{3.13}$$

$$\frac{dP}{dt} = -KNP - \mu P + b\lambda_2 I_2. \tag{3.14}$$

The system equilibria are given by

$$\alpha S^*\left(1 - \frac{N^*}{C}\right) - K_S S^* P^* = 0, \tag{3.15}$$

$$\overline{\alpha} I_1^*\left(1 - \frac{N}{C}\right) + K_1 S^* P^* - \lambda_1 I_1^* = 0, \tag{3.16}$$

$$K_2 S^* P^* + \lambda_1 I_1^* - \lambda_2 I_2^* = 0, \tag{3.17}$$

$$-KN^* P^* - \mu P^* + b\lambda_2 I_2^* = 0. \tag{3.18}$$

As seen in Fig 3.3, a non-trivial steady state is possible for only small range of temperature in around optimum transition temperature (T_1). It is difficult to solve

the entire system (3.15)-(3.18) analytically across the entire range of temperature variation. Instead, we analyse the model with two different ranges of temperature. The first one assumes that constant temperature is lower than critical temperature T_1. The second scenarios assumes that the temperature is constant but is higher than T_1. Let's start with the first scenario such that constant temperature T is smaller than $T_1 - 5$ °C, then we obtain

$$\boxed{\begin{aligned}&\overline{\alpha} \simeq \alpha,\\ &K_1 \simeq K_S = \epsilon K,\\ &K_2 \simeq \lambda_1 = 0.\end{aligned}}$$

It can be clearly seen from given diagrams with related parameters in Fig 3.3. Thus the system becomes as below:

$$\alpha S^* \left[1 - \frac{N^*}{C}\right] - \epsilon K S^* P^* = 0, \tag{3.19}$$

$$\alpha I_1^* \left[1 - \frac{N^*}{C}\right] + \epsilon K S^* P^* - 0 I_1^* = 0, \tag{3.20}$$

$$0 S^* P^* + 0 I_1^* - \lambda_2 I_2^* = 0, \tag{3.21}$$

$$-K N^* P^* - \mu P^* + b\lambda_2 I_2^* = 0, \tag{3.22}$$

I_2^* is zero from Eq (3.21). If we substitute this to Eq (3.22), P^* becomes zero since the parameters and densities cannot be negative. Thus, we have two equations (3.19), (3.20) in this system and there are no lytic bacteria and phages: $I_2^* = P^* = 0$;

$$\alpha S^* \left[1 - \frac{N^*}{C}\right] = 0, \tag{3.23}$$

$$\alpha I_1^* \left[1 - \frac{N^*}{C}\right] = 0. \tag{3.24}$$

In this temperature condition, lytic bacteria and phages cannot survive while susceptible bacteria and infected bacteria in lysogenic cycle might stay alive. The sum of the susceptible and lysogenic bacteria densities in the steady state equals

to carrying capacity. Therefore, the non-trivial steady state is

$$\boxed{(S^*, I_1^*, I_2^*, P^*) = (a, C-a, 0, 0)}$$

where $0 \leq a \leq C$ and a depends on the initial values of S and I_1. To make stability analysis, Jacobian matrix can expressed where $F_1 = \alpha S\left(1 - \frac{N}{C}\right)$ and $F_2 = \alpha I_1\left(1 - \frac{N}{C}\right)$ as below:

$$J_1 = \begin{bmatrix} \frac{\partial F_1}{\partial S} & \frac{\partial F_1}{\partial I_1} \\ \frac{\partial F_2}{\partial S} & \frac{\partial F_2}{\partial I_1} \end{bmatrix}_{(S^*, I_1^*)} = \frac{\alpha}{C} \begin{bmatrix} C - 2S^* - I_1^* & -S^* \\ -I_1^* & C - S^* - 2I_1^* \end{bmatrix} = \frac{\alpha}{C} \begin{bmatrix} -a & -a \\ a - C & a - C \end{bmatrix}.$$

Then, the eigenvalues of Jacobian matrix by solving the equation $\det(EI - J) = 0$ are obtained such that $E_1 = 0$ and $E_2 = -\alpha$. Initial values of S is assumed non-zero as it is primary. Fig 3.19 is an example of the model that the constant temperature is 20 °C, the constant mortality rate is 1 day^{-1} and the initial values of all species equal to each other as 10^5 ml^{-1}. The other parameters are as seen in Table 3.1. We see two straight lines which show the densities of susceptible and lysogenic bacteria while the densities of lytic bacteria and phages go to zero.

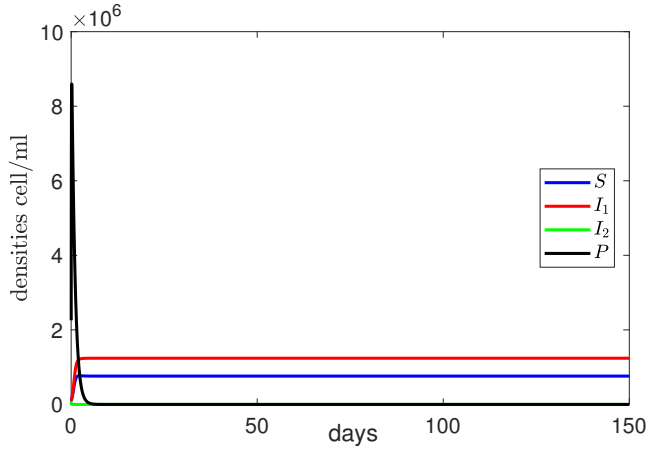

Figure 3.19: The dynamics of the bacteria-phage system predicted by **Model I** with constant temperature as 20 °C and without UV exposure. The fixed parameters are as in Table 3.1, the constant mortality rate is 1 day^{-1} and the initial values of each species are the same as 10^5 ml^{-1}.

According to the second scenario, we assume that the constant temperature value is larger than the optimum transition temperature such as $T > T_1 + 5$. Then some parameters can be found from the diagrams in Fig 3.3:

$$\boxed{\begin{aligned}&\overline{\alpha} = 0\\&K_1 = 0\\&K_2 = K_S = \epsilon K\end{aligned}}$$

Thus the system becomes:

$$\alpha S^*\left[1 - \frac{N}{C}\right] - \epsilon K S^* P^* = 0, \tag{3.25}$$

$$0I_1^*\left[1 - \frac{N}{C}\right] + 0S^*P^* - \lambda_1 I_1^* = 0, \tag{3.26}$$

$$\epsilon K S^* P^* + \lambda_1 I_1^* - \lambda_2 I_2^* = 0, \tag{3.27}$$

$$-KNP^* - \mu P^* + b\lambda_2 I_2^* = 0. \tag{3.28}$$

It is obvious that $\boxed{I_1^* = 0}$ from Eq (3.26) which means there is no lysogenic infection. The new system will be only lytic infection:

$$\alpha S^*\left[1 - \frac{N}{C}\right] - \epsilon K S^* P^* = 0, \tag{3.29}$$

$$\epsilon K S^* P^* - \lambda_2 I_2^* = 0, \tag{3.30}$$

$$-KNP^* - \mu P^* + b\lambda_2 I_2^* = 0, \tag{3.31}$$

Eq (3.30) says $\lambda_2 I_2^* = \epsilon K S^* P^*$. It is substituted to Eq (3.31), then common P^* factors (for nonzero P^*) are cancelled and S^* can be expressed by I_2^* such that

$$-KS^* - KI_2^* - \mu + b\epsilon K S^* = 0$$

$$\Rightarrow \boxed{S^* = \frac{I_2^* K - \mu}{K(b\epsilon - 1)}} \tag{3.32}$$

From the last finding and Eq (3.30), P^* can expressed in terms of I_2^* such that

$$\epsilon K S^* P^* = \lambda_2 I_2^* \;\Rightarrow P^* = \frac{\lambda_2 I_2^*}{\epsilon K S^*} = \frac{\lambda_2 I_2^*}{\epsilon K \frac{I_2^* K - \mu}{K(b\epsilon - 1)}}$$

$$\Rightarrow \boxed{P^* = \frac{(b\epsilon - 1)\lambda_2 I_2^*}{\epsilon(I_2^* K - \mu)}} \tag{3.33}$$

Common factors (S^*) is cancelled in Eq (3.29) and it is rearranged as

$$\alpha C - \alpha S^* - \alpha I_2^* - \epsilon C K P^* = 0. \tag{3.34}$$

Overall, Eqs (3.32) and (3.33) are substituted to Eq (3.34) and rearranged as

$$\alpha C - \alpha \frac{I_2^* K - \mu}{K(b\epsilon - 1)} - \alpha I_2^* - \cancel{\epsilon} C K \frac{(b\epsilon - 1)\lambda_2 I_2^*}{\cancel{\epsilon}(I_2^* K - \mu)} = 0,$$

$$\Rightarrow \alpha C I_2^* K - \alpha C \mu - \frac{\alpha K}{b\epsilon - 1} I_2^{*2} + \frac{\alpha \mu}{b\epsilon - 1} I_2^* + \frac{\alpha \mu}{b\epsilon - 1} I_2^* - \frac{\alpha \mu^2}{K(b\epsilon - 1)}$$
$$- \alpha K I_2^{*2} + \alpha \mu I_2^* - C K b \epsilon \lambda I_2^* + C K \lambda_2 I_2^* = 0,$$

$$\Rightarrow I_2^{*2}\Big(\frac{\alpha K}{b\epsilon - 1} + \alpha K\Big) - I_2^*\Big(\alpha C K + 2\frac{\alpha \mu}{b\epsilon - 1} + \alpha \mu - C K b \epsilon \lambda_2 + C K \lambda_2\Big)$$
$$+ \Big(\alpha C \mu + \frac{\alpha \mu^2}{K(b\epsilon - 1)}\Big) = 0. \tag{3.35}$$

Then, I_2^* can be found by discriminant

$$\boxed{I_2^* = \frac{-x_2 \pm \sqrt{x_2^2 - 4x_1 x_3}}{2x_1}}$$

where Eq (3.35) is expressed by $x_1 I_2^{*2} + x_2 I_2^* + x_3 = 0$. Thus, S^* and P^* can be calculated by being substituted I_2^* to Eq (3.32) and Eq (3.33), respectively. One can see that in a warm environment, lysogenic cycle in viral infection would not be possible. The stability of the equilibrium is given by the corresponding Jacobin

matrix

$$J_1 = \begin{bmatrix} \frac{\partial F_1}{\partial S} & \frac{\partial F_1}{\partial I_2} & \frac{\partial F_1}{\partial P} \\ \frac{\partial F_2}{\partial S} & \frac{\partial F_2}{\partial I_2} & \frac{\partial F_2}{\partial P} \\ \frac{\partial F_3}{\partial S} & \frac{\partial F_3}{\partial I_2} & \frac{\partial F_3}{\partial P} \end{bmatrix}_{(S^*, I_2^*, P^*)}$$

$$= \begin{bmatrix} \frac{\alpha}{C}(C - 2S^* - I_1^*) - \epsilon K P^* & -\frac{\alpha S^*}{C} & -\epsilon K S^* \\ \epsilon K P^* & \epsilon K S^* & -\lambda_2 \\ -K P^* & -K S^* + b\lambda_2 & -K N^* - \mu \end{bmatrix}$$

where

$$F_1 = \alpha S\left(1 - \frac{N}{C}\right) - K_S S P,$$

$$F_2 = K_2 S P - \lambda_2 I_2,$$

$$F_3 = -K N P - \mu P + b\lambda_2 I_2.$$

For example, the densities of species are shown for the period of 150 days, where the temperature is assumed constant 45 °C and the initial density of each species is 10^5 as in Fig 3.20. To make stability analysis, we assumed that the constant mortality rate is 1 day^{-1} and other parameters are as in Table 3.1. Then,

$$S^* = 1.43 \times 10^6,$$

$$I_2^* = 5.15 \times 10^7,$$

$$P^* = 2.40 \times 10^{10},$$

$$J_1 = \begin{bmatrix} -1177 & -12.5 & 0 \\ 719.7 & 0 & 20 \\ -2399 & 2000 & -6.3 \end{bmatrix} \Rightarrow \det(EI - J_1) = \begin{bmatrix} E + 1177 & 12.5 & 0 \\ -719.7 & E & -20 \\ 2399 & -2000 & E + 6.3 \end{bmatrix}.$$

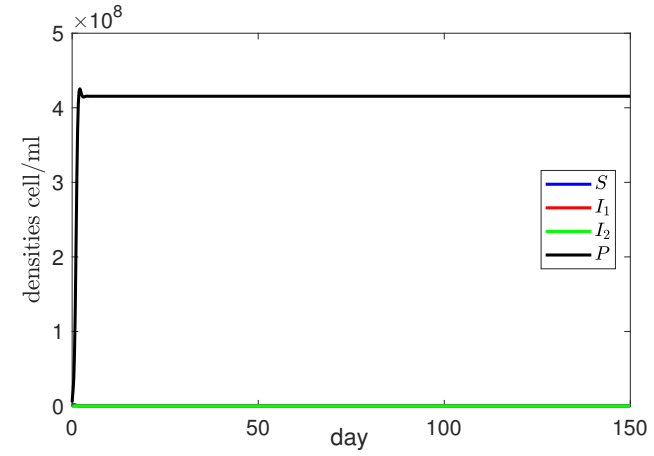

(a)

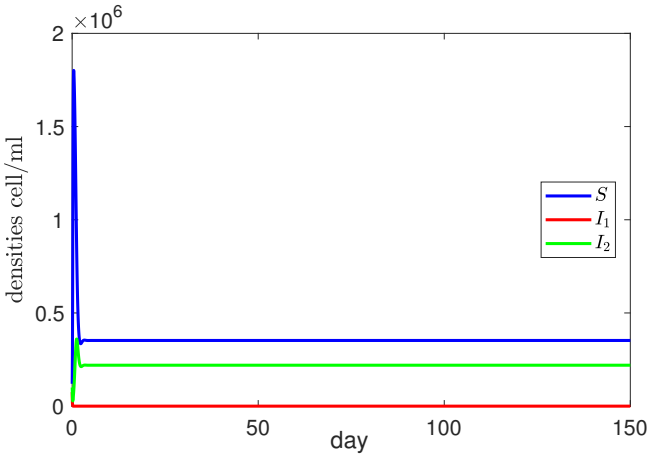

(b)

Figure 3.20: The dynamics of the bacteria-phage system predicted by **Model I** with constant temperature as 45 °C and without UV exposure. The fixed parameters are as in Table 3.1, the constant mortality rate is 1 day^{-1} and the initial values of each species are the same as 10^5 ml^{-1}. The densities of all species are shown in (a) whereas only bacteria densities are shown in (b).

The eigenvalues are as below: $E_1 = -1170$ and $E_{2,3} = -6.5815 \pm 202i$. Therefore, the steady state is stable and it is shown with the diagrams. The density of lysogenic bacteria goes zero.

3.3.3 Analysis the model with different lysogenic growth rate

Finally, we find that some structural modifications of the above models can result in different outcomes and completely different dynamical regimes. In particular, the assumption that the growth rates for the lysogenic and phage-free bacteria are the same for all temperatures (i.e. $\overline{\alpha}(T) = \alpha(T)$) would result in different dynamics in nutrient rich environment (Fig 3.21). Namely, for large values of C the susceptible bacteria S completely disappear from the system: the resulting dynamics consist of oscillating densities of I_1 and I_2, i.e. all bacteria becomes

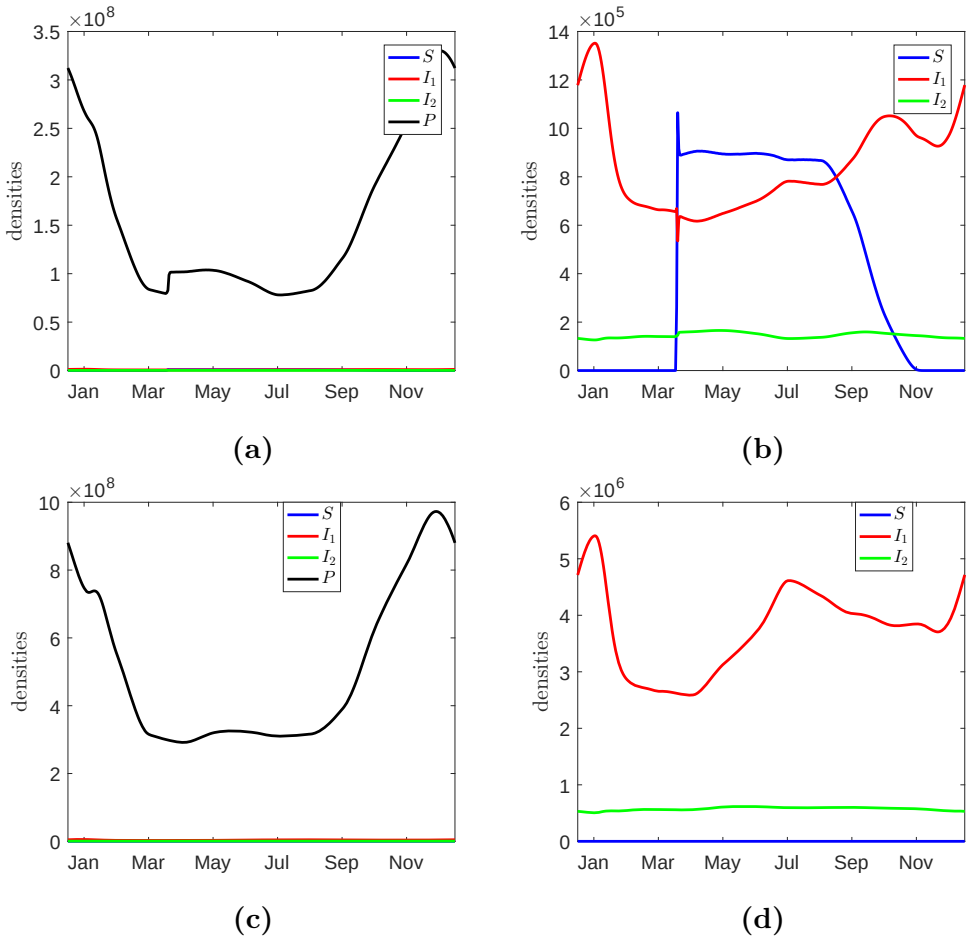

Figure 3.21: Seasonal dynamics of the bacteria-phage system predicted by **Model I** for the temperature and solar radiation records corresponding to **Nakhon Phanom** province in terms of the same growth rates of susceptible and lysogenic bacteria ($\overline{\alpha}(T) = \alpha(T)$ at any temperature values for $C = 2 \times 10^6$ in (a),(b) and for $C = 8 \times 10^6$ (c),(d).

infected (see Fig 3.21(d)). The number of phages is highly oscillating through the day but their daily averaged density stays fairly constant through the year as shown in Fig 3.21(c). Susceptible bacteria don't appear around 5 months in cold seasons with these growth rates (Fig 3.21(b)). Another assumption is that there is no growth of lysogenic bacteria ($\overline{\alpha}(T) = 0$) at any time. All other parameters are fixed as in Table 3.1. In that case, susceptible bacteria can survive at any time even though their density decreases in winter for Nakhon Phanom Province (Fig 3.22(b)). Increase carrying capacity makes change the dynamics as shown in Figs 3.22(c),(d).

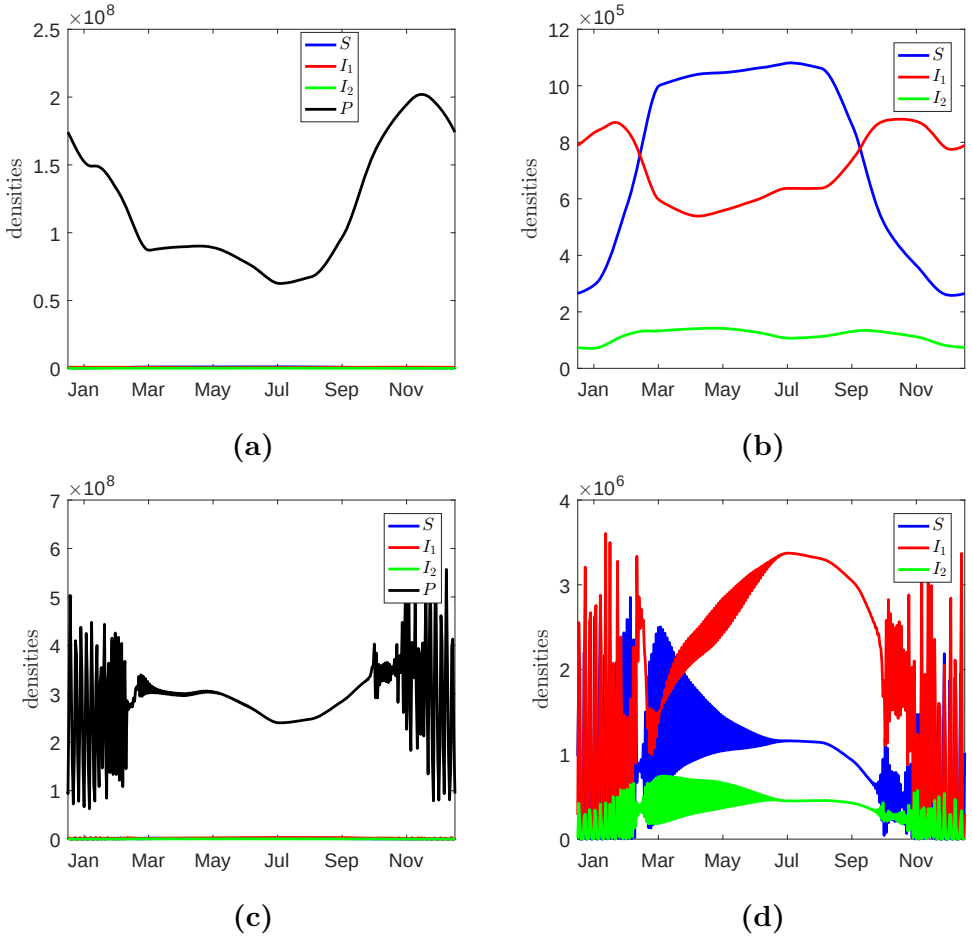

Figure 3.22: Seasonal dynamics of the bacteria-phage system predicted by **Model I** for the temperature and solar radiation records corresponding to **Nakhon Phanom** province in terms of $\overline{\alpha}(T) = 0$ at any temperature values for $C = 2 \times 10^6$ in (a),(b) and for $C = 8 \times 10^6$ in (c),(d).

3.4 Summary for chapter 3

Melioidosis is the infectious disease caused by *B. pseudomallei* in Southeast Asia and around the world. In this chapter, we studied interaction these bacteria and their phages in a well-mixed environment as the stagnant water in the rice field in temporarily fluctuating environment (daily and seasonal variations). This interaction occurs via two types of viral infection: lytic and lysogenic. Our computations were based on realistic estimates of biological parameters (see Table 3.1) and on the historical data on temperature as well as solar radiation (see Figs 3.6, 3.4). The switching between lytic and lysogenic infections would be observed every day across the whole year.

In our study we consider two different modelling frameworks: ODE-based and DDE-based. Both models predict similar results in terms of seasonal and daily dynamics of bacteria-phage interaction. Our simulation predicts high variations of *B. pseudomallei* and phages numbers both daily and seasonally. We find that elevated numbers of susceptible phage-free bacteria S are observed in warm seasons with a high solar radiation. We find that the observed seasonal patterns of dynamics in models are the result of interplay between variations temperature, UV radiation and the nutrient supply level. Model dynamics strongly depends on carrying capacity C. For large C, the regular daily rhythm of variation of species densities becomes perturbed (Fig 3.13(d)). This observation is similar to the classical paradox of enrichment in predator-prey models in well-mixed environment.

On the other hand, some modification of models would change some of our results, for instance considering $\overline{\alpha}(T) = \alpha(T)$. Also, keeping constant temperature or UV index showed their influences on seasonal variation of species densities. Lastly, Mathematical analysis of the equilibrium of Model I with two scenarios: the first says the highest temperature within year is below T_1 and the second the lowest temperature within year is above T_1.

A more accurate description would include considering bacteria in soil. In

this case the distribution of environmental factors such as temperature, nutrients, mortality of phages, etc, will be highly heterogeneous and this might potentially dampen high amplitude oscillations of host-pathogen observed in homogeneous environment as it happens in some predator-prey models [81]. This would be addressed in the next chapter.

Chapter 4

Modelling of seasonal spatio-temporal dynamics of bacteria-phage interaction in soil

4.1 Introduction

A highly pathogenic bacteria *Burkholderia pseudomallei* cause the disease *Melioidosis* which is currently number three out of the most fatal infections after AIDS and tuberculosis [63]. Bacteria grow in water and soil in the endemic areas of South-East Asia and Northern Australia. Soil is a very complicated ecosystem which includes an extraordinary diversity of B. pseudomallei population in melioidosis-endemic areas [64]. Via various means, including human transport, these bacteria can disperse to areas which were initially non-endemic.

In the previous chapter, we examined the dynamics of *B pseudomallei* in the top surface water, where we suggested homogeneity of the environment. However, water in rice field are generally muddy which means non-homogeneous. Also, bacteria are found in the soil below the surface water and can survive until 1 meter depth [72].

This signifies that a more accurate description of bacteria-phage interaction and prediction of their population densities would require considering their heterogeneous spatial distribution in soil. A number of factors determine the distribution of *B. pseudomallei* such as the temperature, pH level, precipitation, water content and the nutrients concentration. In addition, it is well-known that the solar radiation cannot penetrate the soil. This enhances the living condition of their predators (phages) because UV rays may destroy as much as half phages per day in the top water [106]. However, the spatial and temporal dynamics *B. pseudomallei* in their endemic area is not much understood so far and modelling helps in estimating population numbers of bacteria across seasons [72].

In this chapter, we consider a conceptual model of bacteria-phage interaction in vertically spatial space (soil) externally forced by daily and seasonal temperature variations. We suggest that some key parameters as the carrying capacity C of bacteria, mortality of phages μ introduced the previous chapter change with depth. Moreover, temperature dependent parameters (growth rate of susceptible α and lysogenic bacteria $\overline{\alpha}$, transition rates by infection K_1, K_2 and λ_1). We explore the model dynamics within different ranges of the carrying capacity (describing eutrophication of the environment) and compare the results with the previous chapter.

Notations related to chapter 4

t	Time
h	Depth (cm)
T	Temperature ($^\circ C$)
u	Ultraviolet index
$S(t,h)$	Density of susceptible bacteria at time t and depth h
$I_1(t,h)$	Density of infected bacteria in lysogenic cyle at time t and depth h
$I_2(t,h)$	Density of infected bacteria in lytic cyle at time t and depth h
$N(t,h)$	Density of overall bacteria at time t and depth h
$P(t,h)$	Density of bacteriophage at time t and depth h
D_b	Diffusion coefficient of bacteria in soil
D_P	Diffusion coefficient of phages in soil
D_h	Heat diffusion coefficient in soil
ρ_{s}	Bulk density
C_{ps}	Specify heat
k_{s}	Thermal conductivity in soil
$C(h)$	Carrying capacity of bacteria at depth h
C_{surf}	Carrying capacity of bacteria on the soil surface
$\alpha(T)$	Growth rate of susceptible bacteria at temperature T
$\overline{\alpha}(T)$	Growth rate of lysogenic bacteria at temperature T
$\alpha_{\max}$	Maximum intrinsic birth rate of bacteria
$\lambda_1(T)$	Lysogenic process rate to lytic cycle at temperature T
$\lambda_{1\max}$	Maximum lysogenic process rate (transition rate from lysogenic cycle to lytic cycle)
λ_2	Lysis constant
K	Phage adsorption rate
K_S	Effective per bacteria contact rate
ϵ	Adsorption efficiency
$K_1(T)$	Transition rate from susceptible to lysogenic cycle at temperature T
$K_2(T)$	Transition rate from susceptible to lytic cyle at temperature T
T_0	Optimum temperature for growth and lysis ($^\circ C$)
T_1	Optimum transition temperature ($^\circ C$)
$\mu(u)$	Mortality rate of variable u
μ_{m}	Background mortality rate of phages
μ_{s}	Mortality rate of phages on the soil surface
b	Phage replication factor

Units	
$^{\circ}C$	The degree celsius
ml	millilitre
s	second
cm	centimetre
m	metre
kg	kilogram
J	Joule
K	Kelvin
W	Watt

Abbreviation	
Fig	Figure
Eq	Equation

4.2 The model

We model host-parasite interaction between bacteria and bacteriophage in vertically non-homogeneous space (the upper part of soil). The model consists of phage-free bacteria (S) which are susceptible to phage, infected bacteria in lysogenic (I_1) and lytic (I_2) states and free phages (P). Phages and susceptible bacteria take the role of predator (parasite) and prey (host), respectively. The variable h describes the depth level of soil and t is time.

The meaning of the model parameters and the flowchart are the same as in the Model I of the previous chapter and in Fig 3.1 without delay model. α and $\overline{\alpha}$ are growth rates of susceptible and lysgoenic bacteria; K_1, K_2 and λ_1 are transition rates from susceptible to lysogenic and to lytic cycle and from lysogenic cycle to lytic cycle; C is carrying capacity of bacteria; λ_2 is lysis rate; μ is mortality rate of phages; b is burst size; K and K_S are adsorption and infection probabilities of phages; T is temperature variation and u is ultraviolet index, respectively. In addition, D_b and D_P are diffusion coefficients of bacteria and phages.

The model is defined by the system of one-dimensional partial differential equations as below

$$\begin{aligned}
\frac{\partial S(t,h)}{\partial t} &= D_b\frac{\partial^2 S(t,h)}{\partial h^2} + \alpha(T)S\Big[1-\frac{N}{C(h)}\Big] - K_S SP \\
\frac{\partial I_1(t,h)}{\partial t} &= D_b\frac{\partial^2 I_1(t,h)}{\partial h^2} + \overline{\alpha}(T)I_1\Big[1-\frac{N}{C(h)}\Big] + K_1(T)SP - \lambda_1(T)I_1 \\
\frac{\partial I_2(t,h)}{\partial t} &= D_b\frac{\partial^2 I_2(t,h)}{\partial h^2} + K_2(T)SP + \lambda_1(T)I_1 - \lambda_2 I_2 \\
\frac{\partial P(t,h)}{\partial t} &= D_P\frac{\partial^2 P(t,h)}{\partial h^2} - KNP - \mu(u,h)P + b\lambda_2 I_2
\end{aligned} \tag{4.1}$$

where $S(t,h)$, $I_1(t,h)$, $I_2(t,h)$, and $P(t,h)$ are densities of susceptible bacteria, infected bacteria in lysogenic cycle and in lytic cycle and phages at time t and depth h, respectively. The total density of bacteria population is denoted by $N(t,h)$. D_b and D_P are constant diffusion coefficients of bacteria and phages,

respectively. Delay model with space will be considered in the future work.

4.2.1 Parameter estimation

Constant parameters λ_2, K, K_S and b in Model system (3.1) are also constant in this section model and take the same values in Table 3.1. The mortality rate of phages varies with changing UV level on the surface until around 5 cm depth but the sunlight doesn't reach so phages aren't exposed to UV in deeper soil. Thus, we assume constant mortality rate of phages at any depth and time which is called background mortality. We also assume a space-dependent mortality rate which decreases exponentially and becomes almost zero at 5 cm depth of soil because of exposure to UV rays. The overall mortality rate of phages will be as the following

$$\mu(u,h) = \mu_m + \exp(-1.2h)\mu_s(u) \tag{4.2}$$

where $\mu_m = 3$ is constant mortality rate in depth and $\mu_s(u)$ is the mortality rate function around the surface as below:

$$\mu_s(u) = \begin{cases} \mu_c + Y_0 \exp(ku) & \text{in day} \\ \mu_c & \text{at night} \end{cases} \tag{4.3}$$

where u is ultraviolet (UV) index, $Y_0 = 0.0746$ and $k = 0.366$. Thus, we can rearrange it as below

$$\mu(u,h) = \begin{cases} \mu_m + \exp(-1.2h)(Y_0 \exp(ku) & \text{in day} \\ \mu_m & \text{at night} \end{cases} \tag{4.4}$$

or we can clearly say

$$\mu(u,h) = \begin{cases} \mu_m + Y_0 \exp(ku - 1.2h) & \text{in day} \\ \mu_m & \text{at night} \end{cases} \tag{4.5}$$

UV index might be from 0 to 12 and maximum UV index within day is between 8 and 12 for Nakhon Phanom and Sa Kaeo Provinces in Thailand as historical data in Fig 3.4.

We postulate that the carrying capacity is constant with time and seasonal variations as in the previous chapter. We assume that it varies with depth of soil since the number of bacteria with depth decreases according to empirical observations [12]. This might happen because humus and nitrogen contents, pH condition or water content in the soil decrease with depth [72]. There is a little decreasing in moisture condition of the soil from 20-25 cm down to 90 cm of soil even it increases until 20-25 cm from the surface [12]. Brown et al presented the experiment results related to bacteria population densities in several plots and depth levels in [12, p. 290]. We chose the four different plots with 8 depth levels and show them with stars in Fig 4.1. We also calculate regressions of these data

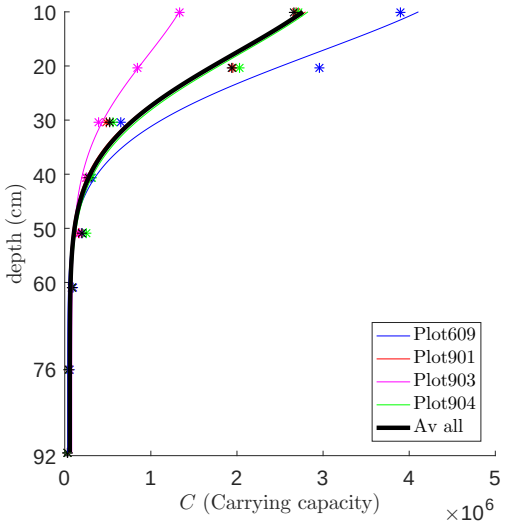

Figure 4.1: The figure shows the densities of bacteria of four different plots in [12]. The density measurement are made for 8 different depth levels of soil starting with 10 cm until 92 cm from the surface. Each colour of Stars and lines shows experimental values and regressions respectively for different plot. The black thick curve shows the average densities of all measurement. It seems that carrying capacity decreases with depth and goes zero.

and showed them with line in the same figures. Using these data, we fit the vertical distribution of the carrying capacity by taking average of the measured bacteria

numbers in four different plots (Fig 4.1). We use the following expression for the carrying capacity as a function of depth:

$$C(h) = C_{\text{surf}} \frac{C_1 \exp\left(-C_2 h^2\right) + C_3}{C_1 + C_3}$$

where $C_1 = 3.2 \times 10^6$, $C_2 = 1.6 \times 10^{-3}$ and $C_3 = 5.9 \times 10^4$ from the above regression funtion (black curve in Fig 4.1). We used GraphPad Prism software to [1] fulfil a non-linear regression. According to the consider function, the carrying capacity has a maximum at the surface and deceases with depth as in Fig 4.2. We suggest that the carrying capacity of the environment is not influenced by seasonal variations.

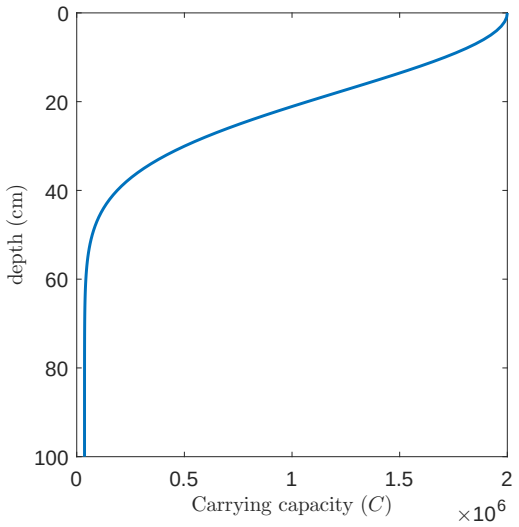

Figure 4.2: The figure shows carrying capacity of bacteria for our model. Its maximum value is 2×10^6 per gram of soil. It decreases greatly until 40 cm from the surface. The function is obtained from average values of the experimental measurement in [12, p. 290].

[1] Scientific 2D graphing and statistics software [1]

Table 4.1: Definitions, units, ranges and the fixed values of constant Parameters

Symbol	**Meaning**	**Unit**	**Range**	**Default Value**
D_b	bacteria diffusion coefficient in soil	$\mathrm{cm}^2\ \mathrm{day}^{-1}$	–	0.1
D_P	phages diffusion coefficient in soil	$\mathrm{cm}^2\ \mathrm{day}^{-1}$	–	0.01
D_h	heat diffusion coefficient in soil	$\mathrm{cm}^2\ \mathrm{day}^{-1}$	–	66.58 [114]
ρ_s	Bulk density	$\mathrm{kg/m}^3$	–	1110.52
C_ps	Specify heat	J/kg K	–	1130
k_s	Thermal conductivity in soil	W/m K	–	0.0967
α_max	maximum growth rate of bacteria	$19 - 27$	day^{-1}	23 [18]
C_surf	bacteria carrying capacity	ml^{-1}	–	2×10^6
K	phage adsorption rate	$\mathrm{ml}^{-1}\mathrm{day}^{-1}$	–	1×10^{-7}
K_S	effective per bacteria contact rate	$\mathrm{ml}^{-1}\mathrm{day}^{-1}$	–	1×10^{-7}
ϵ	adsorption efficiency	–	–	0.3
$\lambda_{1\mathrm{max}}$	maximum lysogenic process rate	day^{-1}	$19.1 - 27.2$	23 [18]
λ_2	constant lysis rate	day^{-1}	–	20 [18]
b	virus replication factor	–	158 ± 54	100 [34]
T_0	Optimum temperature for growth and lysis	°C	$35.6 - 50.6$	38.2 [18]
T_1	optimum transition temperature	°C	$34.81 - 34.84$	34.8
σ	standard deviation of growth rate	°C	$6.7 - 17.4$	9.1
u	ultraviolet index	–	$8 - 12$	–
μ_m	background mortality rate	day^{-1}	–	3
n	transition width	–	$53.7 - 56.3$	55

4.2.2 Vertical and seasonal temperature distribution

Growth rate of susceptible and lysogenic bacteria (α and $\overline{\alpha}$ respectively) and transition rates (K_1, K_2 and λ_1) depend on temperature as defined in Eq (3.3)-(3.7), respectively and so they are temperature dependent variables. Seasonal and daily variations of the surface temperature are assumed the same data as the previous chapter in Fig 3.6. In addition to this variations, the temperature varies with depth of soil in terms of heat equation since the space is non-homogeneous. We model the temperature distribution in soil using heat (diffusion) equation is given by the following:

$$\rho_s C_{ps} \frac{\partial T(t,h)}{\partial t} = k_s \frac{\partial^2 T(t,h)}{\partial h^2} \tag{4.6}$$

$$\Rightarrow \frac{\partial T(t,h)}{\partial t} = D_h \frac{\partial^2 T(t,h)}{\partial h^2} \tag{4.7}$$

where ρ_s, C_{ps} and k_s are bulk density, specific heat and thermal conductivity in soil, respectively. The values of these parameters are from the article Tuntiwaranuruk et al such that $\rho_s = 1110.52$ kg/m^3, $C_{ps} = 1130$ J/kg K and $k_s = 0.0967$ W/m K [114]. Constant diffusion coefficient can be obtained here by

$$\begin{aligned} D_h = \frac{k_s}{\rho_s C_{ps}} = \frac{0.0967}{1110.52 \times 1130} &= 7.7059 \times 10^{-8} \text{ m}^2/\text{s} \\ &= 66.58 \text{ cm}^2/\text{day}. \end{aligned}$$

We use the Dirichlet boundary conditions and assume the boundary values such that

$$T(t,0) = T_s(t)$$
$$T(t,100) = 22^\circ C$$

where T_s is the surface temperature function which is the same as in the previous well-mixed model given by Fig 3.6. We used the same historical weather report

for the surface and calculated heat equation for each time step. The initial value of the temperature distribution $T_s(0)$ is assumed to be linear.

According to heat equation, temperature increases if it is lower and decreases if it is higher with depth until around 20 cm. There are some fluctuation until around 40−45 cm. After this depth level, they approach to the bottom boundary temperature 22 °C and daily temperature variation doesn't appear (see vertical diagram in Fig 4.3).

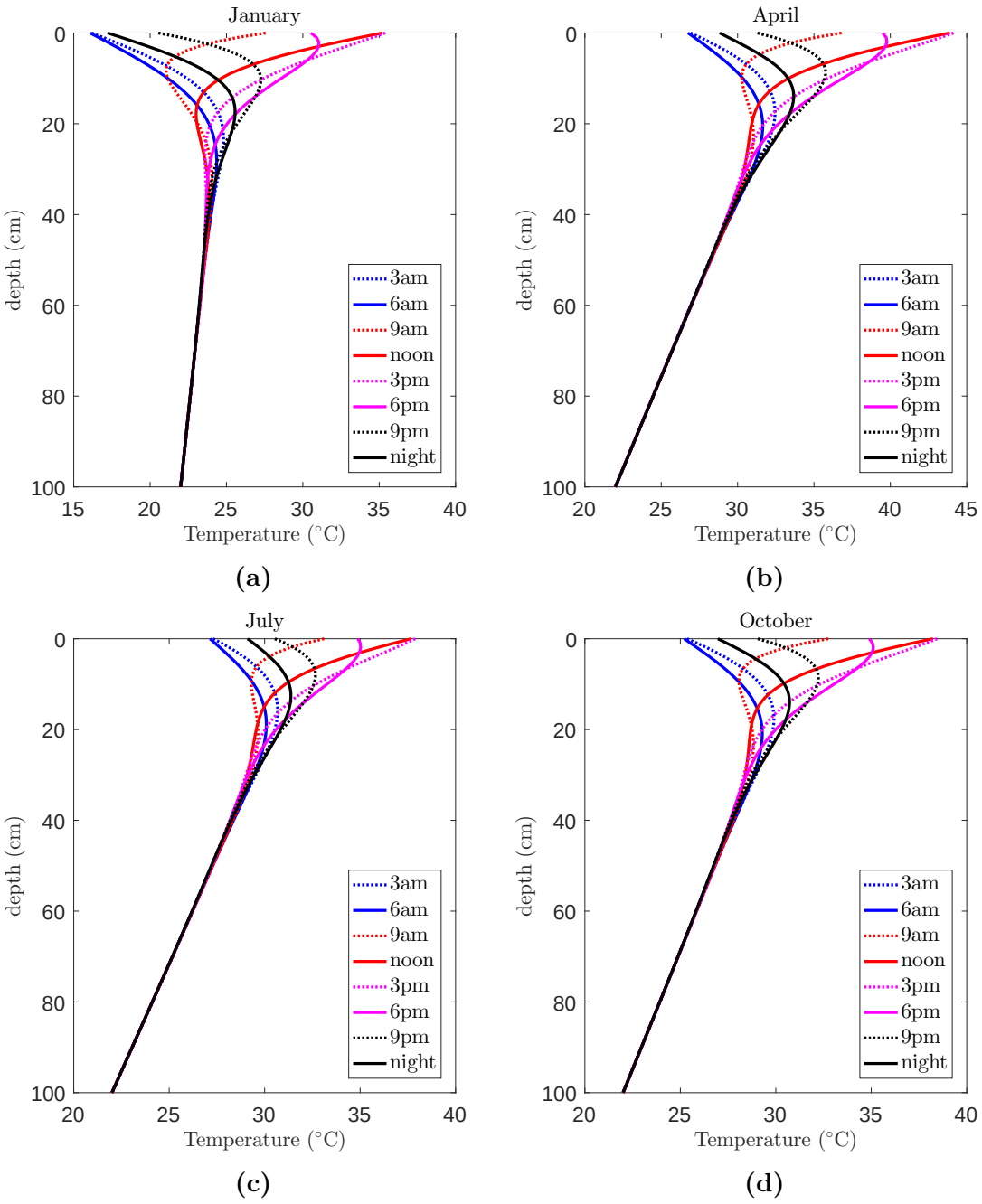

Figure 4.3: This is the result of our computation according to the heat equation. Vertical temperature variation of Nakhon Phanom Province for first day of 4 months (a): January; (b): April; (c): July and (d):October for each 3 hours

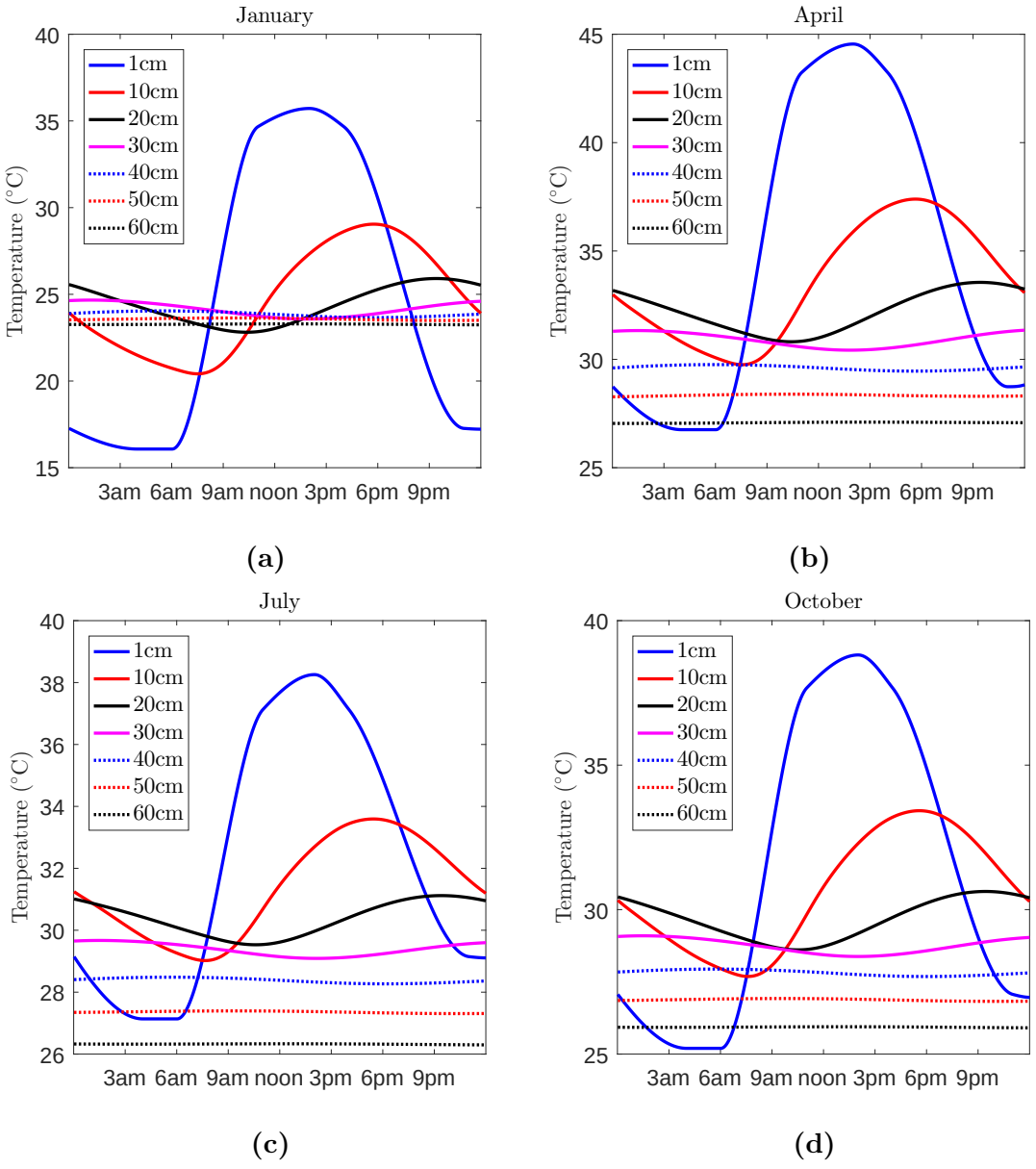

Figure 4.4: Vertical temperature variation of Nakhon Phanom Province for first day of 4 months (a): January; (b): April; (c): July and (d):October for each 3 hours

4.2.3 Diffusion coefficients of bacteria and phages in watery soil

Paddy fields are flooded land which are used for growing rice. Therefore, soil here is either mud or muddy water. There are many effects for distribution of bacteria and phages vertically. For instance, rain water carries bacteria and phage

deeper of soil together with gradient but we ignore them for simplicity. We assume the phage and bacteria vertical diffusion coefficient to be constant.The distribution of *B. pseudomallei* and phages in soil is poorly understood. There is not much information about the diffusion coefficient of the bacteria cells and phages in soil. We estimated the diffusion coefficients of species based on the reasoning below (Modelling).

Diffusion coefficient of bacteria and phage in water are predicted to be 3.5993×10^{-10} $m^2s^{-1} = 0.311$ cm^2day^{-1} and 2.8×10^{-12} $m^2s^{-1} = 0.00242$ cm^2day^{-1}, respectively [124]. However, they should be smaller than that of water in our model. We can explain this with regard to viscosity which is a measurement of the fluid resistance to gradual deformation or thickness of fluid. In this respect, mud has larger viscosity than muddy water whereas it has larger viscosity than water. From Einstein-Stokes equation ($D = \frac{k_b T_K}{6\pi\eta r}$ where k_b is Boltzmann constant [28], T_K is absolute temperature (°K), η is the dynamic viscosity and r is the radius of the spherical particle), the viscosity of liquid is an inverse proportion of the diffusion coefficient [20]. Thus, we can predict the diffusion coefficients of bacteria and phages with known viscosity. For example, honey and peanut viscosity are around 5 and 250 $m^{-1}s^{-1}$.

We also assume that the model has zero-flux boundary condition for all species. We used the same numerical methods as in Chapter 2. We take 0.1 cm spatial step size to get proper results. On the other hand, we need to select optimal time resolution in terms of $\Delta t \leq \frac{(\Delta h)^2}{2D_h}$ where D_h is 66.6 cm/day. That's why it requires too small time step for numerical stability due to large diffusion coefficient

$$\Delta t \leq \frac{0.1^2}{2 \times 66.6} = 7.5 \times 10^{-5} \text{ day}.$$

This causes "out of memory" issue or long time computation in computer. On the other hand, bacteria and phages diffusion coefficients are very low and we don't need to compute this step size for whole model. Instead, we separately compute

heat equation and apply this obtained temperature in depth of soil to our model with larger time resolution (for example $\Delta t = 10^{-3}$ or 5×10^{-4} day).

We compute the average densities of the species (both in terms of spatial and temporal averaging) by using a numerical right Riemann sum. As in Chapter 2, we numerically express the densities of species as vectors (the vectors have 1001 elements for $\Delta h = 0.1$cm in this model) whose elements correspond to the densities for each depth level at time t. Thus, we can find easily the vertically average densities of species at each time step. Daily average densities can be computed using "if" command for each day (via Matlab in this thesis). Thus, each calculation uses 1000 elements. Finally, the values of steps were reduced to compare if the results of simulations remained the same.

4.3 Modelling results

In this study, we observe vertical distribution of *B.pseudomallei* and their predators (phages) according to the seasonal and daily temperature variations. We consider two different types of parameterisations for the mortality rate since the exact shape of such function is not clear from the experimental literature. First, we assume that variable mortality rate depending on sunlight ray on the surface until 5 cm depth in addition to constant mortality rate in any season and at any depth level. The seasonal variation of the population densities according to this mortality rate and other all parameters as mentioned before are shown in Fig 4.5: the densities of bacteria and phages on the surface (a-b); vertical average densities of bacteria until 20 cm (c) and vertical average densities of bacteria until 50 cm (d). However, very high mortality rate of phages in summer (see Section 4.2.1) leads to death of almost all phages on the surface and the density of susceptible bacteria reaches highest values (carrying capacity).

The second parameterisation of the mortality rate consider a spatially homogeneous mortality rate even on the surface by considering rice shading and husk

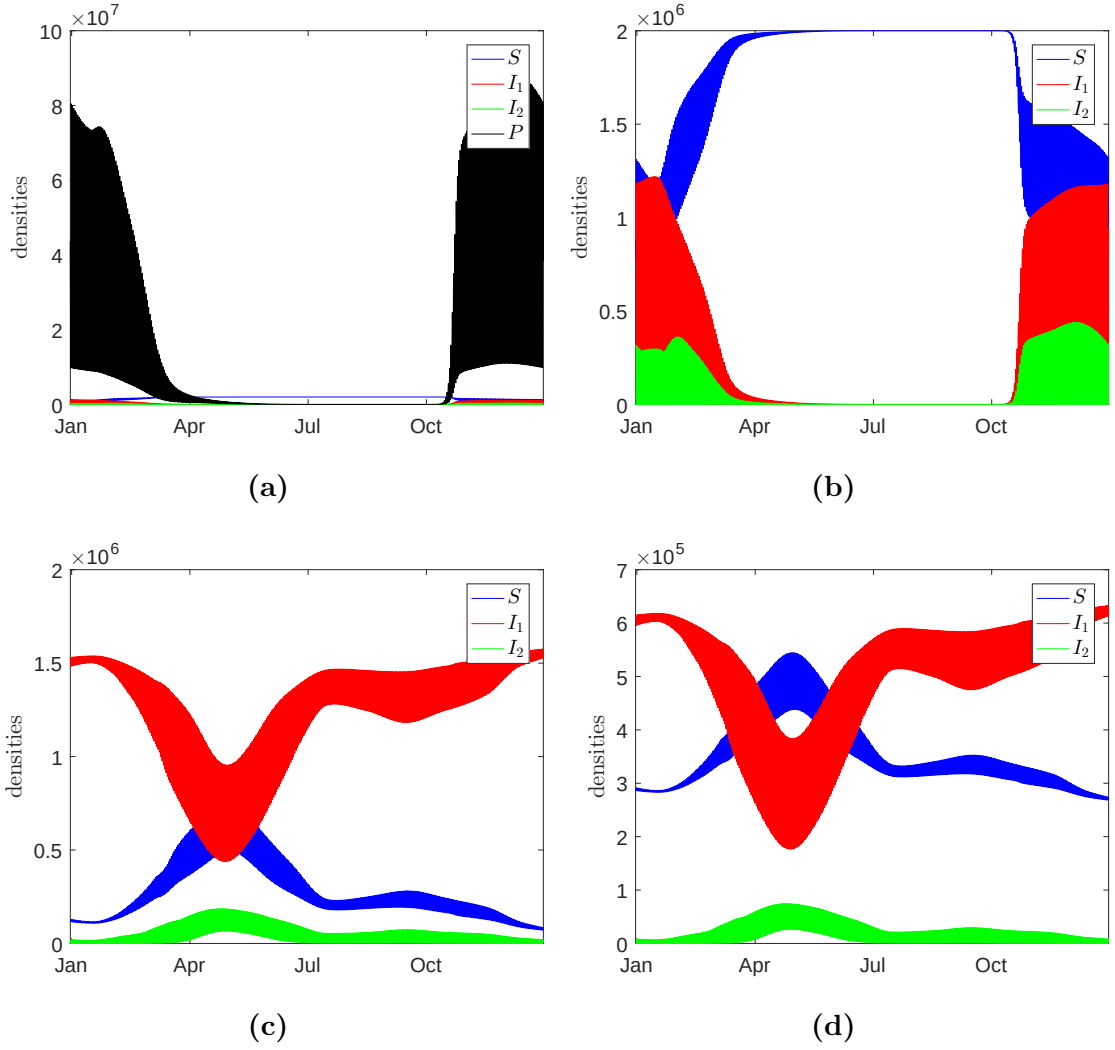

Figure 4.5: (a),(b) show the bacteria and phage population dynamics on the surface of soil for UV dependent mortality rate. (c) and (d) respectively show spatial average densities variation of bacteria until 20 cm and 50 cm

and water which blocks sunlight on the surface. In this case, the densities display smoother seasonal variation due to no UV effect on the surface while they have very large range daily oscillations (see Fig 4.6). Moreover, phages can survive across seasons and susceptible bacteria density is not much high as the previous model. Interestingly, vertical average densities are very similar in the two model (Figs 4.5(c,d); 4.7 and 4.8). The density of susceptible bacteria distributes mostly near the surface and it decreases to zero at around 10 cm. Then, it increase again at around 18 cm and decreases slowly to carrying capacity with depth in Fig 4.9. On the other side, phage density oscillates with depth until around 15 cm, then it

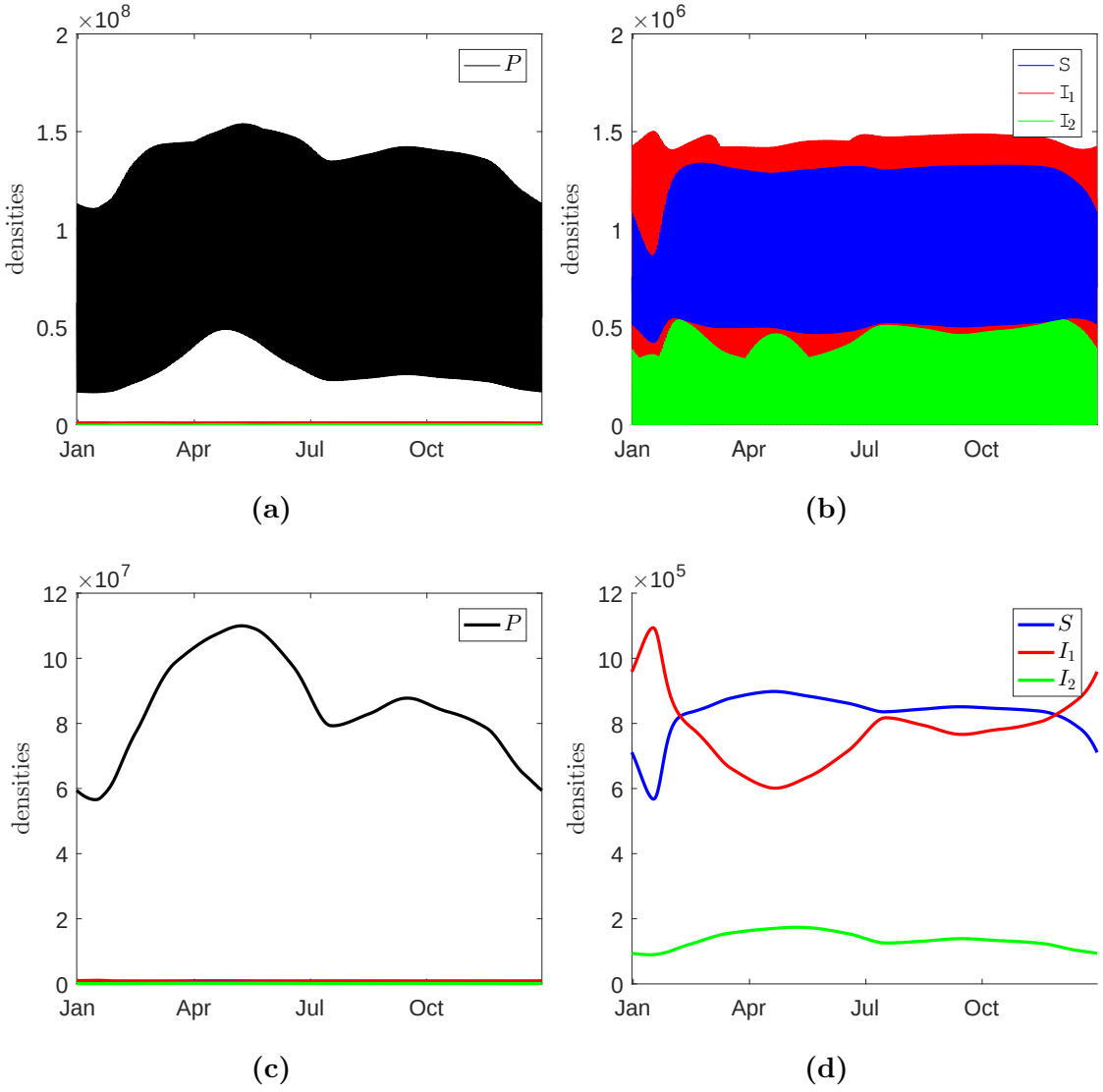

Figure 4.6: (a-b) show the bacteria and phage population dynamics on the surface of soil for constant mortality rate in anywhere. (c) and (d) respectively show daily average densities variation of phages and bacteria on the surface

decreases and becomes almost zero at around 20 cm in Fig 4.12. There is almost no phages at deeper level than 20 cm.

Increasing carrying capacity of bacteria causes oscillation in the densities with time variation. For instance, we showed two different values of carrying capacity as $C = 8\times10^6$ and $C = 1\times10^8$ in Fig 4.13. The oscillations are not related to daily variations. As seen in the figure, increasing carrying capacity increases irregular oscillations. The range between the oscillations decrease with depth for vertical

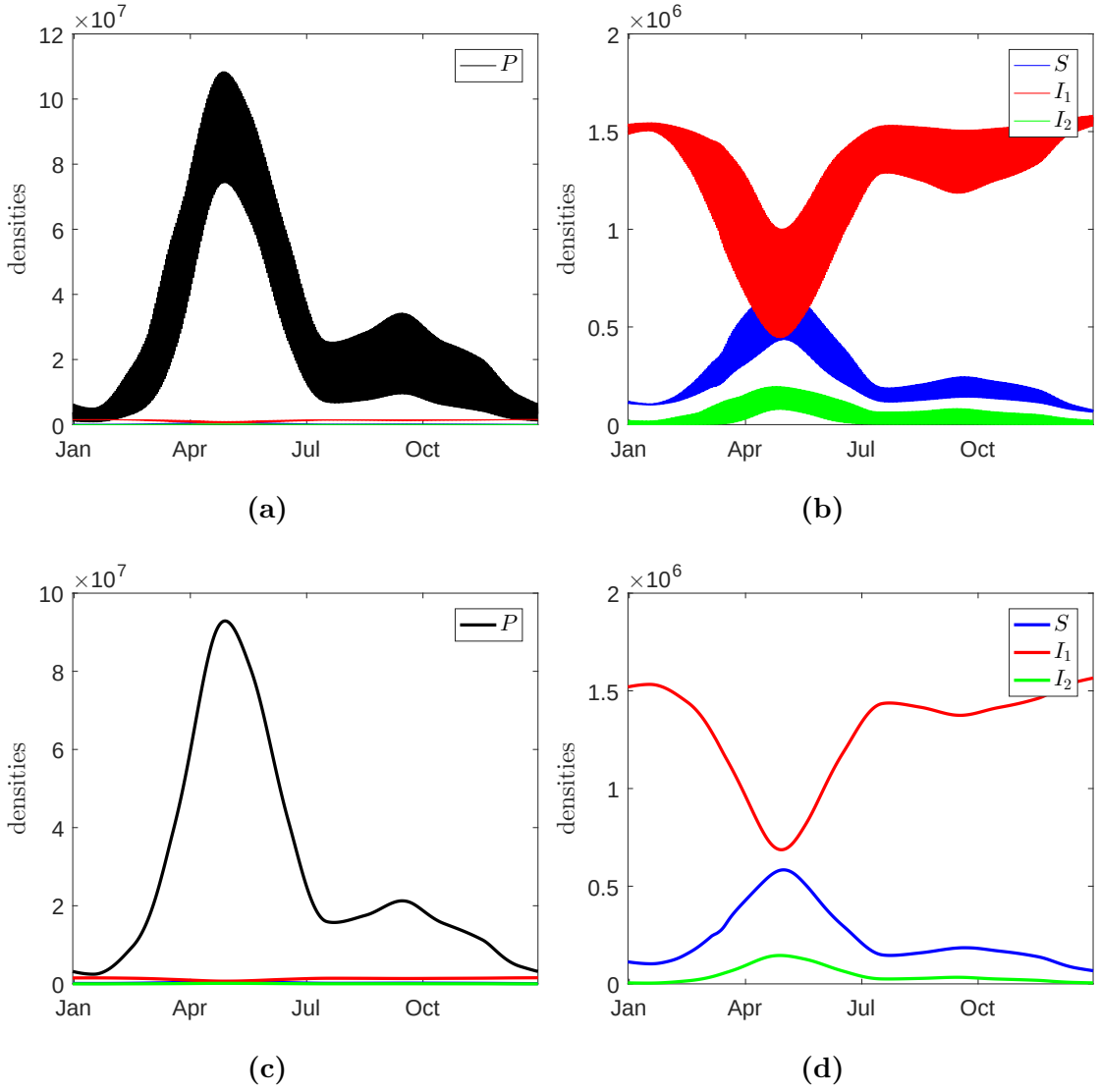

Figure 4.7: (a-b) show the spatial average densities of bacteria and phage population until 20 cm depth of soil for constant mortality rate. (c-d) show both daily and spatially average densities variation of phages and bacteria until 20 cm

average densities until 20 cm and 50 cm as seen in Figs 4.14, 4.15, respectively.

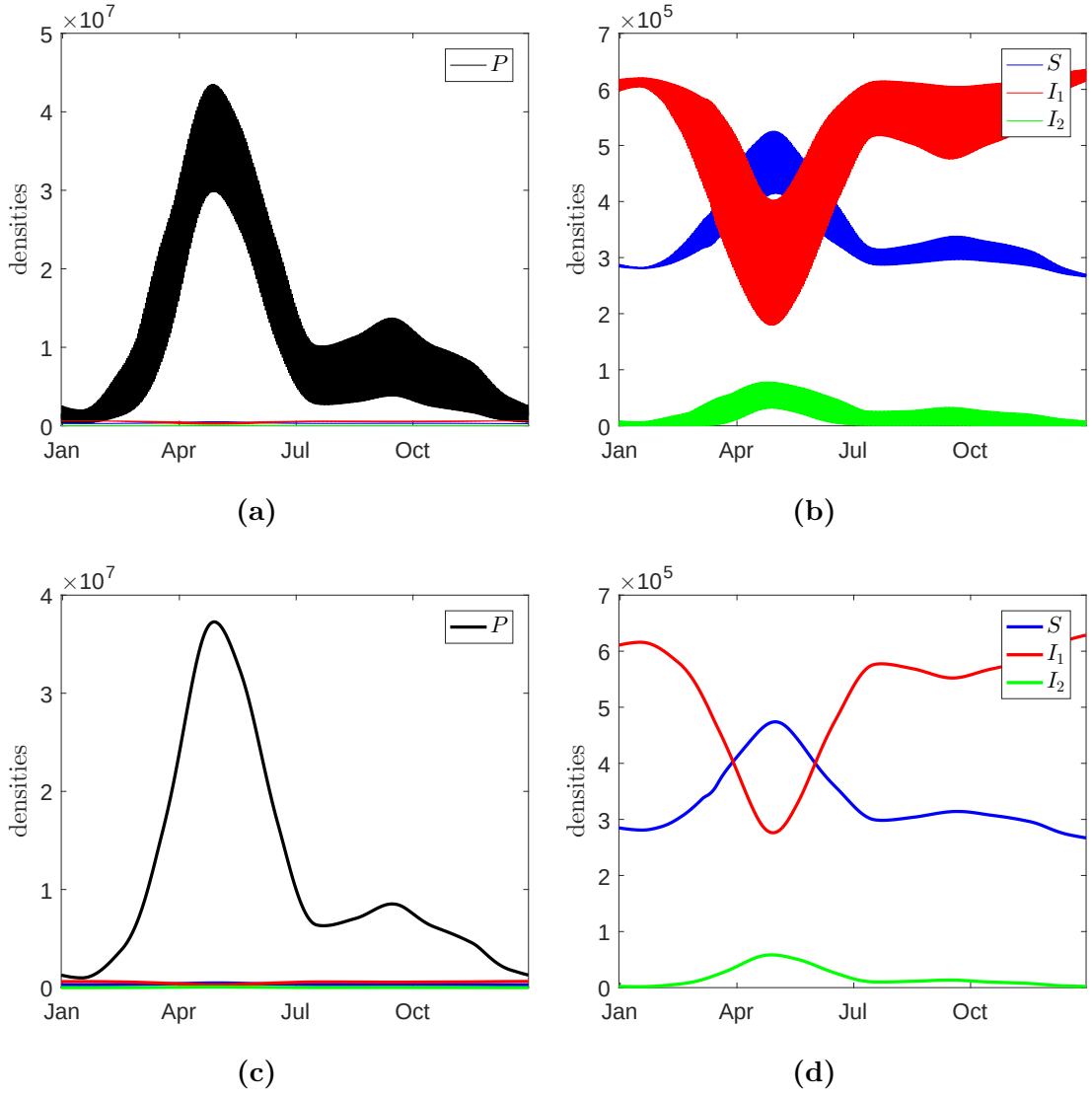

Figure 4.8: (a-b) show the spatial average densities of bacteria and phage population until 50 cm depth of soil for constant mortality rate. (c-d) show both daily and spatially average densities variation of phages and bacteria until 50 cm

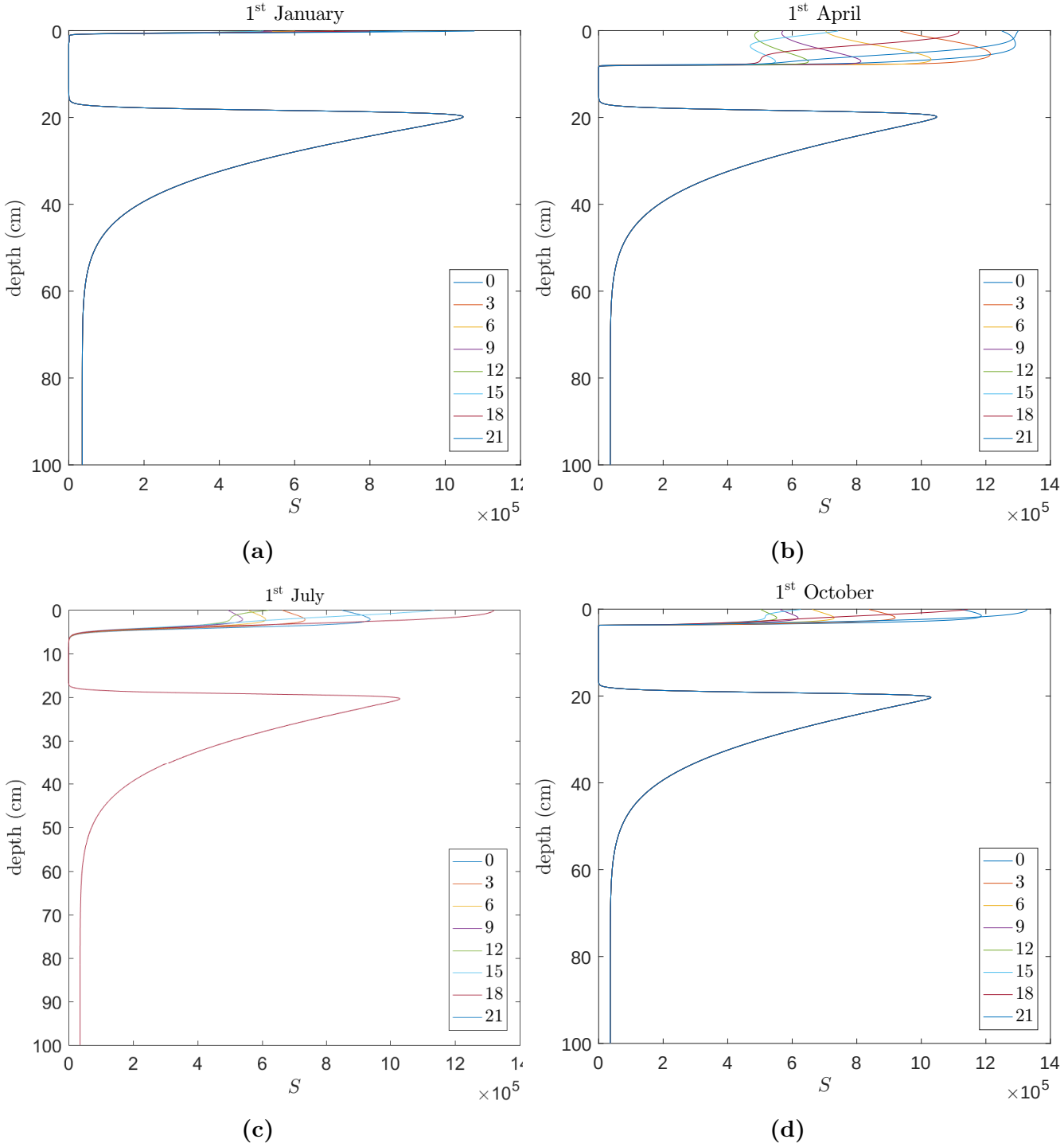

Figure 4.9: Vertical distribution of susceptible bacteria population dynamics in soil on 1st January, 1st April, 1st July and 1st October, respectively.

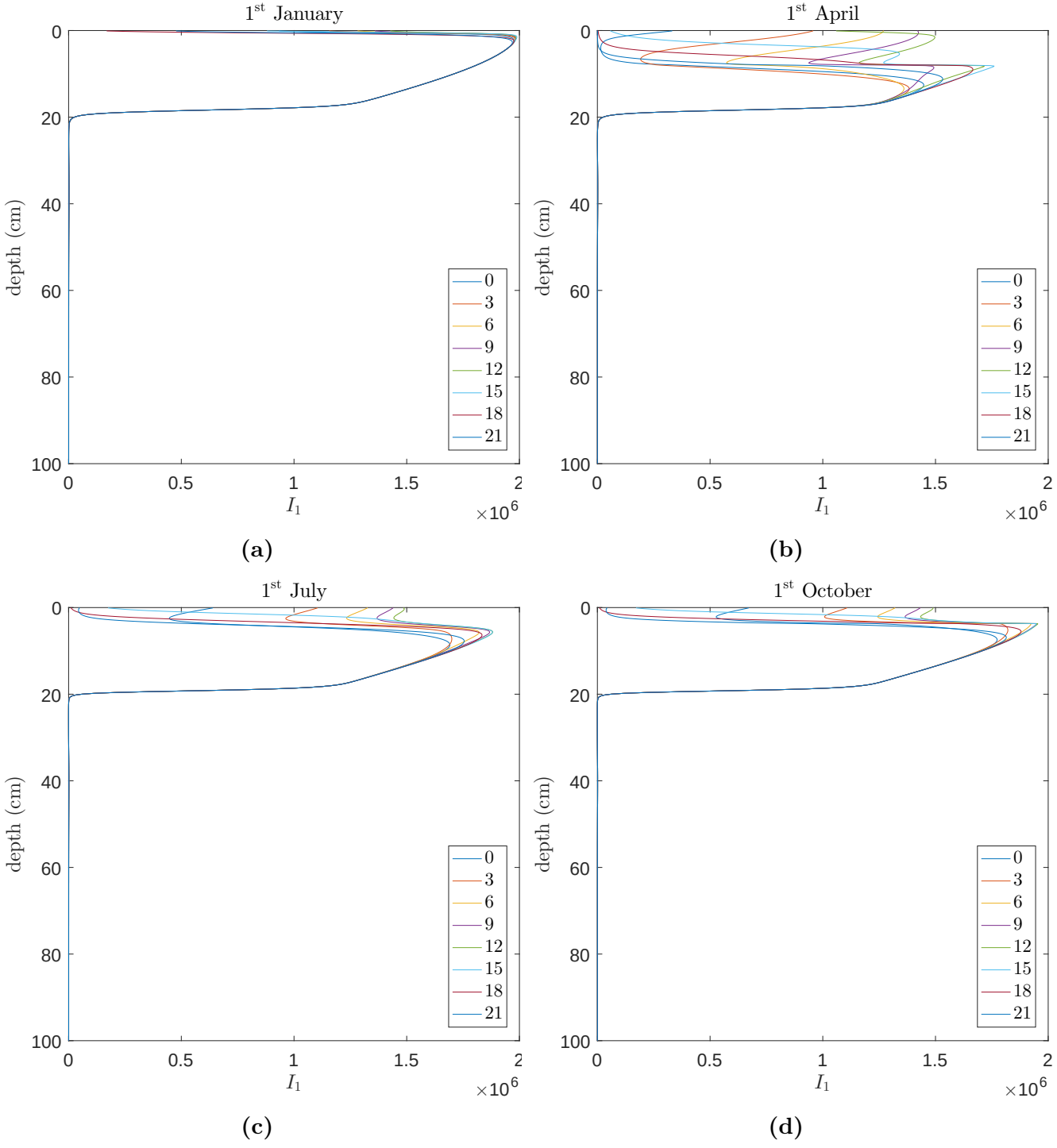

Figure 4.10: Vertical distribution of lysogenic bacteria population dynamics in soil on 1st January, 1st April, 1st July and 1st October, respectively.

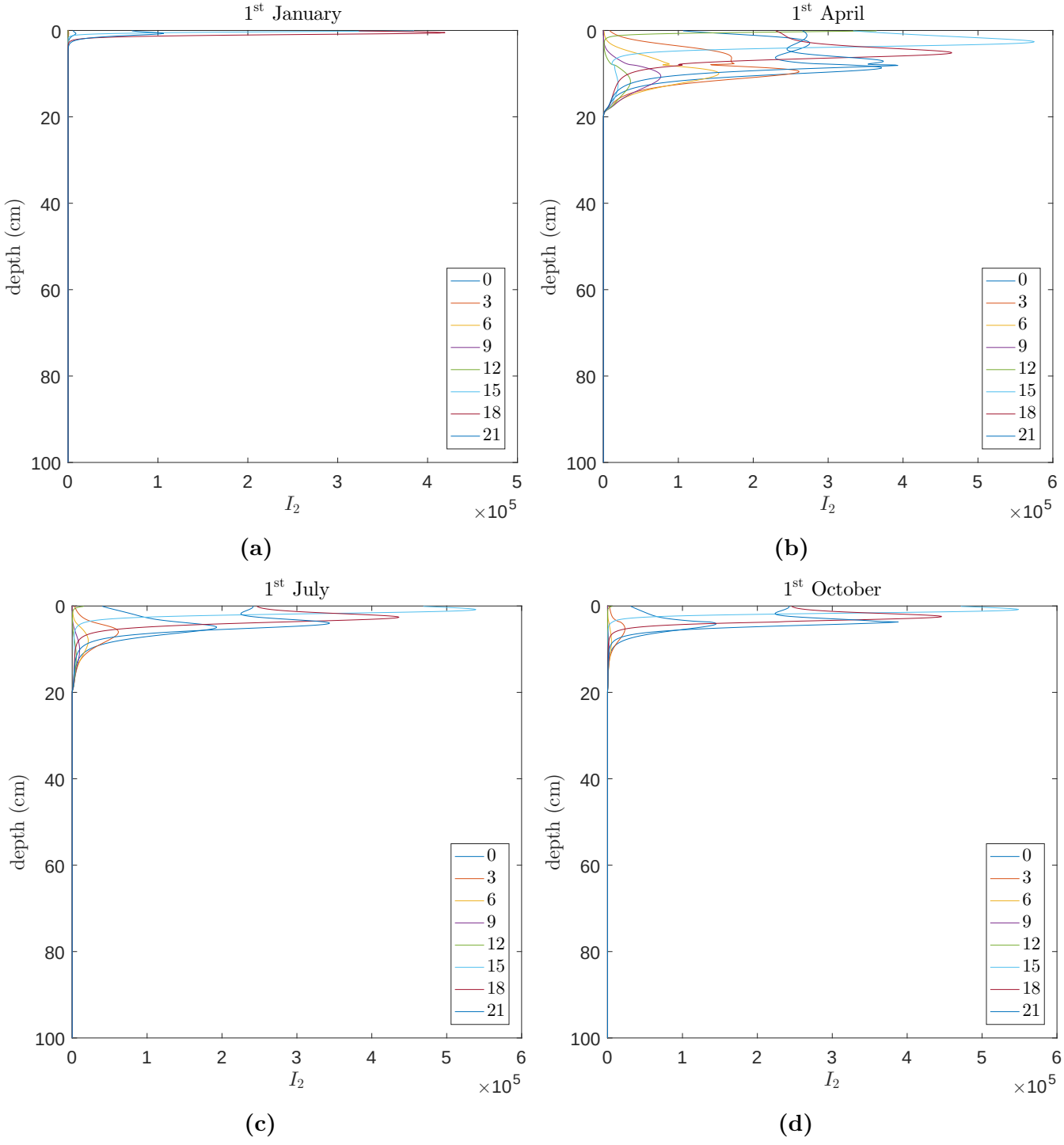

Figure 4.11: Vertical distribution of lytic bacteria population dynamics in soil on 1st January, 1st April, 1st July and 1st October, respectively.

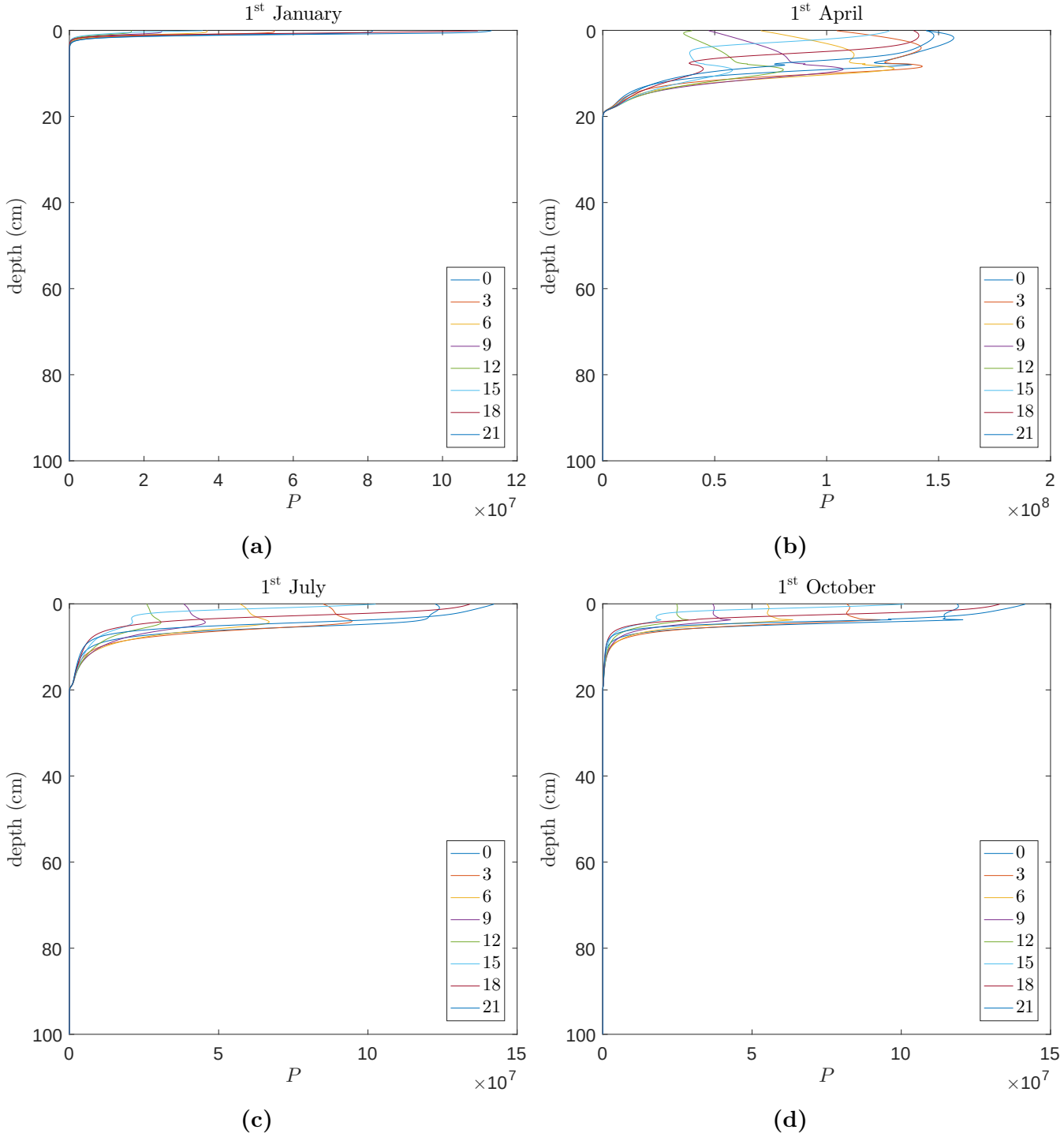

Figure 4.12: Vertical distribution of phages population dynamics in soil on 1st January, 1st April, 1st July and 1st October, respectively.

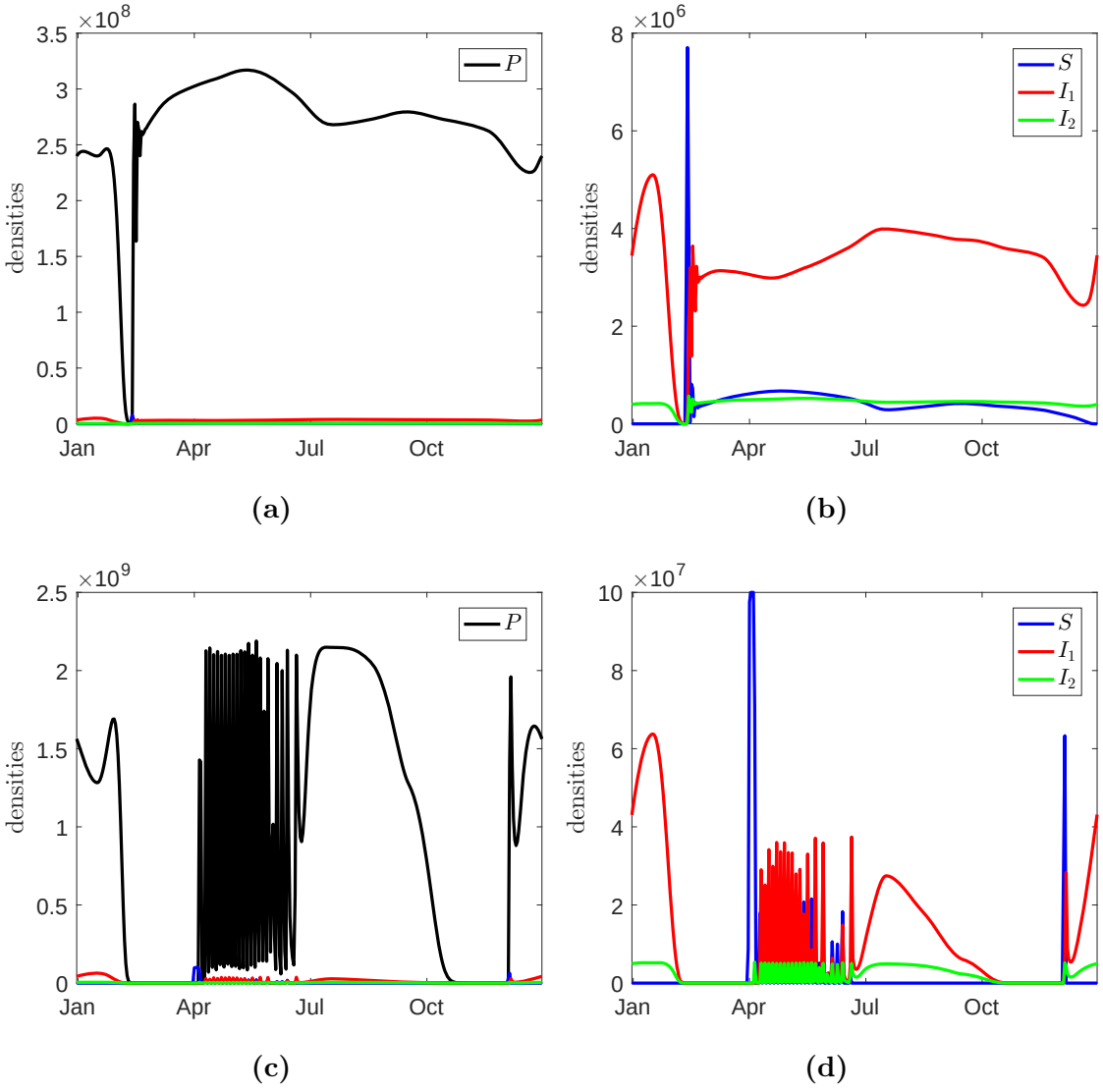

Figure 4.13: Daily average densities of bacteria and phage population dynamics on the surface of soil for different carrying capacity such that (a, b) for $C = 8 \times 10^6$ and (c, d) for $C = 1 \times 10^8$.

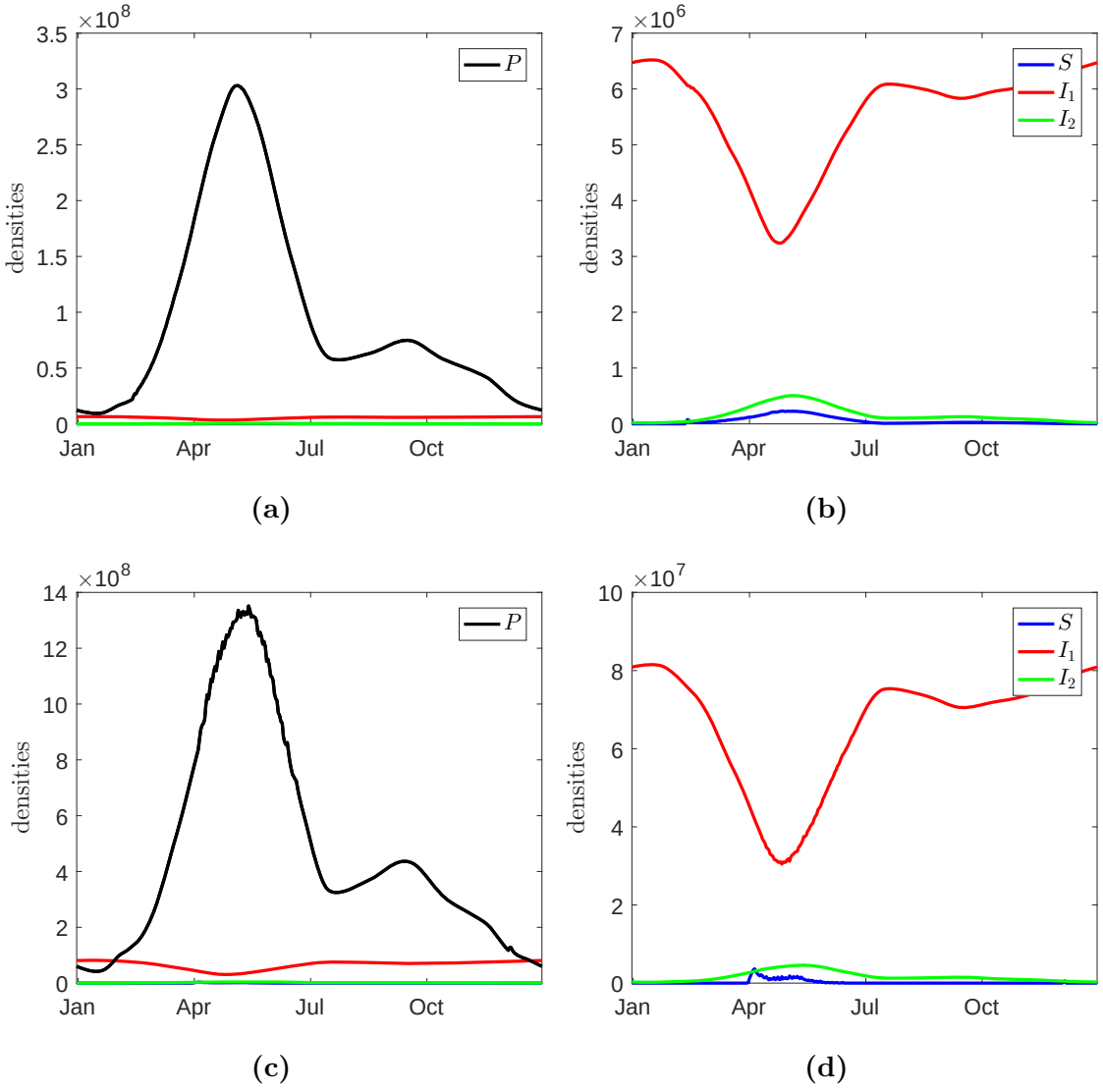

Figure 4.14: Daily and spatially average densities of bacteria and phage population until 20 cm of soil for different carrying capacity such that (a, b) for $C = 8 \times 10^6$ and (c, d) for $C = 1 \times 10^8$.

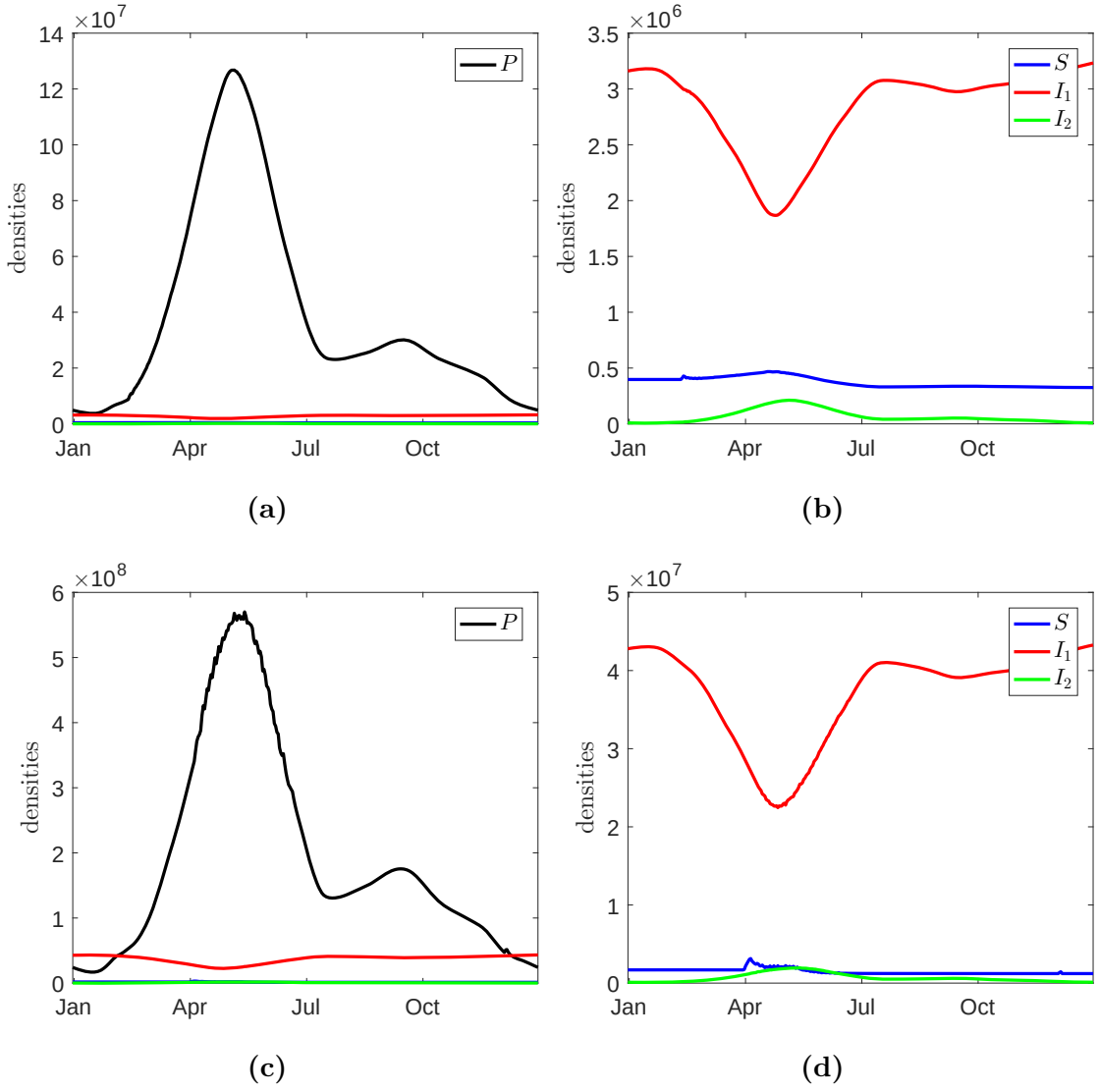

Figure 4.15: Daily and spatially average densities of bacteria and phage population until 50 cm of soil for different carrying capacity such that (a, b) for $C = 8 \times 10^6$ and (c, d) for $C = 1 \times 10^8$.) for $C = 1 \times 10^8$.

4.3.1 Bifurcation Diagram

The mortality rate of phages and carrying capacity of bacteria are important parameters in this model, however, they are not clearly known in experimental literature. We investigate the effect of variation of these parameters on the model dynamics (see Fig 4.16). In that way, we keep the parameters constant except for these two parameters. The result is shown in the bifurcation diagram in Fig 4.16 which is constructed using numerical simulations. We categorise the pattern of dynamics into two regimes (regime I and regime II). Regime I expresses the type of dynamics exhibiting oscillations in species densities due to daily and seasonal variations as shown in Fig 4.6; Regime II corresponds to the pattern of dynamics shown in Fig 4.13. In this regime, there exist some fluctuations in densities which do not match daily and seasonal variations. These two regime can be discerned using dynamics of daily average densities.

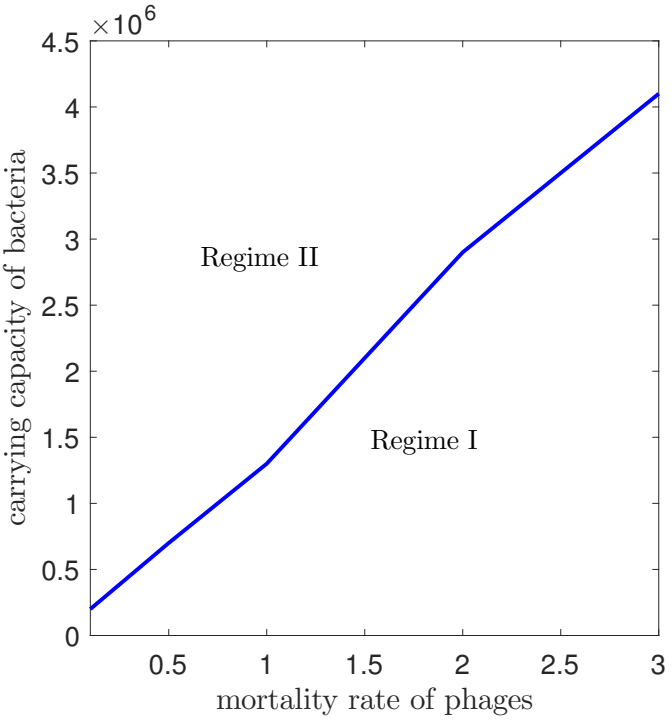

Figure 4.16: Bifurcation diagrams showing possible dynamical regimes in **Nakhon Phanom** province depending on mortality rate of phages (μ) and carrying capacity of bacteria on the surface (C_{surf}). The classification of regimes I-II is explained in the text. Other parameters are taken from Table 4.1 as default values.

4.4 Summary for chapter 4

The third most fatal infectious disease known as textitMelioidosis caused by the pathogenic bacteria *Burkholderia pseudomallei* is mostly reported in Southeast Asian countries as well as the North Australia. In this study, we postulate that the bacteria are controlled by their natural enemies: bacteriophages and we model bacteria–phage interaction in the soil. The main difference between the previous chapter is that here we consider non-homogeneous environment for bacteria and phages caused by the heterogeneity of temperature distribution as well as that of the carrying capacity. This model should be considered as the first step of modelling bacteria-phage interactions in soil since we assume here the simplest possible model based on reaction-diffusion equations: more advanced models should be considered the soil system in more detail (e.g. by including hydrological regimes).

We consider two different parameterisations of the mortality of phages. Our modelling results show that in the case of a homogeneous mortality of phages the spatial distribution of susceptible bacteria is generally very smooth across all seasons unlike in the case of a spatially variable mortality rate with the maximum on the surface. We also find that generally the densities of species in soil shows a seasonal trend both in terms of their distribution and the absolute numbers. For example, in April-July the vertical average densities of susceptible-lytic bacteria and phages increase while the density of lysogenic bacteria decreases (for instance Fig 4.7). This would signify a higher risk of decision acquisition.

We found that for sub-populations of phages and bacteria distributed very close to the surface (from the surface to around 20 cm depth) their density is almost zero except susceptible bacteria. Moreover, their density follows the levels of the carrying capacity after around 18 cm depth as in Fig 4.2. An increase in the carrying capacity causes oscillation in addition to daily and seasonal as in the previous chapter. Moreover, if the mortality rate of phages is increased then irregular oscillation doesn't happen even for a large carrying capacity (see

Fig 4.16). Spatial averaging can also dampen the overall dependence of population numbers on the carrying capacity. The obtained results can resolve the paradox of enrichment of bacteria-phage interaction in soil.

Chapter 5

Conclusion

Mathematical modelling in ecology has started with a single species model; interactions with other species where described by constant parameters [71, 92, Chapter 1]. The initial single species population models have been improved by adding time delay to describe incubation or maturation time, age structure or seasonal variations [13]. Including dynamical predation was a great step in model development. Mathematical models in ecology often assume the space to be homogeneous or assume that the whole system is well-mixed. This makes it easy to mathematically analyse the model properties, in particular to find system equilibria and further perform stability analysis. If the inhabited area is small enough or the species are most homogeneously distributed on the region, then, indeed there is no need the diffusion calculation. The model will only be the reaction form with ODEs. However, in many cases such assumption is too simplistic and including heterogeneity in either vertical or/and horizontal directions might be very efficient to get more realistic results for ecological predictions. By adding the diffusion to the local interaction model described by ordinary differential model we obtain a system of reaction-diffusion equation which can be very rich in terms of dynamical patterns. Such system was firstly studied by Fisher and Kolmogorov et al in 1930s [31, 51].

Species in communities live together and interact with each other. Mathematically, this can be described as dynamical feedbacks affecting the target population. Therefore, population dynamics of each species is affected with the interactions which might be competition within or between species for resources or space; symbiosis; or predator-prey. In this study, we focused on predator-prey (host-parasite) model [92, chapter 3], which is fundamental in nature. Our study covers three main aspects of mathematical modelling of predator-prey interactions which are in the focus of the literature:

- influence of spatially heterogeneity on ecosystem stability and persistence (Chapters 2,4)
- role of external forcing on predator-prey (host-parasite) interactions (Chapter 3,4)
- influence of parametrisation of model terms on modelling outcomes (Chapters 2,3,4).

As important ecological case studies, we considered a tri-trophic plankton interaction across a vertical water column in Chapter 2 and bacteria-phage interaction under temperature variation in Chapters 3,4.

Below we briefly discuss the main results and outline the main findings of Chapters 2,3,4.

5.1 Tri-trophic plankton model (Chapter 2)

In Chapter 2, we considered a top-down control in a tri-trophic system under eutrophication (high nutrient resource for prey) with a fast moving top predator (copepods) and two lower levels which are herbivorous microzooplankton and primary producer, phytoplankton. We assumed that the spatial distribution of copepods is determined that of the two lower trophic levels as contrary to [61],

where it was assumed that the top predators only consumed microzooplankton. The main goal of this chapter is to contribute to solving the paradox of enrichment for omnivorous copepods (which both consume microzooplankton and phytoplankton). Mathematically we used a system of integro-differential equations including diffusion terms to take into account fast movement of top predators as slow movement of intermediate predators.

We took into account different possible scenarios of predation in the same system: considering omnivorous and non-omnivorous top predator; different types of functional responses (food selection without switching and active switching which is only for omnivorous copepods). Also we examined the system without spatial heterogeneity and saw that stabilization of system was impossible in well-mixed space even though the model with carnivorous top predator. However, the stability is possible in spatial model. This confirms some previous findings on the crucial role of space in the top-down control and stabilization of eutrophic ecosystems [24, 96, 81]. Model 1 which has carnivorous copepods result in coexistence for all levels in large range of parameter values Fig 2.2. Primary producer density is very high in this hypothesis Fig 2.6.

However, phytoplankton would also be usually an important resource for copepods (top predator) in addition to intermediate grazers [8, 32, 82]. In that way, we considered more realistic interactions with omnivorous top predator. In this condition, we analysed the model with two different functional responses of copepods. The first one is none-switching functional response (called Disk equation or Holling Type II) as in Eq 2.7. However, this resulted in extinction one of the grazers (copepods or microzooplankton) in almost any realistic values of parameters (see Fig 2.8). Coexistence of all species is only possible very narrow and unrealistic parameter values (see Fig 2.8(d)). Thus, Model 2 has more realistic copepods feeding but the response is unrealistic.

On the other hand, introducing the strong assumption of active switching behaviour of copepods (covered by Model 3) can result in the coexistence of the

entire food web with the density of primary producers remaining low (see Fig 2.12). This conclusion is comparable with the main results of [38], who found that active switching promotes coexistence of microzooplankton and copepods. Interestingly, some experimental works have also confirmed that active switching of copepods can stabilize a tri-trophic planktonic system [37], although these experiments were conducted on such a short time scale that the population dynamics of copepods were neglected.

5.2 Bacteria-phages interaction (Chapters 3−4)

Gram negative bacterium B. Pseudomallei causes a very dangerous infectious disease known as Meliodosis. The disease is hazardous for people in some areas in Southeast Asian countries and North Australia. It kills around 40% of infected people which are generally agricultural workers in rice fields. Recently it was suggested (based on empirical observation) that bacteriophage (phage for short) would potentially control the dynamics of this dangerous bacteria. However, this important controlling mechanism by phages has been disregarded by the large part of the literature related. Therefore the interaction between the bacteria and phages and its modelling are very crucial. The main particularity of the considered bacteria-phage interaction is that it is temperature-dependent. This means that only they lyse (kill) bacteria at high temperatures whereas at lower temperatures they display a lysogenic life cycle Fig 1.6. The switch between infection type (from lytic or lysogenic) would be determined by the ambient temperature [104].

Due to temperature dependent viral infection, mathematical modelling of this type of interaction is very complex. There have been constructed a number of models of bacteria-phage interaction but they all ignored lysogeny and the influence of temperature variation; also they assume phage to be lytic. Thus considering temperature-dependent bacteria-phage interaction it would be insightful for understanding the main features of seasonal dynamics of phage free bacteria which actually cause infection. This work is the first one to build a mathematical model

related to lysogeny. Our mathematical model includes both infected cycles depending on temperature condition (daily and seasonal oscillations) reported for endemic regions in Thailand (e.g. see Fig 3.6).

Almost all parameters in this chapter are from either literature or unpublished experimental results. The experimental results on the temperature dependent lysogeny demonstrated that the switch between lysogenic and lytic way of infection occurs at around $T_1 = 35°\text{C}$ (see Fig 3.2(a)) which was previously underestimated in the literature. Switching between lytic and lysogenic infection happen each day depending on daily temperature variation (Typical ranges in two provinces (Nakhon Phanom and Sa Kaeo) of Thailand showed in Fig 3.6. We also find that the newly estimated value of the adsorption constant of the phages (which was earlier an unknown parameter) allows the persistence of phages in the models. In addition to temperature values, the models are based on historical data on ultraviolet (UV) index since phage mortality strongly depend on UV sun radiation at the surface.

Our model simulation predicts high variations of density of *B. pseudomallei* and phages numbers for both daily and seasonally. We found that elevated numbers of susceptible phage-free bacteria S (meaning a higher disease acquisition risk for agricultural workers) were observed in warm seasons with a high solar radiation. This is consistent with the reported cases of disease acquisition in some regions in Thailand such as Nakhon Phanom [7]. On the other hand, the same publication does not reveal a pronounced annual variation of infection cases in Sa Kaeo as it is observed in the model. Such a discrepancy can be probably explained by different environmental conditions in terms of soil properties (resulting in different carrying capacity C) which would damp the seasonal variation in the system. We found that the observed seasonal patterns of dynamics in models were the result of interplay between variations temperature, UV radiation and the nutrient supply level. Our models also predict highly variable daily oscillations of densities of phage-free, lytic, lysogenic bacteria whereas the overall number of

bacteria remained nearly constant (Fig 3.8). There is also a strong dependence of resultant dynamics on the nutrients content of the environment which is described by the carrying capacity C. We observed that enrichment of the environment (e.g. by heavily using agricultural fertilises or using rice fields as temporally fish farms) would result in outbreaks of high bacterial numbers during warm seasons. In this case, the regular daily rhythm of variation of species densities becomes perturbed: few days characterised by very low densities of bacteria would follow by the periods of high bacterial densities (Fig 3.13(d)).

In our study we considered two different modelling frameworks: ODE-based and DDE-based. Interestingly, both models predicted similar results in terms of seasonal dynamics of bacteria-phage interactions as well as regarding the dependence of patterns on the key model parameters such as C, b and K. This demonstrates the robustness of our modelling approach and strengthen theoretical predictions. On the other hand, some modification of models, for example, considering $\overline{\alpha}(T) = \alpha(T)$ would modify some of our results obtained with systems (1)-(2). In particular, we found the possibility of a complete eradication of phage-free bacteria. A more thorough investigation of the model robustness towards structural changes would be needed. This demonstrates the sensitivity of model outcomes to parameterisation of model terms.

Our modelling approach may suggest few possible directions towards direct testing of our main hypothesis that phages are the main control agent of bacteria. It follows from our model that excluding phages from the system will result in ceasing large amplitude oscillations of densities of bacteria and phages due to host-pathogen cycles and this can be easily checked empirically. In this case, the presence of pronounced variation of density of phage-free bacteria on the scale of the day or several days might indicate a strong control of B. pseudomallei by its phages. Another important indicator of the page control would be measuring the ratio between the bacterial and phage numbers in the field.

Finally, simulations using our models indicate possible directions for disease

management and monitoring of *B. pseudomallei*. In particular, one can estimate the risk of disease acquisition (determined by S) across seasons. In the case the environment does not allow a large number of bacteria (which signifies low values of carrying capacity C), the risky period coincides with high level of UV radiation, which causes mortality of phages (Fig 3.7(a)). Under this scenario, the practical recommendation would be to avoid agricultural activities in the field in the evening (e.g. 9pm) when the number of phage-free bacteria is amplified after the day (see Fig 3.8). In the case of nutrient rich environment - which can be a result of extensive use of fertilises or fish farming – the recommendations would be different. Under a large degree of eutrophication, one should expect high density outbreaks of phage-free bacteria during warm seasons (see Fig 3.13). The duration of such outbreaks can be form several days to a month characterised by high densities of S regardless the time of the day. Thus, a better monitoring of disease under intensive use of fertilises is strongly recommended to report the start of the outbreak. Finally, our numerical experiments with a high background mortality rate μ_c of phages shows that this would cause an increase of susceptible bacteria density S thus enhancing the corresponding risk of disease acquisition. This has a direct application to disease management and control. Some herbicides can also kill the phages thus this using would amplify the risk of disease acquisition and should be implemented with a great care.

In Chapter 3, we built bacteria-phage interactions model in a well-mixed environment as the stagnant water in the rice field. A more accurate description would include considering bacteria in the soil, where the distribution of environmental factors such as temperature, nutrients, mortality of phages, etc will be highly heterogeneous. Thus the well-mixed model from Chapter 3 was extended of a spatial model in Chapter 4. Here we used a reaction-diffusion modelling framework.

In Chapter 4, the mortality rate of phage would be changed since UV cannot penetrate deep inside soil (or watery soil). Therefore, we assumed the mortality

rate is constant with depth and time. Another key parameter is carrying capacity bacteria which is decreases with depth. We saw very smooth density of susceptible bacteria across the year on the surface of soil but highly wide range of daily oscillation. This is because mortality rate of phages were assumed to be constant. However, with depth seasonal effect became clear as seen vertical average densities until 20 cm and 50 cm from the surface in Figs 4.7, 4.8, respectively. The variable μ was also assumed near the surface but the results were not much realistic Fig 4.5. The susceptible bacteria reached the carrying capacity in around 8 month of year since phage goes zero.

From the simulated vertical distributions we can see that switching in infection type (i.e. lytic or lysogenic) appeared in the first 20 cm. After 20 cm only susceptible bacteria can survive (which means disease risk still exist) and the susceptible density keeps carrying capacity as in Fig 4.2.

In this thesis, we constructed two bacteria-phage models which consider in homogeneous and heterogeneous space. For the well-mixed environment (Chapter 3) we compared ordinary differential equation model with a delay model and found only very small differences between the two. This indicates that the model is structurally not sensitive with respect to the modelling approach used. This makes our results promising for future forecasting of bacteria-phage interaction.

5.3 Future perspectives

In this thesis, we construct bacteria-phage model on the surface of water based on ODE and DDE. As a future work, the interaction model in soil (heterogeneous environment) can be strengthened by DDE. Resistant bacteria to phages could be thought as a future work. This causes to death of attacking phages, thus, it prevents new phage replication and release. We examined this with adsorption efficiency but we do not have density of resistant bacteria. Finally, a more accurate model of bacteria dispersal in soil should be used in updated models (e.g. including

vertical transport of bacteria by water). Also, some more advanced numerical methods can be used to take into account smallness of the transition layer, where the mortality of phages sharply drops to low values.

Bibliography

[1] Analyze, graph and present scientific data faster than ever with prism 7! `https://www.graphpad.com/scientific-software/prism/`. Accessed : December 31, 2017.

[2] Alligood, K. T., Sauer, T. D., and Yorke, J. A. (2000). *Chaos: An Introduction to Dynamical Systems*. Springer Science & Business Media.

[3] Beckmann, A. and Hense, I. (2007). Beneath the surface: Characteristics of oceanic ecosystems under weak mixing conditions–a theoretical investigation. *Progress in Oceanography*, 75(4):771–796.

[4] Beretta, E. and Kuang, Y. (1998). Modeling and analysis of a marine bacteriophage infection. *Mathematical Biosciences*, 149(1):57–76.

[5] Beretta, E. and Kuang, Y. (2001). Modeling and analysis of a marine bacteriophage infection with latency period. *Nonlinear Analysis: Real World Applications*, 2(1):35–74.

[6] Bhatia, S. (2016). *Food Biotechnology*. CRC Press.

[7] Bhengsri, S., Baggett, H. C., Jorakate, P., Kaewpan, A., Prapasiri, P., Naorat, S., Thamthitiwat, S., Tanwisaid, K., Chantra, S., Salika, P., et al. (2011). Incidence of bacteremic melioidosis in eastern and northeastern thailand. *The American journal of tropical medicine and hygiene*, 85(1):117–120.

[8] Boyd, C. M., Smith, S. L., and Cowles, T. J. (1980). Grazing patterns of copepods in the upwelling system off peru. *Limnology and Oceanography*, 25(4):583–596.

[9] Boyd, P. W. (2002). Environmental factors controlling phytoplankton processes in the southern ocean1. *Journal of Phycology*, 38(5):844–861.

[10] Breckels, M. N., Bode, N. W., Codling, E. A., and Steinke, M. (2013). Effect of grazing-mediated dimethyl sulfide (dms) production on the swimming behavior of the copepod calanus helgolandicus. *Marine drugs*, 11(7):2486–2500.

[11] Bremermann, H. J. (1983). Parasites at the origin of life. *Journal of mathematical biology*, 16(2):165–180.

[12] Brown, P. E. (1912). *Bacteria at different depths in some typical Iowa soils*. Agricultural Experiment Station, Iowa State College of Agriculture and the Mechanic Arts.

[13] Busenberg, S. and Cooke, K. (1993). Delay differential equations models. In *Vertically Transmitted Diseases: Models and Dynamics*, pages 143–170. Springer Berlin Heidelberg.

[14] Cairns, B. J., Timms, A. R., Jansen, V. A., Connerton, I. F., and Payne, R. J. (2009). Quantitative models of in vitro bacteriophage–host dynamics and their application to phage therapy. *PLoS Pathog*, 5(1):e1000253.

[15] Campbell, A. (1961). Conditions for the existence of bacteriophage. *Evolution*, pages 153–165.

[16] Carlotti, F. and Nival, S. (1992). Moulting and mortality rates of copepods related to age within stage: Experimental results. *Marine ecology progress series. Oldendorf*, 84(3):235–243.

[17] Chavez, F. P., Buck, K. R., and Barber, R. T. (1990). Phytoplankton taxa in relation to primary production in the equatorial pacific. *Deep Sea Research Part A. Oceanographic Research Papers*, 37(11):1733–1752.

[18] Chen, Y., Chen, S., Kao, C., and Chen, Y. (2003). Effects of soil ph, temperature and water content on the growth ofburkholderia pseudomallei. *Folia microbiologica*, 48(2):253–256.

[19] Clokie, M. and Galyov, E. (2017). Unpublished data.

[20] Edward, J. T. (1970). Molecular volumes and the stokes-einstein equation. *J. chem. Educ*, 47(4):261.

[21] Edwards, A. M. and Brindley, J. (1996). Oscillatory behaviour in a three-component plankton population model. *Dynamics and stability of Systems*, 11(4):347–370.

[22] Edwards, A. M. and Brindley, J. (1999). Zooplankton mortality and the dynamical behaviour of plankton population models. *Bulletin of mathematical biology*, 61(2):303–339.

[23] Edwards, C. A., Batchelder, H. P., and Powell, T. M. (2000a). Modeling microzooplankton and macrozooplankton dynamics within a coastal upwelling system. *Journal of Plankton Research*, 22(9):1619–1648.

[24] Edwards, C. A., Powell, T. A., and Batchelder, H. P. (2000b). The stability of an npz model subject to realistic levels of vertical mixing. *Journal of Marine Research*, 58(1):37–60.

[25] Edwards, K. F., Thomas, M. K., Klausmeier, C. A., and Litchman, E. (2015). Light and growth in marine phytoplankton: allometric, taxonomic, and environmental variation. *Limnology and Oceanography*, 60(2):540–552.

[26] Egilmez, H. and Morozov, A. Y. (2016). Tri-trophic plankton models revised: importance of space, food web structure and functional response parametrisation. *Mathematical Modelling of Natural Phenomena*, 11(4):16–33.

[27] Farkas, J. Z., Morozov, A. Y., Arashkevich, E. G., and Nikishina, A. (2015). Revisiting the stability of spatially heterogeneous predator–prey systems under eutrophication. *Bulletin of Mathematical Biology*, 77(10):1886–1908.

[28] Fellmuth, B., Gaiser, C., and Fischer, J. (2006). Determination of the boltzmann constant—status and prospects. *Measurement Science and Technology*, 17(10):R145.

[29] Ferreira, J. M. and Pedro, A. M. (1998). Oscillations of delay difference systems. *Journal of Mathematical Analysis and Applications*, 221(1):364–383.

[30] Fioletov, V. E., Kerr, J. B., and Fergusson, A. (2010). The uv index: definition, distribution and factors affecting it. *Can J Public Health*, 101(4):5–9.

[31] Fisher, R. A. (1937). The wave of advance of advantageous genes. *Annals of Human Genetics*, 7(4):355–369.

[32] Frost, B. (1987). Grazing control of phytoplankton stock in the open subarctic pacific ocean: a model assessing the role of mesozooplankton, particularly the large calanoid copepods neocalanus spp. *Marine ecology progress series. Oldendorf*, 39(1):49–68.

[33] Gabric, A., Murray, N., Stone, L., and Kohl, M. (1993). Modelling the production of dimethylsulfide during a phytoplankton bloom. *Journal of Geophysical Research: Oceans*, 98(C12):22805–22816.

[34] Gatedee, J., Kritsiriwuthinan, K., Galyov, E. E., Shan, J., Dubinina, E., Intarak, N., Clokie, M. R., and Korbsrisate, S. (2011). Isolation and characterization of a novel podovirus which infects burkholderia pseudomallei. *Virology journal*, 8(1):1.

[35] Genkai-Kato, M. and Yamamura, N. (1999). Unpalatable prey resolves the paradox of enrichment. *Proceedings of the Royal Society of London B: Biological Sciences*, 266(1425):1215–1219.

[36] Gentleman, W., Leising, A., Frost, B., Strom, S., and Murray, J. (2003). Functional responses for zooplankton feeding on multiple resources: a review of assumptions and biological dynamics. *Deep Sea Research Part II: Topical Studies in Oceanography*, 50(22):2847–2875.

[37] Gismervik, I. (2006). Top-down impact by copepods on ciliate numbers and persistence depends on copepod and ciliate species composition. *Journal of Plankton Research*, 28(5):499–507.

[38] Gismervik, I. and Andersen, T. (1997). Prey switching by acartia clausi: experimental evidence and implications of intraguild predation assessed by a model. *Marine Ecology Progress Series*, 157:247–259.

[39] Gourley, S. A. and Kuang, Y. (2004). A delay reaction-diffusion model of the spread of bacteriophage infection. *SIAM Journal on Applied Mathematics*, 65(2):550–566.

[40] Hansen, B. W., Bjørnsen, P., and Hansen, B. (1997). Zooplankton grazing and growth: Scaling within the 2-2,000-˜ iii body size range. *Limnol. Oceanogr*, 42:687–704.

[41] Hansen, F. (1993). Phaeocystis blooming enhanced by copepod predation on protozoa-evidence from incubation experiments. *Mar Ecol Prog Ser*, 102:51–57.

[42] Holling, C. (1959a). The components of predation as revealed by a study of small-mammal predation of the european pine sawfly. *The Canadian Entomologist*, 91(05):293–320.

[43] Holling, C. (1961). Principles of insect predation. *Annual review of entomology*, 6(1):163–182.

[44] Holling, C. S. (1959b). Some characteristics of simple types of predation and parasitism. *The Canadian Entomologist*, 91(07):385–398.

[45] Holling, C. S. (1965). The functional response of predators to prey density and its role in mimicry and population regulation. *Memoirs of the Entomological Society of Canada*, 97(S45):5–60.

[46] Hu, G., Wu, X., Zhao, L., Li, R., Wu, T., Xie, C., Pang, Q., and Cheng, G. (2017). An improved model for soil surface temperature from air temperature in permafrost regions of qinghai-xizang (tibet) plateau of china. *Meteorology and Atmospheric Physics*, 129(4):441–451.

[47] Huang, Y., Chen, F., and Zhong, L. (2006). Stability analysis of a prey–predator model with holling type iii response function incorporating a prey refuge. *Applied Mathematics and Computation*, 182(1):672–683.

[48] Hutchinson, G. E. (1948). Circular causal systems in ecology. *Annals of the New York Academy of Sciences*, 50(1):221–246.

[49] Jensen, C. X. and Ginzburg, L. R. (2005). Paradoxes or theoretical failures? the jury is still out. *Ecological Modelling*, 188(1):3–14.

[50] Kharab, A. and Guenther, R. B. (2011). *An introduction to numerical methods: a MATLAB approach*. CRC Press.

[51] Kolmogorov, A. N. (1937). A study of the equation of diffusion with increase in the quantity of matter, and its application to a biological problem. *Moscow Univ. Bull. Math.*, 1:1–25.

[52] Kot, M. (2001). *Elements of mathematical ecology*. Cambridge University Press.

[53] Krug, E. G. (2016). Trends in diabetes: sounding the alarm. *The Lancet*, 387(10027):1485–1486.

[54] Krysiak-Baltyn, K., Martin, G. J., Stickland, A. D., Scales, P. J., and Gras, S. L. (2015). Computational models of populations of bacteria and lytic phage. *Critical reviews in microbiology*, pages 1–27.

[55] Krysiak-Baltyn, K., Martin, G. J., Stickland, A. D., Scales, P. J., and Gras, S. L. (2016). Computational models of populations of bacteria and lytic phage. *Critical reviews in microbiology*, 42(6):942–968.

[56] Lalli, C. and Parsons, T. R. (1997). *Biological Oceanography: An Introduction: An Introduction*. Butterworth-Heinemann.

[57] Lampert, W. (2005). Vertical distribution of zooplankton: density dependence and evidence for an ideal free distribution with costs. *BMC biology*, 3(1):1.

[58] Lenski, R. E. and Levin, B. R. (1985). Constraints on the coevolution of bacteria and virulent phage: a model, some experiments, and predictions for natural communities. *American Naturalist*, pages 585–602.

[59] Levin, B. R., Stewart, F. M., and Chao, L. (1977). Resource-limited growth, competition, and predation: a model and experimental studies with bacteria and bacteriophage. *American Naturalist*, pages 3–24.

[60] Levinton, J. S. (2009). *Marine biology: function, biodiversity, ecology*. Oxford University Press New York.

[61] Lewis, N., Morozov, A., Breckels, M., Steinke, M., and Codling, E. (2013). Multitrophic interactions in the sea: assessing the effect of infochemical-mediated foraging in a 1-d spatial model. *Mathematical Modelling of Natural Phenomena*, 8(06):25–44.

[62] Lewis, N. D., Breckels, M. N., Archer, S. D., Morozov, A., Pitchford, J. W., Steinke, M., and Codling, E. A. (2012). Grazing-induced production of dms can stabilize food-web dynamics and promote the formation of phytoplankton blooms in a multitrophic plankton model. *Biogeochemistry*, 110(1-3):303–313.

[63] Limmathurotsakul, D., Wongratanacheewin, S., Teerawattanasook, N., Wongsuvan, G., Chaisuksant, S., Chetchotisakd, P., Chaowagul, W., Day, N. P., and Peacock, S. J. (2010a). Increasing incidence of human melioidosis in northeast thailand. *The American journal of tropical medicine and hygiene*, 82(6):1113–1117.

[64] Limmathurotsakul, D., Wuthiekanun, V., Chantratita, N., Wongsuvan, G., Amornchai, P., Day, N. P., and Peacock, S. J. (2010b). Burkholderia pseudomallei is spatially distributed in soil in northeast thailand. *PLoS neglected tropical diseases*, 4(6):e694.

[65] Lotka, A. J. (1910). Contribution to the theory of periodic reactions. *The Journal of Physical Chemistry*, 14(3):271–274.

[66] Lotka, A. J. (1920a). Analytical note on certain rhythmic relations in organic systems. *Proceedings of the National Academy of Sciences of the United States of America*, 6(7):410.

[67] Lotka, A. J. (1920b). Undamped oscillations derived from the law of mass action. *Journal of the american chemical society*, 42(8):1595–1599.

[68] Lotka, A. J. (1926). Elements of physical biology. *Science Progress in the Twentieth Century (1919-1933)*, 21(82):341–343.

[69] MacDonald, N. (1978). *Lecture notes in biomathematics*. Springer.

[70] Malacinski, G. M. (2005). *Essentials of molecular biology*. Jones & Bartlett Learning.

[71] Malthus, T. R. (1798). *An Essay on the Principle of Population, as it Affects the Future Imporvement of Society, with Remarks on the Speculations of Mr. Godwin, M. Condorcet, and Other Writers*. The Lawbook Exchange, Ltd.

[72] Manivanh, L., Pierret, A., Rattanavong, S., Kounnavongsa, O., Buisson, Y., Elliott, I., Maeght, J.-L., Xayyathip, K., Silisouk, J., Vongsouvath, M., et al. (2017). Burkholderia pseudomallei in a lowland rice paddy: seasonal changes and influence of soil depth and physico-chemical properties. *Scientific reports*, 7.

[73] Mc Grath, S. and van Sinderen, D. (2007). *Bacteriophage: genetics and molecular biology*. Horizon Scientific Press.

[74] Mellard, J. P., Yoshiyama, K., Litchman, E., and Klausmeier, C. A. (2011). The vertical distribution of phytoplankton in stratified water columns. *Journal of Theoretical Biology*, 269(1):16–30.

[75] Meyer, K., Ridgwell, A., and Payne, J. (2016). The influence of the biological pump on ocean chemistry: implications for long-term trends in marine redox chemistry, the global carbon cycle, and marine animal ecosystems. *Geobiology*, 14(3):207–219.

[76] Meyer, K. M., Vos, M., Mooij, W. M., Hol, W. G., Termorshuizen, A. J., and van der Putten, W. H. (2012). Testing the paradox of enrichment along a land use gradient in a multitrophic aboveground and belowground community. *PloS one*, 7(11):e49034.

[77] Michael, T. H. (2002). Scientific computing: an introductory survey. Accessed: 2017-09-15.

[78] Monod, J. (1949). The growth of bacterial cultures. *Annual Reviews in Microbiology*, 3(1):371–394.

[79] Monon, J. (2012). The growth of bacterial cultures. *Selected Papers in Molecular Biology by Jacques Monod*, page 139.

[80] Morozov, A. and Arashkevich, E. (2008). Patterns of zooplankton functional response in communities with vertical heterogeneity: a model study. *Mathematical Modelling of Natural Phenomena*, 3(03):131–148.

[81] Morozov, A., Arashkevich, E., Nikishina, A., and Solovyev, K. (2010). Nutrient-rich plankton communities stabilized via predator–prey interactions: revisiting the role of vertical heterogeneity. *Mathematical Medicine and Biology*, page dqq010.

[82] Morozov, A., Pasternak, A. F., and Arashkevich, E. G. (2013). Revisiting the role of individual variability in population persistence and stability. *PloS one*, 8(8):e70576.

[83] Morozov, A. and Petrovskii, S. (2013). Feeding on multiple sources: towards a universal parameterization of the functional response of a generalist predator allowing for switching. *PloS one*, 8(9):e74586.

[84] Morozov, A., Sen, M., and Banerjee, M. (2012). Top-down control in a patchy environment: Revisiting the stabilizing role of food-dependent predator dispersal. *Theoretical population biology*, 81(1):9–19.

[85] Morozov, A. Y. (2010). Emergence of holling type iii zooplankton functional response: bringing together field evidence and mathematical modelling. *Journal of theoretical biology*, 265(1):45–54.

[86] Morozov, A. Y. (2013). Incorporating complex foraging of zooplankton in models: Role of micro-and mesoscale processes in macroscale patterns. In *Dispersal, Individual Movement and Spatial Ecology*, pages 223–259. Springer.

[87] Morozov, A. Y., Banerjee, M., and Petrovskii, S. V. (2016). Long-term transients and complex dynamics of a stage-structured population with time delay and the allee effect. *Journal of theoretical biology*, 396:116–124.

[88] Mougi, A. and Nishimura, K. (2008). The paradox of enrichment in an adaptive world. *Proceedings of the Royal Society of London B: Biological Sciences*, 275(1651):2563–2568.

[89] Moussaoui, A. and Bouguima, S. M. (2016). Seasonal influences on a prey–predator model. *Journal of Applied Mathematics and Computing*, 50(1-2):39–57.

[90] Murdoch, W. (1973). The functional response of predators. *Journal of Applied Ecology*, 10:335–342.

[91] Murdoch, W. W. (1969). Switching in general predators: experiments on predator specificity and stability of prey populations. *Ecological monographs*, 39(4):335–354.

[92] Murray, J. D. (2007). *Mathematical biology: I. An introduction*. Springer-Verlag.

[93] Ngamsang, R., Potisap, C., Boonmee, A., Lawongsa, P., Chaianunporn, T., Wongratanacheewin, S., Rodrigues, J. L., and Sermswan, R. W. (2015). The contribution of soil physicochemical properties to the presence and genetic diversity of burkholderia pseudomallei. *The Southeast Asian journal of tropical medicine and public health*, 46(1):38–50.

[94] Oaten, A. and Murdoch, W. W. (1975). Switching, functional response, and stability in predator-prey systems. *American Naturalist*, pages 299–318.

[95] Payne, R. J. and Jansen, V. A. (2001). Understanding bacteriophage therapy as a density-dependent kinetic process. *Journal of Theoretical Biology*, 208(1):37–48.

[96] Petrovskii, S., Li, B.-L., and Malchow, H. (2004). Transition to spatiotemporal chaos can resolve the paradox of enrichment. *Ecological Complexity*, 1(1):37–47.

[97] Polis, G. A. and Holt, R. D. (1992). Intraguild predation: the dynamics of complex trophic interactions. *Trends in Ecology & Evolution*, 7(5):151–154.

[98] Raymont, J. E. (1980). *Plankton & Productivity in the Oceans: Volume 1: Phytoplankton*. Oxford.

[99] Rosenzweig, M. L. et al. (1971). Paradox of enrichment: destabilization of exploitation ecosystems in ecological time. *Science*, 171(3969):385–387.

[100] Rosenzweig, M. L. and MacArthur, R. H. (1963). Graphical representation and stability conditions of predator-prey interactions. *American Naturalist*, pages 209–223.

[101] Roy, S. and Chattopadhyay, J. (2007). Towards a resolution of 'the paradox of the plankton': A brief overview of the proposed mechanisms. *Ecological complexity*, 4(1):26–33.

[102] Ryabov, A. B., Morozov, A., and Blasius, B. (2015). Imperfect prey selectivity of predators promotes biodiversity and irregularity in food webs. *Ecology letters*, 18(11):1262–1269.

[103] Sahoo, B. and Poria, S. (2011). Dynamics of a predator-prey system with seasonal effects on additional food. *International Journal of Ecosystem*, 1(1):10–13.

[104] Shan, J., Korbsrisate, S., Withatanung, P., Adler, N. L., Clokie, M. R., and Galyov, E. E. (2014). Temperature dependent bacteriophages of a tropical bacterial pathogen. *Frontiers in microbiology*, 5:599.

[105] Siekmann, I., Malchow, H., and Venturino, E. (2008). An extension of the beretta-kuang model of viral diseases. *Mathematical Biosciences and Engineering*, 5(3):549–565.

[106] Sinton, L. W., Hall, C. H., Lynch, P. A., and Davies-Colley, R. J. (2002). Sunlight inactivation of fecal indicator bacteria and bacteriophages from waste stabilization pond effluent in fresh and saline waters. *Applied and Environmental Microbiology*, 68(3):1122–1131.

[107] Skalski, G. T. and Gilliam, J. F. (2001). Functional responses with predator interference: viable alternatives to the holling type ii model. *Ecology*, 82(11):3083–3092.

[108] Smith, H. L. (2008). Models of virulent phage growth with application to phage therapy. *SIAM Journal on Applied Mathematics*, 68(6):1717–1737.

[109] Smith, H. L. and Trevino, R. (2009). Bacteriophage infection dynamics: multiple host binding sites. *Mathematical Modelling of Natural Phenomena*, 4(6):109–134.

[110] Stewart, F. M. and Levin, B. R. (1973). Partitioning of resources and the outcome of interspecific competition: a model and some general considerations. *American Naturalist*, pages 171–198.

[111] Suttle, C. A. and Chen, F. (1992). Mechanisms and rates of decay of marine viruses in seawater. *Applied and Environmental Microbiology*, 58(11):3721–3729.

[112] Tang, K. W. and Taal, M. (2005). Trophic modification of food quality by heterotrophic protists: species-specific effects on copepod egg production and egg hatching. *Journal of Experimental Marine Biology and Ecology*, 318(1):85–98.

[113] Trung, T. T., Hetzer, A., Göhler, A., Topfstedt, E., Wuthiekanun, V., Limmathurotsakul, D., Peacock, S. J., and Steinmetz, I. (2011). Highly sensitive direct detection and quantification of burkholderia pseudomallei bacteria in environmental soil samples by using real-time pcr. *Applied and environmental microbiology*, 77(18):6486–6494.

[114] Tuntiwaranuruk, U., Thepa, S., Tia, S., and Bhumiratana, S. (2006). Modeling of soil temperature and moisture with and without rice husks in an agriculture greenhouse. *Renewable energy*, 31(12):1934–1949.

[115] Uitz, J., Claustre, H., Morel, A., and Hooker, S. B. (2006). Vertical distribution of phytoplankton communities in open ocean: An assessment based on surface chlorophyll. *Journal of Geophysical Research: Oceans (1978–2012)*, 111(C8).

[116] Vallina, S. M., Ward, B., Dutkiewicz, S., and Follows, M. (2014). Maximal feeding with active prey-switching: A kill-the-winner functional response and its effect on global diversity and biogeography. *Progress in Oceanography*, 120:93–109.

[117] Verhulst, P. (1845). Recherches mathématiques sur la loi d'accroissement de la population, nouveaux mémoires de l'académie royale des sciences et belles-lettres de bruxelles, art. 1. 18:1–45.

[118] Volterra, V. (1926). Fluctuations in the abundance of a species considered mathematically. *Nature*, 118:558–560.

[119] Waage, P. and Gulberg, C. M. (1986). Studies concerning affinity. *J. Chem. Educ*, 63(12):1044.

[120] Wang-ngarm, S., Chareonsudjai, S., and Chareonsudjai, P. (2014). Physicochemical factors affecting the growth of burkholderia pseudomallei in soil microcosm. *The American journal of tropical medicine and hygiene*, 90(3):480–485.

[121] Weitz, J. S. and Dushoff, J. (2008). Alternative stable states in host–phage dynamics. *Theoretical Ecology*, 1(1):13–19.

[122] Wright, E. (1946). The non-linear difference-differential equation. *The Quarterly Journal of Mathematics*, (1):245–252.

[123] Wright, E. M. (1955). A non-linear difference-differential equation. *J. reine angew. Math*, 194(1-4):66–87.

[124] Zemb, O., Manefield, M., Thomas, F., and Jacquet, S. (2013). Phage adsorption to bacteria in the light of the electrostatics: a case study using e. coli, t2 and flow cytometry. *Journal of virological methods*, 189(2):283–289.